Replies to reviewer #2

At the outset, we thank the reviewer for positive and constructive comments that improved the quality of the manuscript.

Comment: Figure 5: Why CER of the ice show a decreasing trend and CER of water showing an increasing trend over BOB beyond 30°C? Whereas over AS, both CER liquid and Ice shows an increasing trend?

Reply: *The main reason for studying CER at different SST is to understand whether or not the observed differences originated at the formation of cloud stage. For that, CER for water is sufficient. Therefore, figure and text related to CER for ice are removed from the revised manuscript.*

Regarding reviewers' query, yes, there are some small differences in the variation of CER for ice and water with SST above 30 °C, but they are not significant.

Comment: Figure 5: Why CER of ice (water) shows a reverse trend beyond 30°C (28.5°C) over AS and BoB.

Reply: *The CER depends on the ambient atmospheric aerosol concentration and availability of water vapor. The variation of AOD with SST is substantial over the AS while it is marginal over the BOB. As the SST increases AOD decreases and TCWV increases results in increase in CER over the AS and is more prominent at higher SSTs (where the decrease of AOD with SST is quite substantial). On the other hand, the decrease in AOD with SST is quite marginal over BOB and in fact, AOD increases from 30 °C to 31 °C. Therefore, the CER for water continuously increases with rapid increase beyond 28 °C over AS, while the increase is marginal over BOB.*

Comment: Figures 2 and 5: Higher values of reflectivities beyond 8 km beyond 30°C over AS is due to the higher values of CER liquid (Fig. 5)? That means higher convection over AS than BOB?

Whether similar explanation holds good for LTS over AS?

Reply: *The differences in Z over AS and BOB at and above 8 km is very small (within 1 dBZ) and not significant. Therefore, we are not attributing these to any physical or microphysical processes.*

Referee #4

At the outset, we thank the reviewer for positive and constructive comments that improved the quality of the manuscript.

Comment: This study investigated the variability in the vertical structure of precipitation as a function of sea surface temperature using TRMM precipitation radar measurements. I think the paper lacks focus, inadequate analysis, and insufficient literature review. The intent of the paper digresses at some point by incorporating the aerosol/cloud radiation analysis without a context jumbling both convective dynamics and radiative impacts of aerosols on clouds. Given the scope, the section with aerosol and radiation properties is redundant. Most of the analysis lacks context. Overall, the quality and the content of the present paper are poor.

Reply: *The aim of the present study is to understand differences in the variation of vertical structure of precipitation with SST over the Arabian Sea and Bay of Bengal. SST being the main driving force to trigger precipitating systems through air-sea interactions, the occurrence of precipitation top height and intensity profiles (reflectivity) as a function of SST are studied. Besides SST, the vertical structure can be modified by aerosols (or CCN, mostly at the cloud formation stage) and thermodynamics of the ambient atmosphere. In the revised manuscript, all these parameters are considered to explain the differences in the vertical structure. Aerosols are considered only for understanding variation in cloud effective radius, nevertheless their radiative effects (direct, indirect, etc.) are not considered in the present study. Recent studies, indeed, have shown the impact of aerosols (PM_{10}) on the vertical structure of precipitation (Gao et al., 2018 and references therein).*

We have rewritten the introduction with more focus on the above aspects and highlighting the known differences in various aspects/parameters over AS and BOB. The literature survey is also improved considerably in the revised manuscript by adding appropriate references (Guo et al. 2018; Nuijens et al. 2017; Weller et al. 2016; Sathiyamoorthy et al. 2013; Takayabu et al. 2010; Bhat et al. 2001; Ramanathan et al. 2001; Gadgil 2000; Krishnamurti 1981; Narayanan and Rao 1981;).

Comment: Introduction lacks discussion on how Arabian Sea and Bay of Bengal regions are distinctly different in its background state, which would help them explain the further analysis on convective profiles. Though the authors have claimed to have studied the "causative mechanisms" of SST with the vertical structure of precipitation in the introduction, no suggestions based on the analysis performed have been discussed in the later sections. Mere correlation doesn't explain the causality, which needs carefully controlled model experiments with a rigor to assess the confounding factors controlling the SST and precipitation relationship.

Reply: *The introduction of the revised manuscript is modified by considering all the suggestion of the reviewer. The role of the surrounding seas on the rainfall over the Indian landmass is stated and the differences between the two seas are clearly mentioned with proper references in the revised manuscript as follows:*

Indian summer monsoon (ISM) is one of the most complex weather phenomena, involving coupling between the atmosphere, land and ocean. At the boundary of the ocean and atmosphere air-sea interactions play a key role for the coupled Earth system (Wu and Kirtman 2005; Feng et al. 2018). SST – precipitation relations are the important measures for the air-sea interactions on different temporal scales (Woolnough et al., 2000; Rajendran et al. 2012). Recent studies (Wang et al. 2005; Rajeevan et al. 2012; Chaudhari et al. 2013; 2016; Weller et al. 2016; Feng et al. 2018) have shown that the simulation of ISM can be improved with the exact representation of sea surface temperature (SST) - precipitation relationship. SST modulates the meteorological factors that influence the formation and evolution of different kinds of precipitating systems over tropical oceans (Gadgil et al. 1984; Schumacher and Houze, 2003; Takayabu et al. 2010; Oueslati and Bellon 2015).

The studies dealing with SST and cloud/precipitation population considered whole Indian Ocean as a single entity (Gadgil et al. 1984; Woolnough et al., 2000; Rajendran et al. 2012; Sabin et al. 2012; Meenu et al. 2012; Nair and Rajeev 2014; Roxy 2014; Nair et al. 2017). But in reality the BOB and the AS of Indian Ocean possesses distinctly different features. The summer monsoon experiment (MONEX) showed the influence of the AS and the BOB on the rainfall produced over the Indian sub-continent (Krishnamurti 1985; Houze and Churchill 1987; Gadgil 2000; Bhat et al.2001) and also proved how these two seas are different with respect to the other, in terms of SST, back ground atmosphere and the occurrence of precipitating systems. The SST in the AS cools between 10°N and 20°N during the monsoon season whereas warming is seen in other Oceans between the same latitudes (Krishnamurthi 1981). SST variability is large over the AS than the BOB at seasonal and intraseasonal scales (Sengupta et al. 2001; Roxy et al. 2013). The monsoonal winds are stronger over the AS than BOB (Findlater 1969). Also, lower-tropospheric thermal inversions are more frequent and stronger over the AS than BOB (Narayanan and Rao 1981; Sathiyamoorthy et al. 2013). Thus, the atmospheric and sea surface conditions and in turn the occurrence of different kinds of precipitating systems are quite different over the BOB and the AS during the ISM period (June to September - JJAS). For instance, long-term measurements of tropical rainfall measuring mission (TRMM) precipitation radar (PR) have shown that shallow systems are more prevalent over the AS, while deeper systems occur frequently over the BOB (Liu et al. 2007; Romatschke et al. 2010; Saikranthi et al. 2014; Houze et al. 2015).

The aforementioned studies mainly focused on the morphology of vertical structure of precipitation, but, none of them studied the variation of vertical structure of precipitation (in terms of occurrence and intensity) with SST and the differences in the vertical structure over AS and BOB. On the other hand, information on the vertical structure of precipitation is essential for improving the accuracy of rainfall estimation (Fu and Liu 2001; Sunilkumar et al. 2015), understanding the dynamical and microphysical processes of hydrometeor growth/decay mechanisms (Houze 2004; Greets and Dejene 2005; Saikranthi et al. 2014; Rao et al. 2016) and for improving the latent heating retrievals (Tao et al. 2006). SST being the main driving force to trigger precipitating systems through air-sea interactions (Sabin et al. 2012; Nuijens et al. 2017), can alter the vertical structure of precipitation (Oueslati and Bellon 2015). Therefore, the present study aims to understand the variation of vertical structure of precipitation (in terms of precipitation top height and intensity) with SST over the AS and BOB. Besides the SST, vertical structure can be modified by aerosols (or CCN, mostly at the cloud formation stage) and thermodynamics of the ambient atmosphere. For instance, recent studies have shown the impact of surface aerosols (PM_{10}) in altering the vertical structure of precipitation (Gao et al., 2018). All these parameters, therefore, are considered in the present study to explain the differences in the vertical structure.

Comment: Given the non-linear influence of sea surface temperature on the variability of precipitation structure, it would be an oversimplification to look at the influence of SST on the mean structure of radar echoes. It would have been interesting to classify the mean structure further into different cloud types (e.g., shallow/congestus/deep/) and assess the variability of these populations in terms of factors (e.g., winds, stability) that are co-associated with SSTs. There are no insights been provided on why the differences in the variabilities of vertical structure exist between AS and BOB. It is important to investigate if more variability over the AS is due to fluctuations in the winds/SSTs or both. From figure 2, it is evident that AS region has more seasonality in term of air-sea variables compared to BOB. Given the influence of more variables, merely analyzing indirect relationships of precipitation structure with SSTs would be futile. One way to analyze is to look at the variability of large-scale parameters (e.g., stability, vertical velocity, wind speed) for a given SST, and look at the cloud population in terms of these co-associated variables. By doing so, one would prioritize the combination of factors that lead to different convection type. SST influence on the clouds is of the first order; however, it is also important to show the temporal variation, highlighting the seasonal evolution of cloud types collocated with SSTs and other variables.

Reply: *We agree with the reviewer that all the forcing/controlling parameters (SST, winds, vertical wind velocity, stability, etc.) need to be considered for understanding the vertical structure of precipitation. We did the same in the revised version of the manuscript. Also, we studied the vertical structure of two types of precipitation (deep and shallow) as suggested by the reviewer. Since, stratiform rain is the trailing portions of convective complexes (Houze et al. 2015) and is not directly driven by the SST, it's relation with SST is not dealt separately.*

Comment: The stability measure (LTS) used here is appropriate for stratiform clouds, which may not be appropriate for convective clouds in these regions. One may use static stability profiles instead.

Reply: *As suggested by the reviewer instead of LTS the static stability (profiles of θ_e) is used in the revised manuscript to explain the convective strength as a function of SST.*

Replies to short comments

At the outset thank Mr. B. Guha for reading our manuscript and suggesting comments.

Comment: (a) The article title highlights aspect of the variability of vertical structure of precipitation with sea surface temperature (SST). However, the authors explore the relationships between the SST and other variables such as AOD, CER ice and CER liquid, total column water vapour etc. that may not directly represent the vertical structure of precipitation.

***Reply:** The generation and growth of clouds and precipitating systems depend on the triggering mechanisms (over Oceans, it is primarily SST) and ambient dynamical and thermodynamical environment (Houze et al., 2015). Changes in SST have the potential of altering the type of precipitating system and the vertical structure of precipitation (Oueslati and Bellon 2015). Besides the SST, vertical structure can be modified by aerosols (or CCN, mostly at the cloud formation stage) and thermodynamics of the ambient atmosphere. For instance, recent studies have shown the impact of surface aerosols (PM_{10}) in altering the vertical structure of precipitation (Gao et al., 2018 and references therein). We, therefore, need to understand the observed variations exist at the cloud formation stage or manifested during the descent of precipitation particles to the ground. The cloud effective radius (CER for water) (depend on aerosols and TCWV) is a good proxy to understand the cloud microphysical processes. While, vertical velocity, winds, stability parameters are considered to depict the ambient atmosphere, which can alter the vertical structure of precipitation. All these parameters are considered in the present study to understand the vertical structure of precipitation over AS and BOB.*

Comment: (b) The figure 1 shows the regions considered in this study with background colour representing the mean SST during SWM period over AS and BOB. It is clearly evident that the regions of interest depict significant spatial heterogeneity in the SST (_ 2 degrees C). In such a scenario, (in the figures 4, 5 and 6) I think the standard deviation should be present in those figures.

***Reply:** We wish to inform the reviewer that the segregation of SST data into different bins (26° to 31℃ with 1 interval) is done not by averaging the spatial data, rather using 1° X 1° gridded data. Therefore, there is no need to average the SST data. Instead, we provided standard deviation/standard error of mean values for CER, AOD, TVWV and vertical profiles of Z in the revised manuscript.*

Comment: (c) I would recommend to use MODIS level 2 data products for AOD, CER-ice and CER-liquid for exploring the relationships between different variables. Further, the authors have not mentioned from where the total column water vapour data was obtained. Even the combined uncertainty from different sources of data (e.g., TRMM, MODIS and ECMWF Interim Reanalysis) was not accounted for when establishing the relationships.

***Reply:** The total column water vapor data are taken from the ERA-Interim reanalysis and this information is included in the revised manuscript. The spatial resolutions of MODIS level-2* *and ERA-Interim SST are different. Thus, to know the values of AOD and CER at different SSTs, again the MODIS level-2 dataset needs to be regridded. Instead of regridding, we have used equal spatial lengths MODIS level-3 and SST datasets.*

Comment: (d) It would be nice if the authors establish the mechanism on why the contrasting relationships were observed over BOB and AS. The authors shall note that SST depends on other factors such as turbidity of the sea water and sea surface albedo, which in turn depend on other variables including wind speed and chlorophyll concentration. While the authors have ignored these essential variables, the relationships with AOD, CER ice, CER-liquid and total column water vapour alone cannot provide the variability in SST in the regions of interest.

Reply: *We do agree that SST over open Oceans depends on many factors. But our interest is not to show how precipitating systems alter the SST over the AS and BOB. Rather, we focused on the variation of vertical structure of precipitation (in terms of precipitation top height and intensity) with SST over the AS and the BOB and the factors responsible for the variations in the vertical structure over both these oceans.*

Variability of vertical structure of precipitation with sea surface temperature over the Arabian Sea and the Bay of Bengal as inferred by TRMM PR measurements

Kadiri Saikranthi[1], Basivi Radhakrishna[2], Thota Narayana Rao[2] and

Sreedharan Krishnakumari Satheesh[3]

[1] *Department of Earth and Climate Science, Indian Institute of Science Education and Research (IISER), Tirupati, India.*

[2] *National Atmospheric Research Laboratory, Department of Space, Govt. of India, Gadanki - 517112, India.*

[3] *Divecha Centre for Climate Change, Centre for Atmospheric and Oceanic Sciences, Indian Institute of Science, Bangalore - 560012, India.*

Address of the corresponding author

Dr. K. Saikranthi,

Department of Earth and Climate Science,

Indian Institute of Science Education and Research (IISER),

Tirupati,

Andhra Pradesh, India.
Email: ksaikranthi@gmail.com

Abstract

Tropical ~~Rainfall Measuring Mission (TRMM) Precipitation Radar (PR) 2A25 reflectivity profiles data during the period 1998 - 2013~~rainfall measuring mission precipitation radar measurements are used to ~~study~~examine the ~~differences in the~~variation of vertical structure of precipitation ~~and its variation~~ with sea surface temperature (SST) over the Arabian Sea (AS) and ~~the~~ Bay of Bengal (BOB). ~~Even though the AS and the BOB are parts of the Indian Ocean, they exhibit distinct features in vertical structure of precipitation and its variation with SST.~~ The variation of reflectivity and precipitation echo top ~~occurrence~~ with SST is remarkable over the AS but ~~trivial~~small over the BOB. The ~~median~~ reflectivity increases with SST ~~at all heights~~ (from 26°C to 31°C) by ~1 dBZ and 4 dBZ above and below ~~10~~6 km ~~altitude, but the increase~~, respectively, over the AS while, its variation is ~~prominent below the freezing level height~~< 0.5 dBZ over the BOB. The transition from shallow storms at lower SSTs (≤ 27°C) to deeper storms at higher SSTs is strongly associated with the decrease in stability and mid-tropospheric wind shear over the AS. ~~On the other hand, irrespective of altitude, reflectivity profiles are same~~ Contrary, the storms are deeper at all SSTs over the BOB~~. To understand these differences, variation of aerosols, cloud~~ due to weaker stability and ~~water vapor with SST is studied over these seas.~~mid-tropospheric wind shear. At lower SSTs ~~less than 27°C~~, the observed high aerosol optical depth (AOD) and low total column water vapor (TCWV) over ~~the~~ AS results in small ~~Cloud~~ cloud effective radius (CER) ~~values~~ and ~~low~~weaker reflectivity. As SST increases, AOD decreases and TCWV increases~~, which result in~~ leading to large CER and high reflectivity. ~~Over~~The changes in these parameters with SST are marginal over the BOB ~~the change in AOD, TCWV~~ and hence the CER ~~with SST~~and reflectivity. The predominance of collision-coalescence process below the bright band is ~~marginal. Thus,~~responsible for the observed negative slopes in the

reflectivity over both the seas. The observed variations in reflectivity ~~profiles seem to be present from~~ are originated at the cloud formation stage ~~itself~~ over both the seas and these variations are magnified during the descent of hydrometeors to ground.

Formatted: Indent: First line: 1.27 cm

1. Introduction

Indian summer monsoon (ISM - June through September) is one of the most complex weather phenomena, involving coupling between the atmosphere, land and ocean. At the boundary of the ocean and atmosphere air-sea interactions play a key role for the coupled Earth system (Wu and Kirtman 2005; Feng et al. 2018). ~~SST~~The sea surface temperature (SST) – precipitation relations are the important measures for the air-sea interactions on different temporal scales (Woolnough et al., 2000; Rajendran et al. 2012). Recent studies (Wang et al. 2005; Rajeevan et al. 2012; Chaudhari et al. 2013; ~~Chaudhari~~2016; Weller et al. 2016; Feng et al. 2018) have shown that the simulation of ISM can be improved with the exact representation of ~~sea surface temperature (~~SST~~)~~ - precipitation relationship.

~~The dynamics of Madden-Julian oscillation (MJO) campaign (DYNAMO) portrayed the importance of understanding the link between SST and convective initiation at MJO scales (Yoneyama et al. 2013). With known differences in SST between Western Pacific and~~

Formatted: Pattern: Clear (White)

~~Indian Ocean, Barnes and Houze (2013) showed the occurrence of shallow systems maximized during the suppressed phases of MJO while the deep wide convective systems occurred during the active phases of MJO.~~ SST modulates the meteorological factors that influence the formation and evolution of different kinds of precipitating systems over tropical oceans (Gadgil et al. 1984; Schumacher and Houze, 2003; Takayabu et al. 2010; Oueslati and Bellon 2015).

Formatted: Pattern: Clear

The ~~relationships between the~~studies dealing with SST and cloud/precipitation ~~have been studied in variety of contexts during the past three decades. The non-linear relationship of SST-precipiation/cloud occurrence~~population considered whole Indian Ocean as a single entity (Gadgil et al. 1984; Woolnough et al., 2000; Rajendran et al. 2012; Sabin et al. 2012; Meenu et al. 2012; Nair and Rajeev 2014; Roxy 2014~~; Nair et al. 2017) is well documented over the Indian Ocean. The probability of organized convection increases with SST up to a critical value of ~ 28°C (Gadgil et al. 1984). Sabin et al. (2012) and Meenu et al. (2012) showed that the convection is no longer dependent on SST at SSTs greater than 30°C. Later, by considering the time lag between the SST and rainfall Roxy (2014) argued that this upper threshold can exceed till 31°C. Sengupta et al. (2001) showed that the intraseasonal variability of SST is not same over the entire Indian Ocean. Later, Roxy et al. (2013) estimated the time lag for SST and precipitation to be 2 and 5 weeks for~~). But in reality the Bay of Bengal (BOB) and the Arabian Sea (AS~~), respectively. Through this study they found that the response of precipitation to SST anomalies is faster over the AS than the BOB. Also, the summer~~) of Indian Ocean possess distinctly different features. The monsoon experiment (MONEX) ~~showed the influence of the AS and the BOB on the rainfall produced over the Indian sub-continent (Krishnamurti 1985; Houze and Churchill 1987) and also proved~~and Bay of Bengal monsoon experiment (BOBMEX) have shown how these two seas are different with respect to ~~the~~each other~~ oceans,~~ in terms of SST, back ground atmosphere and the occurrence of precipitating systems~~.~~

~~Knowing the differences~~ (Krishnamurti 1985; Houze and Churchill 1987; Gadgil 2000; Bhat et al. 2001). The SST in the AS cools between 10 °N and 20 °N during the monsoon season whereas warming is seen in other global Oceans between the same latitudes (Krishnamurthi 1981). SST variability is large over the AS than the BOB at seasonal and intraseasonal scales (Sengupta et al. 2001; Roxy et al. 2013). The monsoonal winds (in particular the low-level jet) are stronger over the AS than BOB (Findlater 1969). Also, lower-tropospheric thermal inversions are more frequent and stronger over the AS than BOB (Narayanan and Rao 1981; Sathiyamoorthy et al. 2013). Thus, the atmospheric and sea surface conditions ~~over the AS~~ and ~~the BOB during June and September (JJAS)~~in turn the occurrence of ~~various~~different kinds of precipitating systems ~~over these two seas is studied in Liu et al. (2007), Romatschke et al. (2010), Saikranthi et al. (2014), Houze et al. (~~are quite different over the BOB and the AS during the ISM period. For instance, long-term measurements of tropical rainfall measuring mission (TRMM) precipitation radar (PR) have shown that ~~2015). These studies showed that the occurrence of~~ shallow systems ~~is~~are more prevalent over the ~~Arabian Sea~~AS, while deeper systems ~~are abundant in~~occur frequently over the BOB (Liu et al. 2007; Romatschke et al. 2010;~~Bay of Bengal. Recently,~~ Saikranthi et al. ~~(~~2014, 2018; Houze et al. 2015).~~) showed that the observed differences in the occurrence of various kinds of precipitating systems is exist even in El Niño and La Niña periods also, but with variable magnitudes. Aforementioned~~

The aforementioned studies mainly ~~focussed~~focused on the ~~variation of surface rainfall,~~ morphology of vertical structure of precipitation, ~~occurrence of cloudiness with SST over the Indian Ocean. But~~but, none of them studied the variation of vertical structure of precipitation (in terms of occurrence and intensity) with SST~~. The strength of the convective~~

Formatted: Pattern: Clear (White)

Formatted: Pattern: Clear (White)

Formatted: Pattern: Clear (White)

Formatted: Pattern: Clear (White)

Formatted: Pattern: Clear (White)

Formatted: Pattern: Clear (White)

Formatted: Pattern: Clear (White)

~~forcing strongly depends on SST (Sabin et al. 2012)~~ and ~~changes~~the differences in ~~SST have the potential of altering~~the vertical structure over AS and BOB. On the other hand, information on the vertical structure of precipitation~~ (Oueslati and Bellon 2015).~~

~~The vertical structure of precipitation information~~ is essential for improving the accuracy of rainfall estimation (Fu and Liu 2001; Sunilkumar et al. 2015), understanding the dynamical and microphysical processes of hydrometeor growth/decay mechanisms (Houze 2004; Greets and Dejene 2005; Saikranthi et al. 2014; Rao et al. 2016) and ~~flash rates (Liu et al. 2012), and~~ for improving the latent heating retrievals (Tao et al. 2006). ~~Also, most of~~SST being the ~~earlier studies dealing with SST and cloud/precipitation population considered whole Indian ocean as a single entity. But in reality the BOB and the AS of Indian ocean possesses distinctly different features, like SST and its variability over seasonal and intraseasonal scales (Sengupta~~main driving force to trigger precipitating systems through air-sea interactions (Sabin et al. 2012; Nuijens et al. 2017), can alter the ~~2001; Roxy et al. 2013), the monsoonal wind speeds (Findlater 1969) and also the type of rain (Liu et al. 2007; Romatschke et al. 2010; Saikranthi et al. 2014; Rao et al. 2016). Knowing the importance of~~ vertical structure of precipitation ~~and SST modulation of background atmospheric conditions, in~~ (Oueslati and Bellon 2015). Therefore, the present study ~~we have studied~~aims to understand the variation of vertical structure of precipitation ~~with SST and their causative mechanisms over different regions of Indian ocean, in particular over~~(in terms of precipitation top height and intensity) with SST over the AS and BOB. Besides the SST, vertical structure can be modified by aerosols (or CCN, mostly at the cloud formation stage) and thermodynamics of the ambient atmosphere. For instance, recent studies have shown the ~~BOB and~~impact of surface PM_{10} aerosols in altering the ~~AS.~~ vertical structure of precipitation (Guo et al., 2018). All these parameters, therefore, are considered in the present study to explain the differences in the vertical structure.

Formatted: Font color: Custom Color(RGB(34,34,34))

Formatted: Font color: Custom Color(RGB(34,34,34))

Formatted: Font color: Custom Color(RGB(34,34,34))

~~The present paper is organized as follows. Section 2 describes the data and method of analysis. The variation of the vertical structure of precipitation with SST over BOB and AS is studied in section 3. Section 4 discusses the factors influencing the variation of vertical structure over BOB and AS. The results are summarized in Section 5.~~

2. Data

The present study utilizes 16 years (1998-2013) of ~~Tropical rainfall measuring mission (~~TRMM~~) precipitation radar (PR)~~-PR's 2A25 (version 7) dataset~~ during the southwest monsoon season (June to September). TRMM-PR dataset~~, comprising of vertical profiles of attenuation corrected reflectivity ~~with 17 dBZ as minimum detectable signal~~ (Iguchi et al. 2009~~). Comparing TRMM-PR data with Kwajalein S-band radar data Schumacher and Houze (2000) showed that TRMM-PR misses 15% of the echo area observed above 0°C levels due to the sensitivity threshold (17 dBZ). Through this study they concluded that TRMM-PR highly under samples weaker echoes from ice particles associated with stratiform rain aloft but manages to capture most of the near-surface precipitation accumulation.~~), during the ISM. The range resolution of TRMM-PR reflectivity profiles is 250 m with a horizontal footprint size of ~4.3 and 5 km before and after the boosting of its orbit from 350 km to 403 km, respectively. It scans ±17° from nadir with a beam width of 0.71° covering a swath of 215 km (245 km after the boost). The uniqueness of TRMM-PR data ~~uniqueness~~ is its ability in pigeonholing the precipitating systems into convective, stratiform and shallow rain. This classification is based on two methods namely the horizontal method (H - method) and the vertical method (V - method) ~~using the bright band identification and the reflectivity profile~~ (Awaka et al. 2009). The original TRMM-PR 2A25 vertical profiles of attenuation corrected reflectivity are gridded to a three dimensional Cartesian coordinate system with a spatial resolution of 0.05° × 0.05°. The detailed methodology of interpolating the TRMM-PR reflectivity data into the 3D Cartesian grid is discussed in Houze et al. (2007). This dataset is available at the University of Washington website (http://trmm.atmos.washington.edu/).

To understand the observed variations in the vertical structure of precipitation in the light of microphysics of clouds, Moderate Resolution Imaging Spectroradiometer (MODIS) AQUA satellite level 3 data (MYD08) are considered. In particular, the daily atmospheric products of aerosol optical depth (AOD) (Hubanks et al. 2008~~),~~) and cloud effective radius (CER) ~~ice, and CER~~ liquid (Platnick et al. 2017) during the period 2003 and 2013 have been used. MODIS AOD dataset is a collection of aerosol optical properties at 550 nm wavelength, as well as particle size information. Level 2 MODIS AOD is derived from radiances using either one of the three different algorithms, i.e., over ocean Remer et al. (2005) algorithm, over land the Dark-Target (Levy et al. 2007) algorithm and for brighter land surfaces the Deep-Blue (Hsu et al. 2004) algorithm. CER is nothing but the weighted mean of the size distribution of cloud drops i.e., the ratio of third moment to second moment of the drop size distribution. In the level 3 MODIS daily dataset, aerosol and cloud products of level 2 data pixels with valid retrievals within a calendar day are first aggregated and gridded to a daily average with a spatial resolution of 1° × 1°. For CER grid box values, CER values are weighted by the respective ice/liquid water cloud pixel counts for the spatiotemporal aggregation and averaging processes.

The background atmospheric structure (winds and total column water vapor) and SST information are taken from the European Centre for Medium Range Weather Forecasting (ECMWF) Interim Reanalysis (ERA) (Dee et al. 2011).~~).~~ ERA-Interim runs 4DVAR assimilation twice daily (00 and 12 UTC) to determine the most likely state of the atmosphere at a given time (analysis). The consistency across variables in space and ~~in~~ time (during 12-hour intervals) is thus ensured by the atmospheric model and its error characteristics as specified in the assimilation. ERA-Interim is produced at T255 spectral resolution (about

0.75°, ~ 83 km) with a temporal resolution of 6h for upper air fields and 3h for surface fields. ~~The performance of the data assimilation system and the strengths and limitations of ERA-Interim datasets are found in Dee et al. (2011).~~ The original 0.75° × 0.75° spatial resolution gridded dataset is rescaled to a resolution of 0.125° × 0.125°. The temporal resolution of the dataset used in the present study is 6h (00, 06, 12 and 18 UTC). The equivalent potential temperature (θ_e) is estimated from the ERA-Interim datasets using the following formula (Wallace and Hobbs 2006):

$$\theta_e = \theta exp\left(\frac{L_V w_s}{C_p T}\right) \qquad (1)$$

where θ is the potential temperature, L_v is the latent heat of vaporization, w_s is the saturation mixing ratio, C_p is the specific heat at constant pressure and T is the absolute temperature.

Formatted: Indent: First line: 0 cm

The variation of vertical structure of precipitation with SST are studied by considering the dataset between 63 °E ~~-~~ – 72 °E and 8 °N~~-~~ – 20 °N over the AS and 83 °E ~~-~~ – 92 °E and 8 °N ~~-~~ – 21 °N over the BOB. These regions of interest along with the ~~SWM~~ISM seasonal mean SST over the two seas are depicted in Fig. 1. These regions are selected in such a way that the costal influence on SST is eluded from the analysis. As ~~small amount of~~ the rainfall is ~~observed~~scanty over the western AS (west ~~to~~ of 63°E latitude) during ~~SWM~~the ISM (Saikranthi et al. 2018), this region is also not considered in the present analysis. The seasonal mean SST is higher over the BOB than in the AS by more than 1 °C during the ~~SWM~~ISM season ~~corroborating the findings of~~, in agreement with Shenoi et al. (2002). The nearest space and time matched SST data from ERA-Interim are assigned to the TRMM-PR and MODIS observations for further analysis.

3. Variation of vertical structure of precipitation with SST

The occurrence (in terms of %) of conditional precipitation echoes (Z ≥ 17 dBZ) at different altitudes as a function of SST over the AS and the BOB is shown in Fig. 2. The variation of precipitation ~~echoes~~ echo occurrence frequency with SST is quite different over both the seas. ~~It increases with increase in SST over~~ The top of the ~~AS, but remains nearly same over the BOB. Higher occurrence of~~ precipitation echoes extends to higher ~~heights~~altitudes with increasing SST over the AS, while such variation is not quite evident over the BOB. Precipitation echoes are confined to ≤ 8 km at lower SST (< 28~~°~~ °C) over the AS, but exhibits a gradual rise in height with increase in SST. ~~Confinement of~~ Large population density of precipitation echoes ~~to lower heights~~ at lower ~~SST~~altitudes is mainly due to the abundant occurrence of shallow ~~systems~~storms over the AS (Saikranthi et al. 2014; Rao et al. 2016). Interestingly, ~~high~~the occurrence of precipitation echoes is seen at higher ~~heights~~altitudes even at lower SSTs over the BOB, indicating the presence of deeper storms. Such systems exist at all SST's over the BOB.

To examine the variation of reflectivity profiles with SST, median profiles of reflectivity in each SST bin are computed over the AS and the BOB separately for deep and shallow systems and are depicted in Figs. ~~3a & 3d~~3 & 4, respectively. The space- and time-matched conditional reflectivity profiles are grouped into 1°C SST bins and then the median is estimated at each height, only if the number of conditional reflectivity pixels (Figs. 3c~~ &~~; 3f; 4c & 4f) is greater than 500. ~~It is clear from Figs. 3a & 3d that the~~ The median reflectivity profiles corresponding to the deep systems are distinctly different over the AS and the BOB~~,~~ (Figs. 3a & 3d), even at the same SST. Over the AS, reflectivity ~~profiles show only~~of deep systems at different SSTs shows small variations (≤ 1 dBZ) ~~with SST~~ above ~~(> 5 km)~~ the melting region~~,~~, (> 5 km), but ~~vary~~varies significantly (~ 4.5 dBZ) below the melting level (< 5 km). These variations in reflectivity profiles with SST are negligible (< 0.5 dBZ) over the BOB~~. Below~~ both above and below the melting ~~layer, the~~ region. The reflectivity increases from ~~24~~ ~ 26.5 dBZ to ~~~28~~ 31 dBZ~~.~~, with increase in SST from 26 °C to 30 °C over the AS, but it is almost the same (~~~28dBZ~~ 30dBZ) at all SST's over the BOB~~. The standard deviation of reflectivity also exhibits similar variation as that of median profiles with SST over the AS and the BOB. In general the~~ below the melting layer. The standard deviation of reflectivity, representing the variability in reflectivity within the SST bin, is ~~larger over the BOB than the AS~~similar at all SSTs over both the seas except for the 26 °C SST over AS. At this SST, the standard deviation is lesser by ~ 1 dBZ than that of other SSTs.

~~The median reflectivity profiles show a gradual increase with decreasing altitude from ~ 10 km to 6 km and an abrupt enhancement is seen just below 6 km over both the seas. The sudden enhancement at the freezing level~~The median reflectivity profiles of shallow storms depicted in Figs. 4a & 4d also show a gradual increase in reflectivity from 20 dBZ to ~ 22 dBZ as SST changes from 26 °C to 31 °C at the precipitation top altitude over the AS and don't show any variation with SST over the BOB. However at 1 km altitude, except at 26 °C SST over the AS, the reflectivity variation with SST is not substantial over both the seas. The standard deviation of reflectivity profiles show ~ 1 dBZ variation with SST (from 26 °C to 31°C) at all altitudes over the AS and don't show any variation over the BOB. The standard deviation of reflectivity for shallow storms varies from 3 to 4 dBZ at the precipitation top altitude and 4.5 to 5.3 dBZ at 1 km altitude over the AS while it shows ~ 4 dBZ at precipitation top and ~ 5.5 dBZ at 1 km altitude over the BOB.

4. Factors affecting the vertical structure of precipitation and their variability with SST

The formation and evolution of precipitating systems over oceans depend on dynamical, thermodynamical and microphysical factors, like SST, wind shear, vertical wind velocity, stability, CER, etc., and need to be considered for understanding the vertical structure of precipitation (Li and Min 2010; reamean et al. 2013; Chen et al. 2015; Shige and Kummerov 2016; Guo et al 2018).

4.1. Dynamical and thermodynamical factors:

To understand the role of stability/instability, θ_e values computed from (1) using the ERA-Interim datasets during the ISM period over the AS and the BOB are averaged for a season and are depicted in Figs. 5(a) & 5(b), respectively. The surface θ_e (at 1000 hPa) values are larger over the BOB than those over AS for the same SST, indicating that the instability and convective available potential energy (CAPE) could be higher over the BOB. Indeed, higher CAPE is seen over the BOB (Fig. S1, calculated following Emanuel 1994) than AS at all SSTs by a magnitude > 300 J kg^{-1}. The θ_e increases with SST from 358 °K to 368 °K from 27 °C to 31 °C and from 350 °K to 363 °K from 26 °C to 31 °C over the BOB and the AS, respectively. The CAPE also increases with rise in SST over both the seas. To know the stability of the atmosphere θ_e gradients are considered. Irrespective of SST, positive gradients in θ_e are observed between 900 and 800 hPa levels over the AS indicating the presence of strong stable layers. The strength of these stable layers decreases with increasing SST. These stable layers are formed mainly due to the flow of continental dry warm air from Arabian Desert and Africa above the maritime air causing temperature inversions below 750 hPa level over the AS during the ISM period (Narayanan and Rao 1981). However over the BOB, such temperature inversions are not seen in the lower troposphere.

To understand the effect of wind field on the vertical structure of precipitation, profiles of ISM seasonal mean vertical wind velocity and vertical shear in horizontal wind at various SSTs over the AS and the BOB are shown in Figs. 5(c), 5(d) & 5(e), 5(f) respectively. The updrafts are prevalent at all SSTs throughout the troposphere over the BOB, whereas downdrafts are seen in the mid-troposphere (between 200 and 600 hPa levels) up to 27 °C and updrafts in the entire troposphere at higher SSTs over the AS. Also, the magnitude of the vertical wind velocity varies significantly with SST in the mid-troposphere over the AS. Over the BOB, the magnitude of updrafts increases with altitude in the lower and middle troposphere, but doesn't vary much with SST. In the mid-troposphere, updrafts are stronger by > 0.02 Pa S^{-1} over the BOB than over the AS. The profiles shown in Fig. 5(e) & 5(f) are the mean vertical shear in horizontal wind estimated following Chen et al. (2015) at different levels with reference to 950 hPa level. The wind shear increases with increasing altitude at all the SSTs up to 400 hPa, but the rate of increase is distinctly different between the AS and the BOB at SSTs less than 28 °C and nearly the same at higher SSTs. The wind shear decreases systematically with SST (~ 1.5 m s^{-1} for 1° increase in SST) in the middle troposphere over the AS while the change is minimal over the BOB (~ 2 m s^{-1} for 27 °C and 31 °C).

Chen et al. (2015) highlighted the importance of mid-tropospheric wind shear in generating mesoscale local circulations, like low-level cyclonic and upper-level anticyclonic circulations. This feature is apparent over the AS, where down drafts are prevalent in mid-upper troposphere and updrafts in the lower troposphere at lower SSTs. As SST increases, the wind shear decreases and the updraft increases in the mid-troposphere. However, over the BOB the wind shear is relatively week when compared to the AS and hence the updrafts are seen up to 200 hPa level at all SSTs. The weaker CAPE and stable mid-troposphere coupled with upper- to mid- tropospheric downdrafts at lower SSTs over the AS inhibit the growth of precipitating systems to higher altitudes and in turn precipitate in the form of shallow rain. This result is in accordance with the findings of Shige and Kummerow (2016) that showed the static stability at lower levels inhibits the growth of clouds and promotes the detrainment of clouds over the Asian monsoon region and is considered as an important parameter in determining the precipitation top height. As SST increases large CAPE and updrafts in the middle troposphere collectively support the precipitating systems to grow to higher altitudes, as evidenced in Fig. 2a. On the other hand, large CAPE and updrafts in the middle troposphere prevalent over the BOB at all SSTs are conducive for the precipitating systems to grow to higher altitudes as seen in Fig. 2b.

4.2. Microphysical factors ~~is primarily due to the aggregation of hydrometeors and change in dielectric factor from ice to water (Fabry and Zawadzki 1995; Rao et al. 2008; Cao et al. 2013). Below the bright band, the raindrops can grow by collision-coalescence process and reduce their size either by breakup or by evaporation processes. The collision – coalescence results in negative slope in the reflectivity profile, whereas breakup and evaporation results in positive slope (Liu and Zipser 2013; Cao et al. 2013; Saikranthi et al. 2014). The observed negative slope in the median reflectivity profiles below the bright band region indicates the low-level hydrometeor growth over both the seas. This hydrometeor growth below melting region indicates the predominance of collision-coalescence process than the collision-breakup process over both the seas. The magnitude of the slope is nearly equal over both the seas, indicating that the rate of growth, on average, is nearly equal.~~

~~**4. Factors affecting the vertical variation of reflectivity with SST**~~

~~The formation and evolution of precipitating systems depends on the stability of the boundary layer, dynamics and thermodynamics of the ambient atmosphere. To know the stability of the marine boundary layer at various SSTs the lower tropospheric stability (LTS) is considered. LTS is defined as the difference in potential temperature between 700 hPa (θ_{700}) and surface (θ_0) i.e., $LTS = \theta_{700} - \theta_0$ that represents the strength of the inversion caps by the planetary boundary layer (Wood and Bretherton 2006). The LTS values were computed from the ERA-Interim temperature data during SWM season over the selected regions and are depicted in Fig. 4(a). LTS decreases with SST up to 29°C and increases a little at further SSTs over both the seas however when compared to the BOB the LTS values are larger over the AS at all SSTs. The stability of the planetary boundary layer is very high at lower SSTs and as SST increases the stability decreases drastically over the AS up to 29°C and increases a little at further SSTs. On the other hand the variability in planetary boundary layer stability with SST is trivial over the BOB. Also shown in Fig. 4(b) is the convective available potential energy~~

Formatted: Indent: First line: 0 cm

~~(CAPE) at different SSTs over both the Seas. CAPE is calculated following Emanuel (1994). CAPE increases with rise in SST over both the seas while its magnitude is relatively large over the BOB than the AS at all SSTs. The large LTS and small CAPE values at lower SSTs over the AS don't allow the precipitating systems to grow to higher altitudes and in turn precipitate in the form of warm rain. As SST increases LTS decreases drastically and CAPE increases and hence the precipitating systems can grow to higher altitudes. Though LTS increases above 29°C the instability created by the large CAPE can penetrate the planetary boundary layer and favours the formation of deeper systems. On the other hand LTS values are lower and remain almost same at all SSTs and large CAPE values over the BOB are conducive for the precipitating systems to grow to higher altitudes as depicted in Fig. 2.~~

Formatted: Font: Bold

The observed differences in reflectivity profiles of precipitation with SST could be originated at the cloud formation stage ~~or in the evolution stage or due to both. In order to understand this, the variation of mean CER for ice and liquid at different SST's over the AS and the BOB is depicted in Figs. 5a & 5b, respectively. The mean is calculated only when the number of data points is larger than 100 in each SST bin. It is evident from Figs. 5a & 5b that both CER ice and liquid increase with rise in SST substantially over the AS but the increase is marginal over the BOB. For example, as SST rises from 26°C to 31°C, the CER ice and liquid vary from 20 µm to 32 µm and 14.7 µm to 20.8 µm, respectively over the AS, whereas they vary, respectively, from 29 µm to 31 µm and 18.5 µm to 19.5 µm over the BOB. Also, the cloud droplets are small in size at lower SSTs and bigger at higher SSTs over the AS, whereas they are big over the BOB irrespective of SST. These smaller sized hydrometeors at low SSTs are responsible for the observed small reflectivities above the melting layer over the AS than the BOB as reflectivity is more sensitive to the particle size than the droplet concentration ($Z \propto D^6$). At higher SSTs, the CER values are approximately equal over both~~

~~the seas and in turn the observed reflectivities (Fig. 5). This suggests that the variations seen in vertical profiles of reflectivity are originating in the cloud itself.~~

~~Numerous studies have examined the aerosol effects on cloud formation through heterogeneous nucleation and precipitation~~itself or manifested during the evolution stage or due to both. Information on AOD and CER would be ideal to infer microphysical processes at the cloud formation stage. CER values are mainly controlled by the ambient aerosols concentration and the available moisture (Twomey 1977; Albrecht 1989; Tao et al. 2012; and Rosenfeld et al. 2014). For fixed liquid water content, as the concentration of aerosols increases, the number of cloud drops increases and ~~droplet size reduces~~ CER decreases (Twomey 1977). ~~Utilizing the aircraft measurements over Indian sub-continent Ramanathan et al. (2001) showed that the cloud drop number density increase with increasing aerosol number density both over continental and maritime regions. Connolly et al. (2009), Li and Min (2010), Niemand et al. (2012), Creamean et al. (2013), and Fan et al. (2014) showed that dust also act as ice nuclei through heterogeneous nucleation and these ice nuclei directly change the ice nucleation processes that determine the initial number concentration and size distribution of ice crystals. Thus, to~~ To understand the ~~role~~variation of ~~aerosols in~~AOD and TCWV and the ~~observed variations in the~~resultant CER with SST, the ~~seasonal~~ mean AOD ~~variation with~~and TCWV for different SST ~~is~~ bins are plotted in ~~Fig~~Figs. 6a ~~for the SWM.~~& 6b. The mean and standard error are calculated only when the number of data points is more than 100 in each SST bin. AOD decreases from 0.62 to 0.31 with rise in SST from 26 °C to 31 °C over the AS but only from 0.42 to 0.36 as SST varies from 27 °C to 30 °C and then increases ~~with rise in SST~~at higher SSTs over the BOB. ~~Also shown in Fig. 6b is the~~The variation of ~~total column water vapor (~~TCWV~~)~~ with SST ~~over both the seas. TCWV~~(Fig. 6b) shows a gradual increase with SST over the AS while it decreases initially from 27°C to 28°C, and then increases ~~with SST over the BOB. At a given SST the TCWV is more in the~~

~~BOB than in the AS. More number of aerosols and relatively low TCWV over the AS results in large number of cloud drops with reduced size (Twomey 1977; Ramanathan 2001). These reduced size cloud drops are responsible for the observed small CER values at SSTs less than 28°C. As SST rises the AOD decreases and TCWV increases such that the cloud particles grow in size which in turn increases CER. On the other hand, the change in AOD and TCWV (and as a result in CER) is not prominent with SST over the BOB, as seen in the Fig. 5.~~over the BOB. At a given SST the TCWV is more in the BOB (> 8 mm) than in the AS.

~~To understand the transport of aerosols at low and mid-levels the wind magnitudes and directions at 850 hPa and 500 hPa levels are shown in Fig. 7. The strong lower tropospheric winds produce sea salt particles as well as transport dust from the Horn of Africa and the mid tropospheric winds transport dust from the Arabian Desert over the AS (Li and Ramanathan 2002). On the other hand the continental aerosols from India landmass are transported to the BOB both at low and mid troposphere.~~ The decrease in AOD and an increase in TCWV with SST result in an increase in CER (14.7 µm to 20.8 µm from 26°C to 31°C) over the AS (Fig. 7). On the other hand, CER doesn't show much variation with SST (18.5 µm to 19.5 µm from 27°C to 31°C) over BOB due to smaller variations in AOD and TCWV. This also shows that the cloud droplets are smaller in size at lower SSTs over the AS than BOB, while they are bigger and nearly equal in size at higher SSTs. Since, reflectivity is more sensitive to the particle size ($Z \propto D^6$), the smaller-sized hydrometeors at lower SSTs over the AS yield weaker reflectivity than over the BOB (both for deep and shallow systems). As the SST increases, CER as well as the reflectivity increases over the AS. At higher SSTs, the CER values are approximately equal over both the seas and in turn the observed reflectivities (Figs. 3a & 4a). This suggests that the variations seen in the reflectivity are originated in the cloud formation stage itself.

The hydrometeors also evolve during their descent to the ground due to several microphysical processes. These processes can be inferred from the vertical structure of precipitation or vertical profiles of reflectivity. The median reflectivity profiles of deep systems show a gradual increase from ~ 10 km to 6 km and an abrupt enhancement is seen just below 6 km over both the seas (Figs. 3a & 3d). The sudden enhancement at the freezing level (radar bright band)~~Satheesh et al. (2006) showed an increase in AOD with increase in latitude over the AS due to the dust advection from Arabia desert regions during SWM season, whereas SST decreases with increase in the latitude.~~ is primarily due to the aggregation of hydrometeors and change in dielectric factor from ice to water (Fabry and Zawadzki 1995; Rao et al. 2008; Cao et al. 2013). Below the bright band, raindrops grow by collision-coalescence process and reduce their size by either breakup and/or evaporation processes. The collision-coalescence results in negative slope in the reflectivity profile, whereas breakup and evaporation results in positive slope (Liu and Zipser 2013; Cao et al. 2013; Saikranthi et al. 2014; Rao et al. 2016). The observed negative slope (~ - 0.3 dBZ km^{-1}) in the median reflectivity profiles below the bright band indicates dominance of low-level hydrometeor growth over both the seas. The magnitude of the slope decreases with SST over the AS, while it is nearly equal at all SSTs over the BOB. It indicates the growth rate decreases with SST over the AS and remains the same at all SSTs over the BOB. The median reflectivity profiles of shallow systems also show negative slopes (~ -1 dBZ km^{-1}) at all SSTs representing the predominance of low-level hydrometeor growth by collision-coalescence processes over both the seas.

The present analysis shows that the observed reflectivity changes with SST over both the seas originate at the cloud formation stage and magnify further during the descent of hydrometeors to ground.~~In other words the SST is low and AOD is high in northern AS whereas over the southern AS, SST is high and AOD is low. This contrasting spatial~~

~~distribution of AOD and SST could cause a negative correlation between AOD and SST. To examine whether the observed decrease in AOD with increase in SST over the AS is due to the latitudinal variation of AOD or exists at all latitudes, we have segregated the data into 2° latitude bins and plotted the mean AOD with SST for all bins and is depicted in Fig. 8a. In spite of the magnitude, AOD variation with SST is nearly similar at all latitudes of the AS, i.e., the higher AOD is observed at lower SSTs and vice versa. On the other hand the latitudinal variation of AOD with SST over the BOB shown in Fig. 8b also show a decrease in AOD with SST up to 30°C but the magnitude of variation is trivial relative to the AS. As also depicted in Fig. 6a above 30°C AOD increases with SST over the BOB. This indicates that though there is a difference in magnitude of variation, AOD varies with SST over both the seas at all latitudes. This analysis is repeated using the multi-angle imaging spectroradiometer (MISR) dataset (which is not shown here) for small, medium large aerosol particles. Interestingly all three types also show a decrease in AOD with rise in SST over both the seas.~~

5. Conclusions

Sixteen years of TRMM-PR 2A25 reflectivity profiles and 11 years of MODIS AOD and CER data are utilized to understand the differences in variation of vertical structure of precipitation with SST over AS and BOB. ~~This analysis reveals that the variation of reflectivity with SST is~~Precipitation top height increases with SST over the AS indicating that systems grow to higher altitudes with increase in SST while it is almost same at all SSTs representing that the systems are deeper over the BOB. The decrease in stability and mid-tropospheric wind shear with SST over the AS favour the formation of deeper system at higher systems. However the low stability and small wind shear at all SSTs over the BOB help the formation of deeper systems. The variation of reflectivity with SST is found to be remarkable over the AS and marginal over the BOB. The reflectivity increases with rise in

Formatted: No widow/orphan control, Don't adjust space between Latin and Asian text, Don't adjust space between Asian text and numbers

SST over the AS and remains the same at all SSTs over the BOB. This change in reflectivity over the AS is more prominent below the freezing level height (~ 4 dBZ) than the above (~ 1 dBZ). Over the AS, the abundance of aerosols and less moisture at SSTs < 27°C result in high concentration of ~~small diameter~~smaller cloud droplets. As SST increases the aerosol concentration decreases and moisture increases ~~such that~~leading to the formation of bigger cloud droplets~~ are formed~~. Thus, the reflectivity increases with rise in SST over the AS. On the other hand, AOD, TCWV and CER do not show substantial variation with SST over the BOB and hence the change in reflectivity is small. Over the BOB, the mid troposphere is wet and hydrometeor's size at the formation stage is nearly the same at all SSTs. The evolution of hydrometeors during their descent is also similar at all SST's~~, as evidenced by nearly similar~~. The collision-coalescence process is predominant below the bright band region over both the seas and is responsible for the observed negative slope in the reflectivity profiles.

Acknowledgements

The authors would like to thank Prof. Robert Houze and his team for the interpolated 3D gridded TRMM-PR dataset (http://trmm.atmos.washington.edu), ECMWF (http://data-portal.ecmwf.int/) team for providing the ERA-Interim dataset and MODIS (https://ladsweb.modaps.eosdis.nasa.gov/) science team for providing the AOD and CER dataset. The authors express their gratitude to Prof. J. Srinivasan for his fruitful discussions and valuable suggestions in improving the quality of the manuscript. The corresponding author would like to thank Department of Science & Technology (DST), India for providing the financial support through the reference number DST/INSPIRE/04/2017/001185. We thank the two referees for their critical comments in improving the quality of the manuscript.

References

Albrecht, B.A.: Aerosols, cloud microphysics, and fractional cloudiness, *Science*, 245, 1227–1230, 1989.

Awaka, J., Iguchi, T., and Okamoto, K.: TRMM PR standard algorithm 2A23 and its performance on bright band detection, *J. Meteorol. Soc. Jpn*., 87A, 31–52, 2009.

Bhat, G. S., Gadgil, S., Kumar, P. V. H., Kalsi, S. R., Madhusoodanan, P., Murty, V. S., Rao, C. V. P., Babu, V. R., Rao, L.V., Rao, R. R., Ravichandran, M., Reddy, K.G., Rao, P. S., Sengupta, D., Sikka, D. R., Swain, J., and Vinayachandran, P. N.: BOBMEX: The Bay of Bengal Monsoon Experiment, *Bull. Amer. Meteor. Soc.*,~~Barnes, H. C., and Houze, Jr. R. A.: The precipitating cloud population of the Madden-Julian oscillation over the Indian and West Pacific Oceans. *J.*~~ 82, 2217–2244, 2001.

~~Geophys. Res., 118, 6996-7023, doi:10.1002/jgrd.50375, 2013.~~

Cao, Q., Hong, Y., Gourley, J. J., Qi, Y., Zhang, J., Wen, Y., and Kirstetter, P. E.: Statistical and physical analysis of the vertical structure of precipitation in the mountainous west region of the United States using 11+ years of space borne observations from TRMM precipitation radar, *J. Appl. Meteorol. Climatol.*, 52, 408-424, 2013.

Chaudhari, H. S., Pokhrel, S., ~~Mohanty, S., and Saha, S. K.: Seasonal prediction of Indian summer monsoon in NCEP coupled and uncoupled model, *Theor. Appl. Climatol.*, 114, 459–477, doi:10.1007/s00704-013-0854-8, 2013.~~

~~Chaudhari, H. S., Pokhrel, S.,~~ Kulkani, A., Hazra, A., and Saha, S. K.: Clouds-SST relationship and interannual variability modes of Indian summer monsoon in the context of clouds and SSTs: observational and modelling aspects, *Int. J. Climatol.*, doi: 10.1002/ joc.4664, 2016.

Chaudhari, H. S., Pokhrel, S., ~~Connolly, P. J., Möhler, O., Field, P. R., Saathoff, H., Burgess, R., Choularton, T., and Gallagher, M.: Studies of heterogeneous freezing by three different desert dust samples. Atmos. Chem. Phys., 9, 2805–2824, doi:10.5194/acp-9-2805-2009, 2009.~~

Formatted: Font: Times New Roman, 12 pt

Formatted: art_authors, Font: +Body (Calibri), 11 pt

Formatted: art_authors, Font: +Body (Calibri), 11 pt

Formatted: Pattern: Clear

Formatted: Default Paragraph Font, Font: +Body (Calibri), 11 pt, Not Italic

Formatted: art_authors, Font: +Body (Calibri), 11 pt

Formatted: Default Paragraph Font, Font: +Body (Calibri), 11 pt, Not Italic

Mohanty, S., and Saha, S. K.: Seasonal prediction of Indian summer monsoon in NCEP coupled and uncoupled model, *Theor. Appl. Climatol.*, 114, 459–477, doi:10.1007/s00704-013-0854-8, 2013.

Chen, Q., Fan, J., Hagos, S., Gustafson Jr., W. I., and Berg, L. K.: Roles of wind shear at different vertical levels: Cloud system organization and properties, J. Geophys. Res. Atmos., 120, 6551–6574, 2015.

Creamean, J. M., Suski, K. J., Rosenfeld, D., Cazorla, A., DeMott, P. J., Sullivan, R. C., White, A. B., Ralph, F. M., Minnis, P., Comstock, J. M., Tomlinson, J. M., Kimberly A., and Prather, K. A.: Dust and biological aerosols from the Sahara and Asia influence precipitation in the western U.S., *Science*, 339, 1572–1578, doi:10.1126/science.1227279, 2013.

Dee, D. P., et al.: The ERA-Interim reanalysis: Configuration and performance of the data assimilation system, *Q. J. R. Meteorol. Soc.*, 137, 553–597, 2011.

Emanuel, K. A.: Atmospheric convection. Oxford University Press, Oxford, 1994.

Fabry, F., and Zawadzki, I.: Long-term radar observations of the melting layer of precipitation and their interpretation, *J. Atmos. Sci.*, 52, 838–851, 1995.

~~Fan, J., Leung, L. R., DeMott, P. J., Comstock, J. M., Singh, B., Rosenfeld, D., Tomlinson, J. M., White, A., Prather, K. A., Minnis, P., Ayers, J. K., and Min, Q.: Aerosol impacts on California winter clouds and precipitation during CalWater 2011: local pollution versus long-range transported dust, *Atmos. Chem. Phys.*, 14, 81-101, https://doi.org/10.5194/acp-14-81-2014, 2014.~~

Feng, X., Haines, K., Liu, C., de Boisséson, E., and Polo, I., Improved SST-precipitation intraseasonal relationships in the ECMWF coupled climate reanalysis, *Geophys. Res. Lett.*, 45, 3664–3672, 2018.

Formatted: Default Paragraph Font, Font: +Body (Calibri), 11 pt, Not Italic

Formatted: art_authors, Font: +Body (Calibri), 11 pt

Formatted: Default Paragraph Font, Font: +Body (Calibri), 11 pt

Findlater, J.: A major low-level air current near the Indian Ocean during the northern summer, *Q. J. R. Meteorol. Soc.*, 95, 362–380, 1969.

Fu, Y., and Liu, G.: The variability of tropical precipitation profiles and its impact on microwave brightness temperatures as inferred from TRMM data, *J. Appl. Meteorol.*, 40, 2130–2143, 2001.

Gadgil, S., Joseph, P. V., and Joshi, N. V.: Ocean atmosphere coupling over monsoonal regions, *Nature*, 312, 141-143, 1984.

Gadgil, S.: Monsoon–ocean coupling. *Current Sci.*, 78, 309–323, 2000.

Geerts, B., and Dejene, T.: Regional and diurnal variability of the vertical structure of precipitation systems in Africa based on space borne radar data, *J. Clim.*, 18, 893–916, 2005.

Guo, J., Liu, H., Li, Z., Rosenfeld, D., Jiang, M., Xu, W., Jiang, J. H., He, J., Chen, D., Min, M., and Zhai, P.: Aerosol-induced changes in the vertical structure of precipitation: a perspective of TRMM precipitation radar, *Atmos.* Chem. Phys., ~~Houze, R. A~~18, 13329-13343, https://doi.org/10.5194/acp-18-13329-2018, 2018.

~~.: Mesoscale convective systems, *Rev. Geophys.*, 42, RG4003, doi: 10.1029/2004RG000150, 2004.~~

Houze, R. A., and Churchill, D. D.: Mesoscale organization and cloud microphysics in a Bay of Bengal depression, *J. Atmos. Sci.*, 44, 1845–1867, 1987.

Houze, R. A., ~~Wilton, D. C., and Smull, B. F.: Monsoon convection in the Himalayan region as seen by the TRMM precipitation radar, *Q. J. R. Meteorol. Soc.*, **133**, 1389-1411, 2007.~~

~~Houze, R. A.,~~ Rasmussen, K. L., Zuluaga, M. D., and Brodzik, S. R.: The variable nature of convection in the tropics and subtropics: A legacy of 16 years of the Tropical rainfall measuring mission satellite, *Rev. Geophys.*, 53, 994–1021, 2015.

Formatted: Font: Not Bold

Formatted: Default Paragraph Font, Font: +Body (Calibri), 11 pt

Formatted: Default Paragraph Font, Font: +Body (Calibri), 11 pt

Formatted: Default Paragraph Font, Font: +Body (Calibri), 11 pt, Not Italic

Formatted: Default Paragraph Font, Font: +Body (Calibri), 11 pt

Formatted: Font: Not Bold

Houze, R. A., Wilton, D. C., and Smull, B. F.: Monsoon convection in the Himalayan region as seen by the TRMM precipitation radar, *Q. J. R. Meteorol. Soc.*, **133**, 1389-1411, 2007.

Houze, R. A.: Mesoscale convective systems, *Rev. Geophys.*, 42, RG4003, doi: 10.1029/2004RG000150, 2004.

Hsu, N., Tsay, S., King, M., and Herman, J.: Aerosol properties over bright-reflecting source regions, *Geosci. Remote Sens. IEEE Trans.*, 42, 557–569, 2004.

Hubanks, P., King, M., Platnick, S., and Pincus, R.: MODIS atmosphere L3 gridded product algorithm theoretical basis document collection 005 Version 1.1, Tech. Rep. ATBD-MOD-30, NASA, 2008.

Iguchi, T., Kozu, T., Kwiatkowski, J., Meneghini, R., Awaka, J., and Okamoto, K.: Uncertainties in the rain profiling algorithm for the TRMM precipitation radar, *J. Meteor. Soc. Japan*, 87A, 1–30, doi:10.2151/jmsj.87A.1, 2009.

Krishnamurti, T. N.: Summer monsoon experiment – A review. *Mon. Wea. Rev.*, 113, 1590-1626, 1985.

Krishnamurti, T.: Cooling of the Arabian Sea and the onset-vortex during 1979. Recent progress in equatorial oceanography: A report of the final meeting of SCOR WORKING GROUP 47 in Venice, Italy, 1-12, 1981. [Available from Nova Univ., Ocean Science Center, Dania, FL 33004].

Levy, R., Remer, L., Mattoo, S., Vermote, E., and Kaufman, Y.: Second-generation operational algorithm: Retrieval of aerosol properties over land from inversion of moderate resolution imaging spectroradiometer spectral reflectance, *J. Geophys. Res.*, 112, D13, doi:10.1029/2006JD007811, 2007.

Formatted: Strong, Font: +Body (Calibri), 11 pt

Formatted: Default Paragraph Font, Font: +Body (Calibri), 11 pt

Formatted: Font: Not Bold

Li, ~~F., and Ramanathan, V.: Winter to summer monsoon variation of aerosol optical depth over the tropical Indian Ocean, *J. Geophys. Res.*, 107(D16), doi: 10.1029/2001JD000949, 2002.~~

~~Li,~~ R., and Min, Q.-L.: Impacts of mineral dust on the vertical structure of precipitation. J. Geophys. Res., 115, D09203, doi:10.1029/2009JD011925, 2010.

Liu, C., Zipser, E., and Nesbitt, S. W.: Global distribution of tropical deep convection: Different perspectives using infrared and radar as the primary data source, *J. Climate*, 20, 489-503, 2007.

Liu. C., and Zipser, E. J.: Why does radar reflectivity tend to increase downward toward the ocean surface, but decrease downward toward the land surface?, *J. Geophys. Res. Atmos.*, 118, 135-148, doi: 10.1029/2012JD018134, 2013.

~~Liu, C., Zipser, E., and Nesbitt, S. W.: Global distribution of tropical deep convection: Different perspectives using infrared and radar as the primary data source, *J. Climate*, 20, 489-503, 2007.~~

~~Liu, C., Cecil, D., and Zipser, E. J.: Relationships between lightning flash rates and radar reflectivity vertical structures in thunderstorms over the tropics and subtropics. *J. Geophys. Res.*, doi:10.1029/2011JD017123, 2012.~~

Meenu, S., Parameswaran, K., and Rajeev, K.: Role of sea surface temperature and wind convergence in regulating convection over the tropical Indian Ocean, *J. Geophys. Res. Atmos.*, 117, D14102, 2012.

Nair, A. K. M., and Rajeev, K.: Multiyear CloudSat and CALIPSO observations of the dependence of cloud vertical distribution on sea surface temperature and tropospheric dynamics, *J. Clim.*, 27, 672–683, doi:10.1175/JCLI-D-13-00062.1, 2014.

Formatted: Emphasis, Font: +Body (Calibri), 11 pt, Not Italic

~~Nair, A.K.M., Rao, T. N., and Rajeev, K.: Role of cloud feedback in regulating the "pool of inhibited cloudiness" over the Bay of Bengal, *Meteorol. Atmos. Phys.*, https://doi.org/10.1007/s00703-017-0560-7, 2017.~~

~~Niemand, M., Möhler, O., Vogel, B., Vogel,~~ Narayanan, M. S., and Rao, B. M.: Detection of monsoon inversion by TIROS-N satellite, *Nature*, 294, 546-548, 1981.

Nuijens, L., Emanuel, K., Masunaga, H., and L'Ecuyer, T.: Implications of warm rain in shallow cumulus and congestus clouds for large-scale circulations, *Surv. Geophys.*, 38, 1257-1282, 2017.

~~H., Hoose, C., Connolly, P., Klein, H., Bingemer, H., DeMott, P., Skrotzki, J., and Leisner, T.: A particle-surface-area-based parameterization of immersion freezing on desert dust particles, *J. Atmos. Sci.*, 69, 3077-3092, https://doi.org/10.1175/JAS-D-11-0249.1, 2012.~~

Oueslati, B., and Bellon, G.: The double ITCZ bias in CMIP5 models: interaction between SST, large-scale circulation and precipitation. ~~*Climate*~~*Clim. Dyn.*, 44, 585-607, 2015.

Platnick, S., et al.: The MODIS cloud optical and microphysical products: Collection 6 updates and examples from Terra and Aqua, *IEEE Trans. Geosci. Remote Sens.*, 55, 502–525, doi:10.1109/TGRS.2016.2610522, 2017.

Rajeevan, M., Unnikrishnan, C. K., and Preethi, B.: Evaluation of the ENSEMBLES multi-model seasonal forecasts of Indian summer monsoon variability, *Clim. Dyn.*, 38, 2257–2274, 2012.

Rajendran, K., Nanjundiah, R. S., Gadgil, S., and Srinivasan, J.: How good are the simulations of tropical SST–rainfall relationship by IPCC AR4 atmospheric and coupled models?, *J. Earth Sys. Sci.*, 121(3), 595–610, 2012.

~~Ramanathan, V., Crutzen, P. J., Kiehl, J. T., Rosenfeld, D.: Aerosols, climate, and the hydrological cycle, *Science*, 294, 2119-2124, 2011.~~

Formatted: Default Paragraph Font, Font: +Body (Calibri), 11 pt

Formatted: Font: Not Bold

Rao, T. N., Kirankumar, N. V. P., Radhakrishna, B., Rao, D. N., and Nakamura, K.: Classification of tropical precipitating systems using wind profiler spectral moments. Part I: Algorithm description and validation, *J. Atmos. Oceanic Technol.*, 25, 884–897, 2008.

Rao, T. N., Saikranthi, K., Radhakrisna, B., and Rao, S. V. B.: Differences in the climataological characteristics of precipitation between active and break spells of the Indian summer monsoon, *J. Clim.*, 29, 7797-7814, 2016.

Remer, L., Kaufman, Y., Tanr´e, D., Mattoo, S., Chu, D., Martins, J., Li, R., Ichoku, C., Levy, R., Kleidman, R., Eck, T., Vermote, E., and Holben, B.: The MODIS aerosol algorithm, products, and validation, *J. Atmos. Sci*., 62, 947–973, 2005.

Romatschke, U., Medina, S., and Houze, R. A.: Regional, seasonal, and diurnal variations of extreme convection in the South Asian region, *J. Clim.*, 23, 419 –439, 2010.

Rosenfeld, D., et al.: Global observations of aerosol-cloud-precipitation-climate interactions, *Rev. Geophys.*, 52, 750-808, doi:10.1002/2013RG000441, 2014.

Roxy, M~~.: Sensitivity of precipitation to sea surface temperature over the tropical summer monsoon region—and its quantification, *Clim. Dyn.*, 43, 1159-1169, 2014.~~

~~Roxy, M~~., Tanimoto, Y., Preethi, B., Terray, P., and Krishnan, R.: Intraseasonal SST-precipitation relationship and its spatial variability over the tropical summer monsoon region, *Clim. Dyn.*, 41, 45-61, 2013.

Roxy, M.: Sensitivity of precipitation to sea surface temperature over the tropical summer monsoon region—and its quantification, *Clim. Dyn.*, 43, 1159-1169, 2014.

Sabin, T., Babu, C., and Joseph, P.: SST–convection relation over tropical oceans, *Int. J. Climatol.* 33, 1424–1435, 2012.

Saikranthi, K., Radhakrishna, B., Satheesh, S. K., and Rao, T. N.: Spatial variation of different rain systems during El Niño and La Niña periods over India and adjoining ocean, *Clim. Dyn.*, 50, 3671-3685, doi: 10.1007/s00382-017-3833-4, 2018.

Saikranthi, K., Rao, T. N., Radhakrishna, B., and Rao, S. V. B. : Morphology of the vertical structure of precipitation over India and adjoining oceans based on long-term measurements of TRMMPR, *J. Geophys. Res. Atmos.*, 119, 8433–8449, doi: 10.1002/2014JD021774, 2014.

Sathiyamoorthy, V., Mahesh, C., Gopalan, K., Prakash, S., Shukla, B. P., Mathur, A.: Characteristics of low clouds over the Arabian Sea, *J. Geophys. Res*~~Saikranthi, K., ~~. *Atmos.*, 118, 13489-13503, 2013.

~~Radhakrishna, B., Satheesh, S. K., and Rao, T. N.: Spatial variation of different rain systems during El Niño and La Niña periods over India and adjoining ocean, *Clim. Dyn.*, 50, 3671-3685, doi: 10.1007/s00382-017-3833-4, 2018.~~

~~Satheesh, S. K., Moorthy, K. K., Kaufman, Y. J., and Takemura, T.: Aerosol Optical depth, Physical properties and Radiative forcing over the Arabian Sea, *Meteorol. Atmos. Phys.*, 91, 45–62, doi:10.1007/s00703-004-0097-4, 2006.~~

~~Schumacher, C. and Houze, R. A.: Comparison of radar data from the TRMM satellite and Kwajalein oceanic validation site. *J. Appl. Meteor.*, 39, 2151–2164, 2000.~~

Schumacher, C. and Houze, R. A.: Stratiform rain in the tropics as seen by the TRMM precipitation radar, *J. Climate.*, 16, 1739–1756, 2003.

Sengupta, D., Goswami, B. N., and Senan, R.: Coherent intraseasonal oscillations of ocean and atmosphere during the Asian summer monsoon, *Geophys. Res. Lett.*, 28, 4127–4130, 2001.

Formatted: Expanded by 0.2 pt, Pattern: Clear (Custom Color(RGB(252,252,252)))

Formatted: Emphasis, Font: +Body (Calibri), 11 pt, Not Italic

Formatted: Strong, Font: +Body (Calibri), 11 pt

Formatted: Default Paragraph Font, Font: +Body (Calibri), 11 pt

Shenoi, S. S. C., Shankar, D., and Shetye, S. R.: Differences in heat budgets of the near-surface Arabian Sea and Bay of Bengal: Implications for the summer monsoon, *J. Geophys. Res.*, 107(C6), 3052, doi:10.1029/2000JC000679, 2002.

Shige, S. and Kummerow, C.D.: Precipitation-Top Heights of Heavy Orographic Rainfall in the Asian Monsoon Region, *J. Atmos. Sci.*, 73, 3009–3024, 2016.

Sunilkumar, K., Rao, T. N., Saikranthi, K., and Rao, M. P.: comprehensive evaluation of multisatellite precipitation estimates over India using gridded rainfall data, *J. Geophys. Res. Atmos.*, 120, doi:10.1002/2015JD023437, 2015.

Takayabu, Y. N., Shige, S., Tao, W., and Hirota, N.: Shallow and deep latent heating modes over tropical Oceans observed with TRMM PR spectral latent heating Data, *J. Climate*, 23, 2030–2046, 2010.

~~Tao, W.-K., et al.: Retrieval of latent heating from TRMM measurements, *Bull. Am. Meteorol. Soc.*, 87, 1555–1572, 2006.~~

Tao, W.-K., Chen, J.-P., Li, Z., Wang, C., and Zhang, C.: Impact of aerosols on convective clouds and precipitation, *Rev. Geophys.*, 50, RG2001, doi:10.1029/2011RG000369, 2012.

Tao, W.-K., et al.: Retrieval of latent heating from TRMM measurements, *Bull. Am. Meteorol. Soc.*, 87, 1555–1572, 2006.

Twomey, S.: The influence of pollution on the short wave albedo of clouds, *J. Atmos. Sci.*, 34, 1149–1152, 1977.

Wallace, J. M., and Hobbs, P. V.: Atmospheric science: An introductory survey, Second edition, Academic press, pp. 85, 2006.

Wang, B., Ding, Q., Fu, X., Kang, I.-S., Jin, K., Shukla, J., and Doblas-Reyes, F.: Fundamental challenge in simulation and prediction of summer monsoon rainfall, *Geophys. Res. Lett.*, 32, L15711, doi:10.1029/2005GL022734, 2005.

~~Wood, R., and Bretherton, C. S.: On the relationship between stratiform low cloud cover and lower-tropospheric stability, *J. Clim.*, 19, 6425-6432, 2006.~~

Weller, R. A., Farrar, J. T., Buckley, J., Mathew, S., Venkatesan, R., Lekha, J. S., Chaudhuri, D., Kumar, N. S., and Kumar, B. P.: Air-sea interaction in the Bay of Bengal, *Oceanography*, 29(2), 28–37, 2016.

Woolnough, S.J., Slingo, J.M., and Hoskins, B.J.: The relationship between convection and sea surface temperature on intraseasonal timescales, *J. Climate*, 13, 2086–2104, 2000.

Wu, R., and Kirtman, B. P.: Roles of Indian and Pacific Ocean air–sea coupling in tropical atmospheric variability, *Clim. Dyn.*, *25*(2–3), 155–170, 2005.

~~Yoneyama, K., Zhang, C., and Long, C. N.: Tracking pulses of the Madden–Julian oscillation, *Bull. Amer. Meteor. Soc.*, 94, 1871–1891, https://doi.org/10.1175/BAMS-D-12-00157.1, 2013.~~

Formatted: Widow/Orphan control, Adjust space between Latin and Asian text, Adjust space between Asian text and numbers

Formatted: Pattern: Clear

Formatted: Indent: Left: 0 cm, First line: 0 cm

Figure captions

Figure 1: Spatial distribution of ~~SWM~~ISM mean SST (in °C) obtained from ERA-Interim reanalysis data over the AS (63°E-72°E & 8°N-20°N) and the BOB~~.~~ (83°E-92°E & 8°N-21°N). The regions considered in this analysis over these two seas are shown with the boxes.

Figure 2: (a) and (b) represent the altitudinal distribution of occurrence of conditional reflectivity (≥ 17 dBZ) as a function of SST with respect to precipitation occurrence at that particular SST interval over the AS and the BOB, respectively.

Figure 3: (a), (d) and (b), (e) represent vertical profiles of median reflectivity correspond to deep systems and their standard deviation (in dBZ) with SST over the AS ~~(63°E-72°E & 8°N-20°N)~~ and the BOB~~ (83°E-92°E & 8°N-21°N),~~, respectively during the ~~SWM~~ISM season. (c) and (f) show the number of conditional reflectivity pixels at each altitude used for the estimation of the median and standard deviation.

~~**Figure 4:** The variation of mean LTS with SST over the AS (63°E-72°E & 8°N-20°N) and the BOB (83°E-92°E & 8°N-21°N) during the SWM season.~~

Figure 4: Same as Fig. 3 but for shallow precipitating systems.

Figure 5: (a) and (b), respectively, represent the ~~variation~~vertical profiles of mean ~~CER ice~~θ_e (in ~~μm~~K) with SST over the AS and the BOB during the ISM season. (c) and ~~mean CER liquid (in μm) with SST over the AS (63°E-72°E & 8°N-20°N~~(d) and ~~the BOB (83°E-92°E & 8°N-21°N) during the SWM season.~~(e) and (f) are same as (a) and (b) but for mean vertical velocity (in Pa s^{-1}) and wind gradient with reference to 950 hPa level (in m s^{-1}).

Figure 6: (a) ~~The variation~~Mean and standard error of ~~mean~~ AOD and (b) TCWV (in mm) with SST over the AS ~~(63°E-72°E & 8°N-20°N)~~ and the BOB during ISM.

Formatted: Font: Not Bold

Figure 7: Variation of mean and standard error of CER liquid (in μm) with SST over the AS and the BOB ~~(83°E-92°E & 8°N-21°N)~~ during ~~SWM.~~ the ISM season.

~~**Figure 7:** Winds during the SWM season at 850 hPa and 500 hPa levels. The shading colors represent the magnitude of the wind and arrow indicates the direction of the wind.~~

~~**Figure 8:** Latitudinal variation (for every 2° latitude interval) of mean aerosol optical depth over Arabian Sea averaged over 63-72°E.~~

Formatted: Left, Indent: Left: 0 cm, First line: 0 cm, Space After: 8 pt, Line spacing: Multiple 1.08 li

Figures

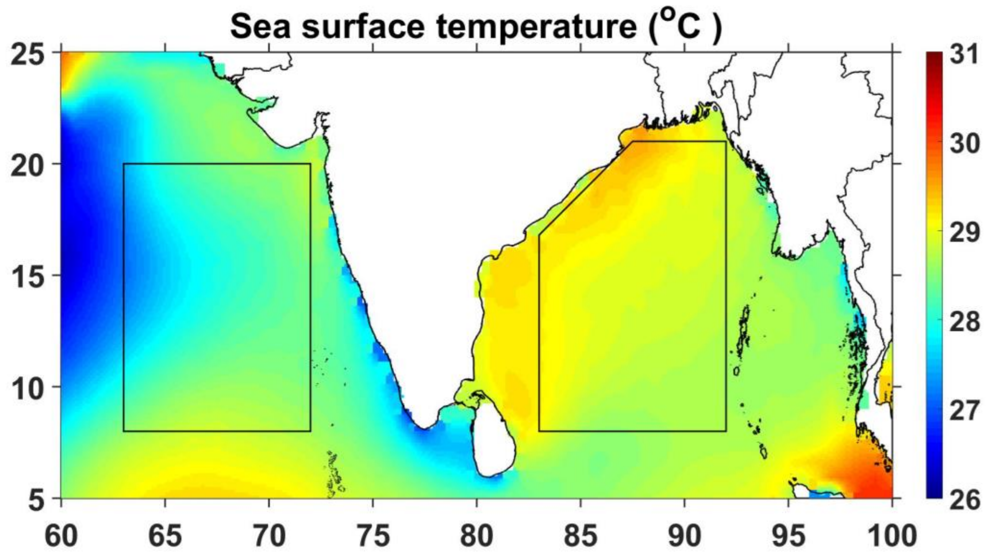

Formatted: Font: (Default) Times New Roman, 12 pt

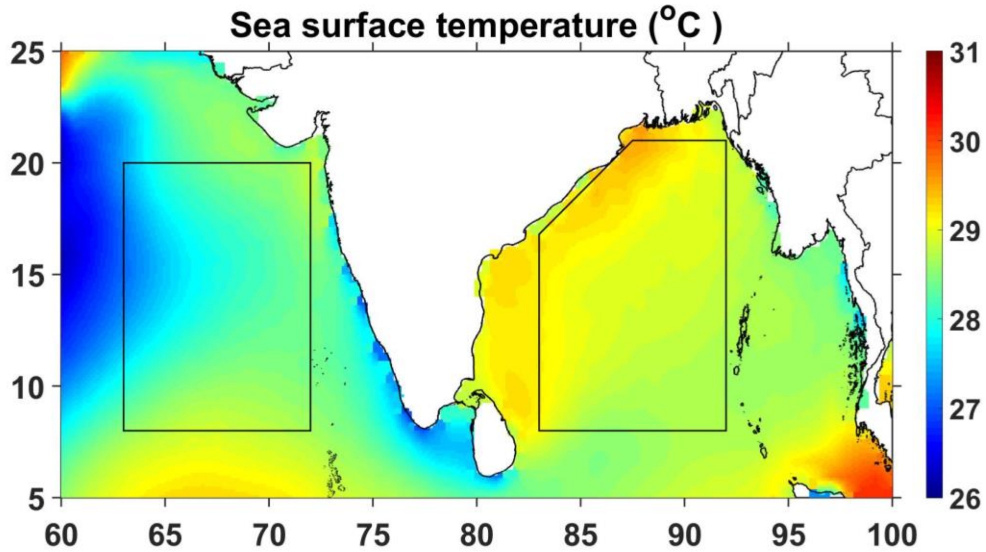

Figure 1: Spatial distribution of ~~SWM~~ISM mean SST (in °C) obtained from ERA-Interim reanalysis data over the AS (63°E-72°E & 8°N-20°N) and the BOB~~.~~ (83°E-92°E & 8°N-21°N). The regions considered in this analysis over these two seas are shown with the boxes.

Formatted: Font: (Default) Times New Roman, 12 pt

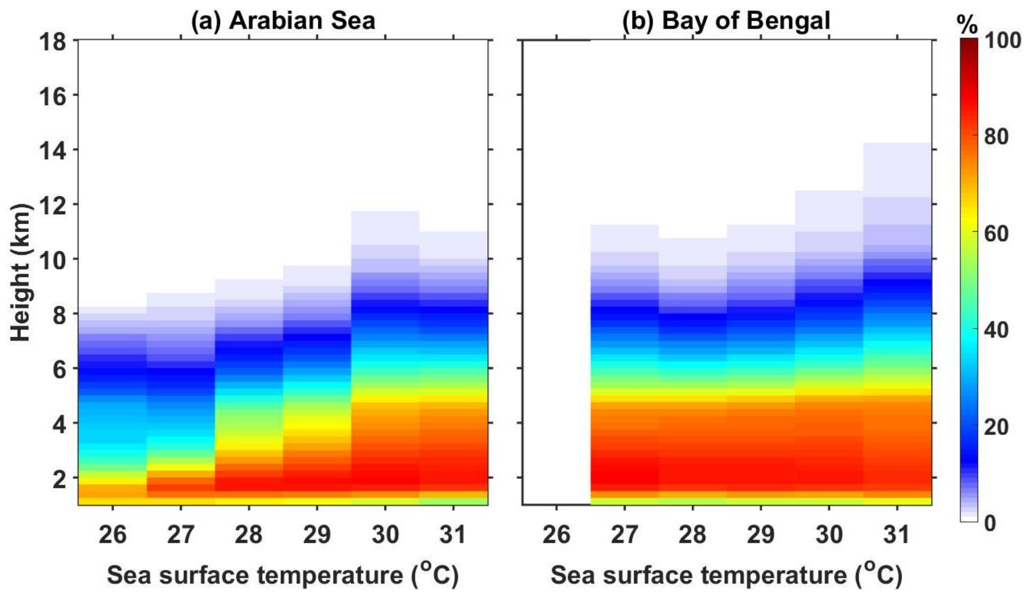

Figure 2: (a) and (b) represent the altitudinal distribution of occurrence of conditional reflectivity (≥ 17 dBZ) as a function of SST with respect to precipitation occurrence at that particular SST interval over the AS and the BOB, respectively.

Formatted: Font: Not Bold, No underline

Formatted: Left, Line spacing: Multiple 1.08 li

Formatted: Font: (Default) Times New Roman, 12 pt

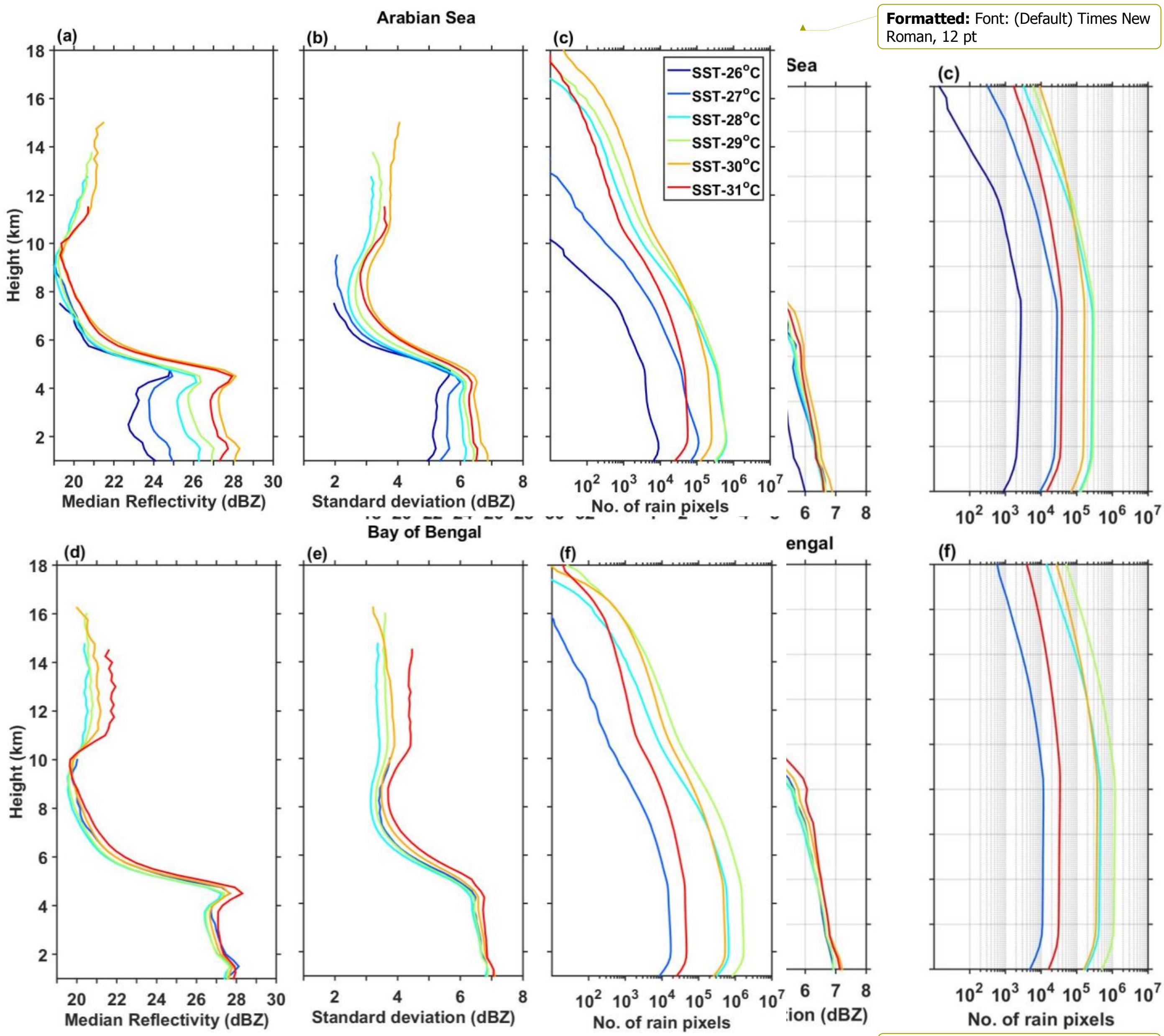

Formatted: Font: (Default) Times New Roman, 12 pt

Figure 3: (a), (d) and (b), (e) represent vertical profiles of median reflectivity correspond to deep systems and their standard deviation (in dBZ) with SST over the AS ~~(63°E-72°E & 8°N-20°N)~~ and the BOB~~ (83°E-92°E & 8°N-21°N),~~, respectively during the ~~SWM~~ISM season. (c) and (f) show the number of conditional reflectivity pixels at each altitude used for the estimation of the median and standard deviation.

Formatted: Indent: Left: 0 cm, Hanging: 1.25 cm

Formatted: Left, Line spacing: Multiple 1.08 li

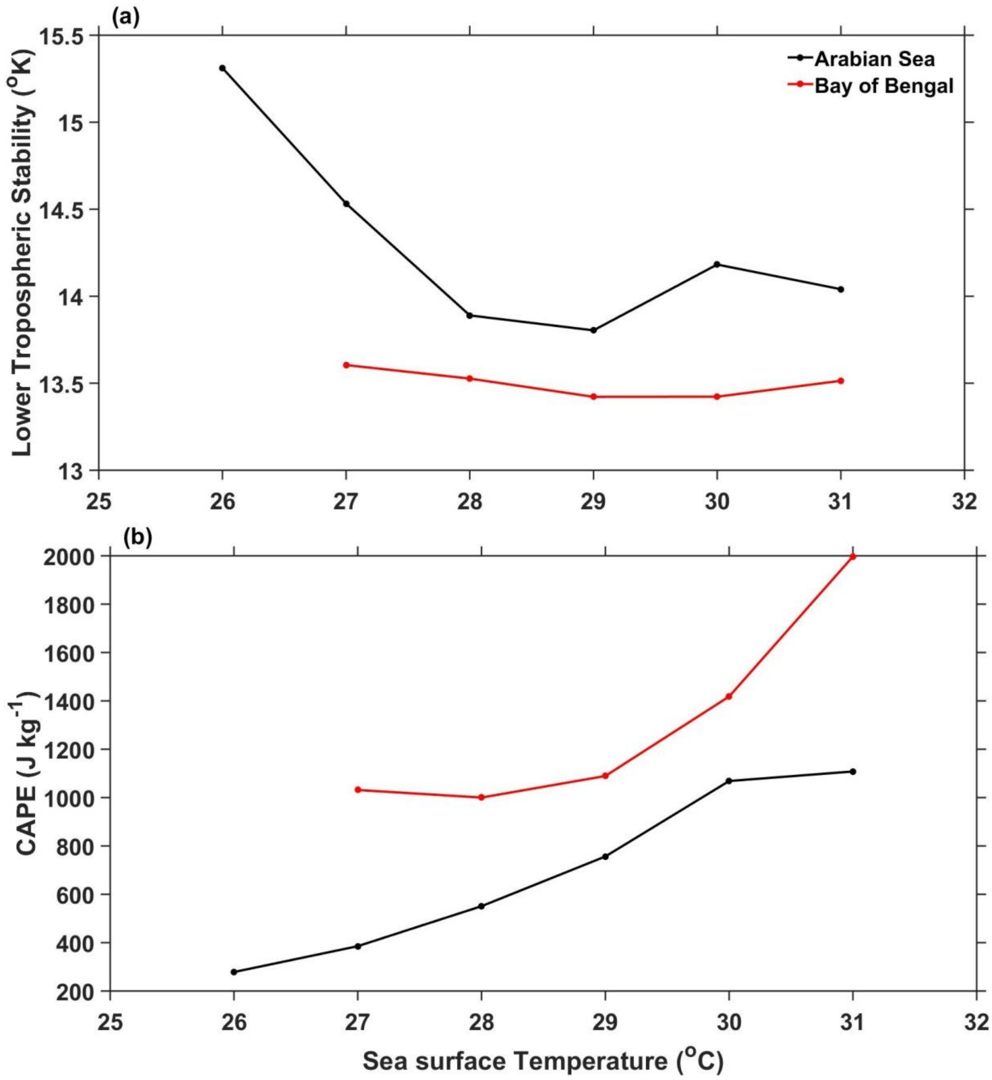

Formatted: Font: (Default) Times New Roman, 12 pt

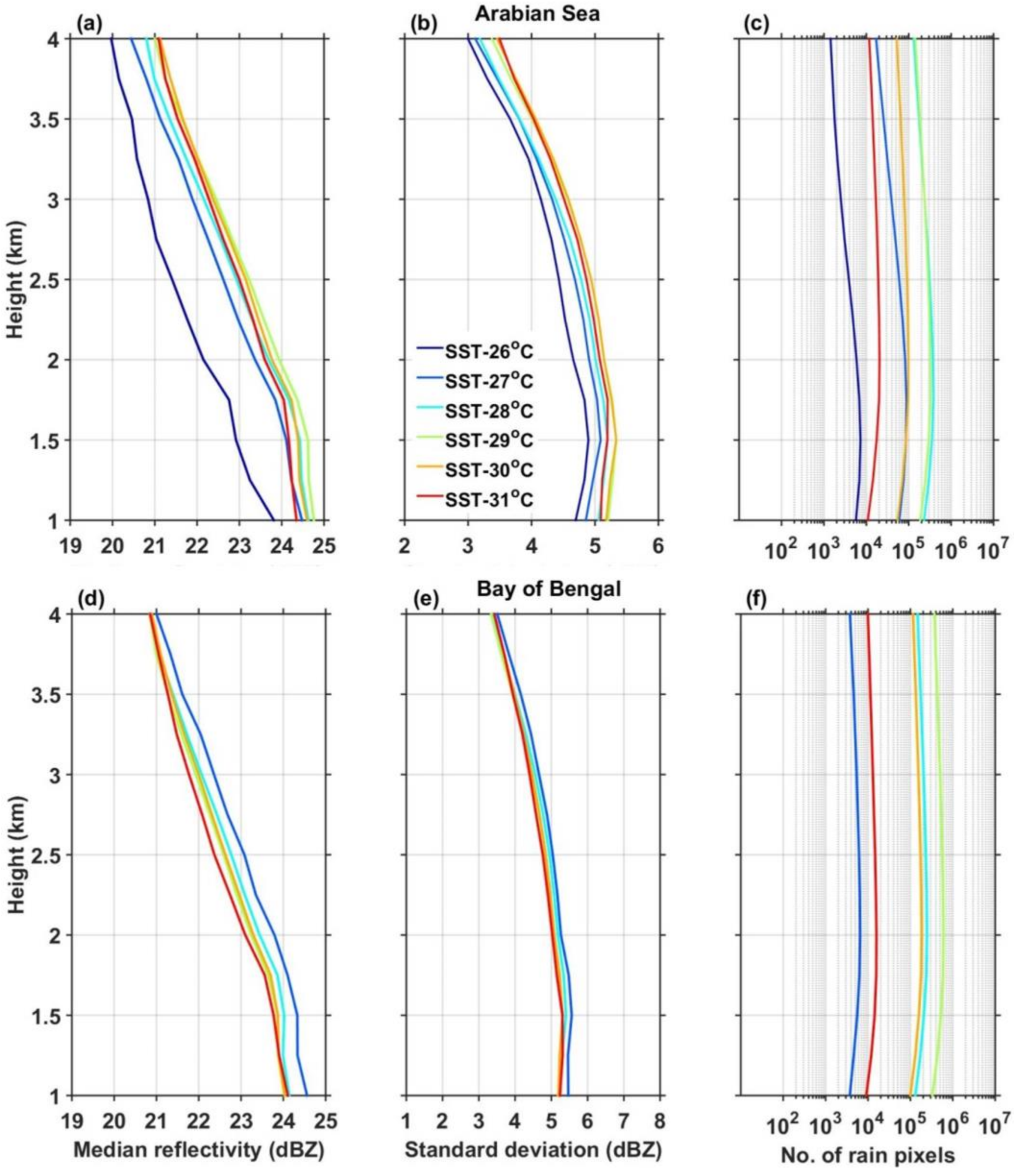

Formatted: Font: (Default) Times New Roman, 12 pt

Figure 4: ~~(a) The variation of mean LTS (in °K) with SST over the AS (63°E-72°E & 8°N-20°N) and the BOB (83°E-92°E & 8°N-21°N) during the SWM season. (b)~~ Same as ~~(a)~~Fig. 3 but for ~~CAPE~~shallow precipitating systems.

Formatted: Indent: Left: 0 cm, Hanging: 1.27 cm, Line spacing: Multiple 1.08 li

Formatted: Left, Line spacing: Multiple 1.08 li

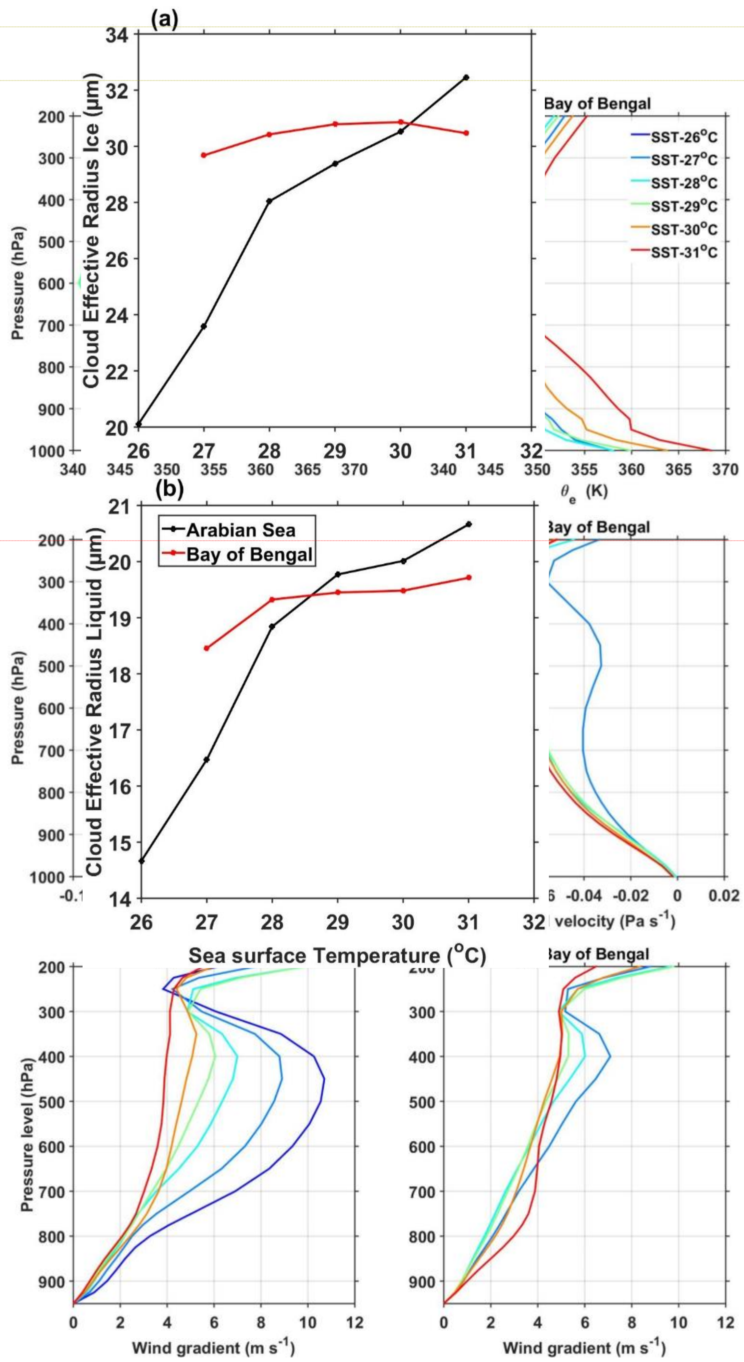

Formatted: Font: (Default) Times New Roman, 12 pt

Formatted: Font: (Default) Times New Roman, 12 pt

Formatted: Left, Line spacing: Multiple 1.08 li

Formatted: Font: Not Bold

Formatted: Left, Indent: Left: 0 cm, First line: 0 cm

Formatted: Indent: Left: 0 cm, Hanging: 1.25 cm

Figure 5: (a) and (b), respectively, represent the ~~variation~~vertical profiles of mean ~~CER ice~~θ_e (in ~~µm) and~~K) with SST over the AS and the BOB during the ISM season. (c) and (d) and (e) and (f) are same as (a) and (b) but for mean vertical velocity (in Pa s^{-1}) and wind gradient with reference to 950 hPa level (in m s^{-1}).

Formatted: Font: (Default) Times New Roman, 12 pt

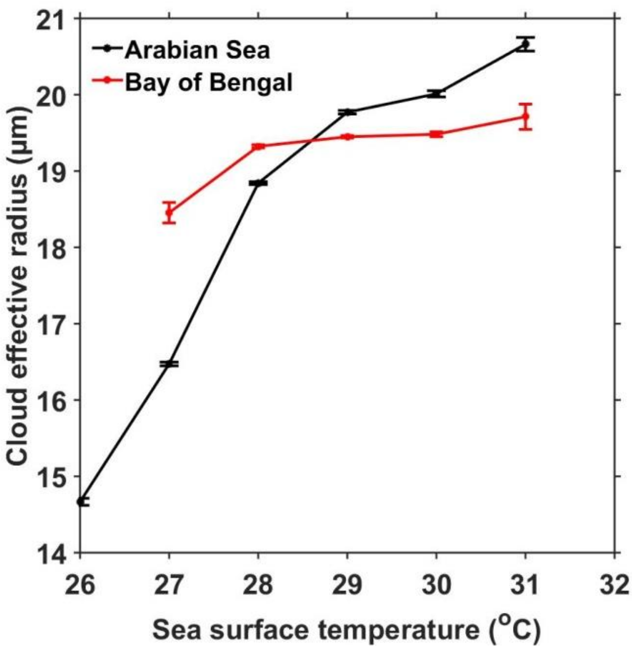

Formatted: Left, Indent: Left: 0 cm, First line: 0 cm, Space After: 8 pt, Line spacing: Multiple 1.08 li

Figure 6: Variation of mean and standard error of CER liquid (in µm) with SST over the AS ~~(63°E-72°E & 8°N-20°N)~~ and the BOB ~~(83°E-92°E & 8°N-21°N)~~ during the ~~SWM~~ISM season.

Formatted: Left, Line spacing: Multiple 1.08 li

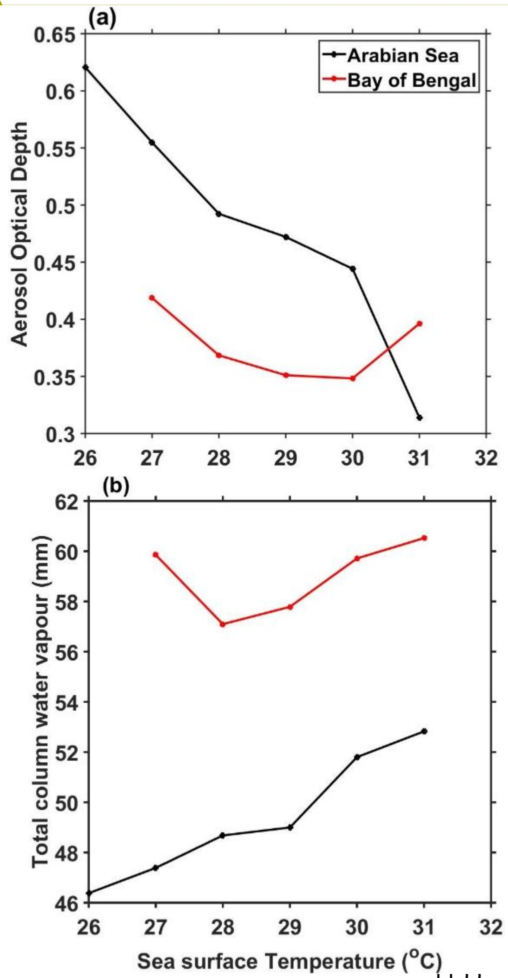

Formatted: Font: (Default) Times New Roman, 12 pt

Formatted: Font: (Default) Times New Roman, 12 pt

Formatted: Font: Not Bold

Formatted: Left, Indent: Left: 0 cm, First line: 0 cm

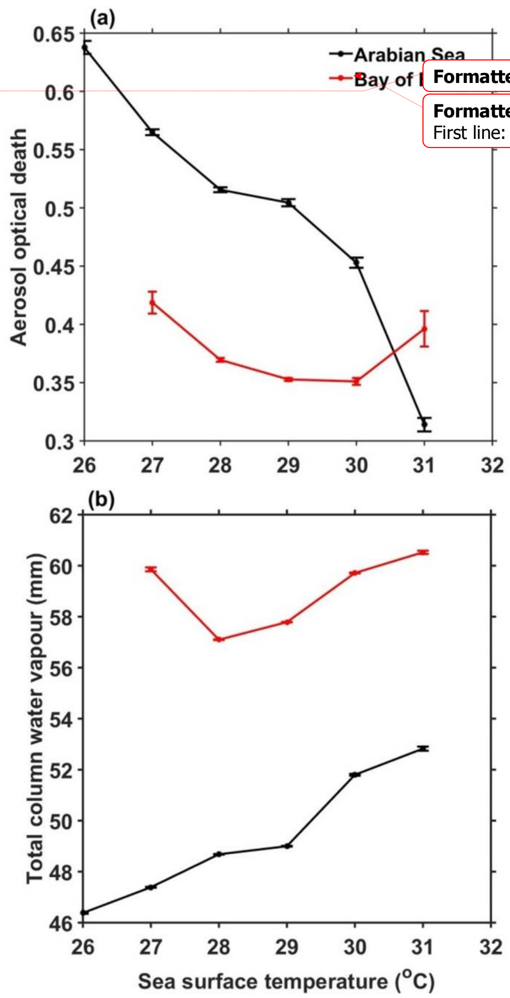

Figure ~~6~~7: (a) ~~The variation~~Mean and standard error of ~~mean~~ AOD and (b) TCWV (in mm) with SST over the AS ~~(63°E-72°E & 8°N-20°N)~~ and the BOB ~~(83°E-92°E & 8°N-21°N)~~ during ~~SWM~~ISM.

Formatted: Font: Not Bold

Formatted: Font: Not Bold

Formatted: Left, Indent: Left: 0 cm, First line: 0 cm

Supplementary material

Satheesh et al. (2006) showed an increase in AOD with increase in latitude over the AS due to the dust advection from Arabia desert regions during ISM season, whereas SST decreases with increase in the latitude. In other words the SST is low and AOD is high in northern AS whereas over the southern AS, SST is high and AOD is low. This contrasting spatial distribution of AOD and SST could cause a negative correlation between AOD and SST as depicted in Fig. 6a. To examine whether the observed decrease in AOD with increase in SST over the AS is due to the latitudinal variation of AOD or exists at all latitudes, we have segregated the data into 2° latitude bins and plotted the mean AOD with SST for all bins and is depicted in Fig. S2. In spite of the magnitude, AOD variation with SST is nearly similar at all latitudes of the AS, i.e., the higher AOD is observed at lower SSTs and vice versa (Fig. S2a). On the other hand the latitudinal variation of AOD with SST over the BOB shown in Fig. S2b also show a decrease in AOD with SST till 30 °C but the magnitude of variation is trivial relative to the AS. Also, as depicted in Fig. 6a AOD increases above 30 °C with SST over the BOB. This indicates that though there is a difference in magnitude of variation, AOD varies with SST over both the seas at all latitudes. This analysis is repeated using the multi-angle imaging spectroradiometer (MISR) dataset (which is not shown here) for small, medium large aerosol particles. Interestingly all three types also show a decrease in AOD with rise in SST over both the seas.

Satheesh, S. K., Moorthy, K. K., Kaufman, Y. J., and Takemura, T.: Aerosol Optical depth, physical properties and radiative forcing over the Arabian Sea, *Meteorol. Atmos. Phys.*, 91, 45–62, doi:10.1007/s00703-004-0097-4, 2006.

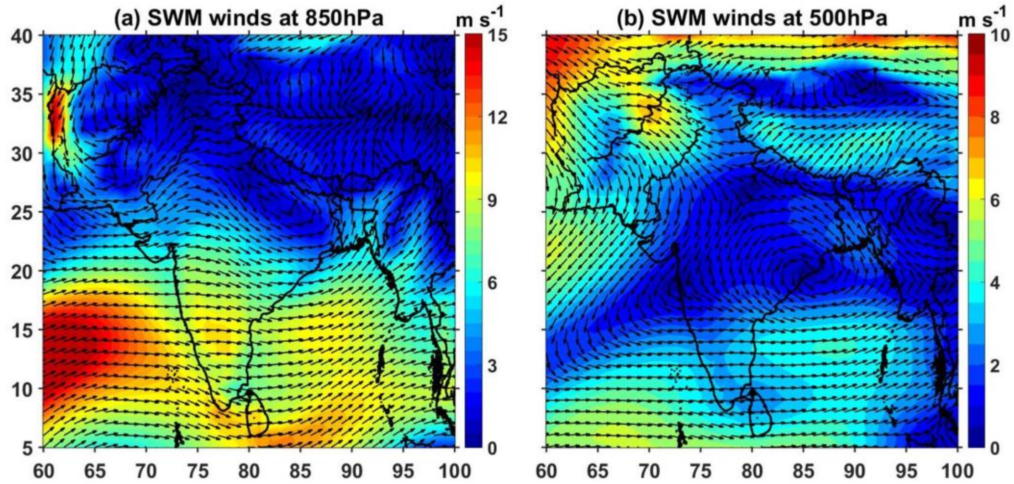

Formatted: Font: (Default) Times New Roman, 12 pt

~~**Figure 7:** Winds during the SWM season at 850 hPa and 500 hPa levels. The shading colors represent the magnitude of the wind and arrow indicates the direction of the wind.~~

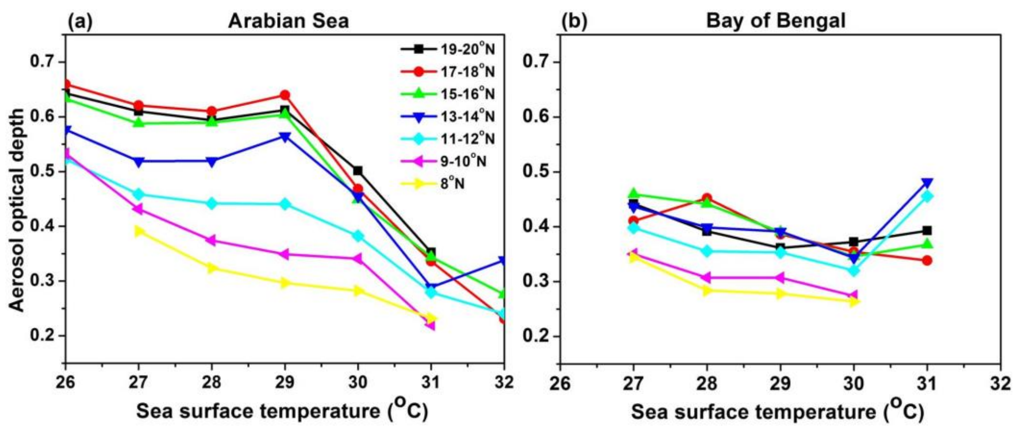

Formatted: Font: (Default) Times New Roman, 12 pt

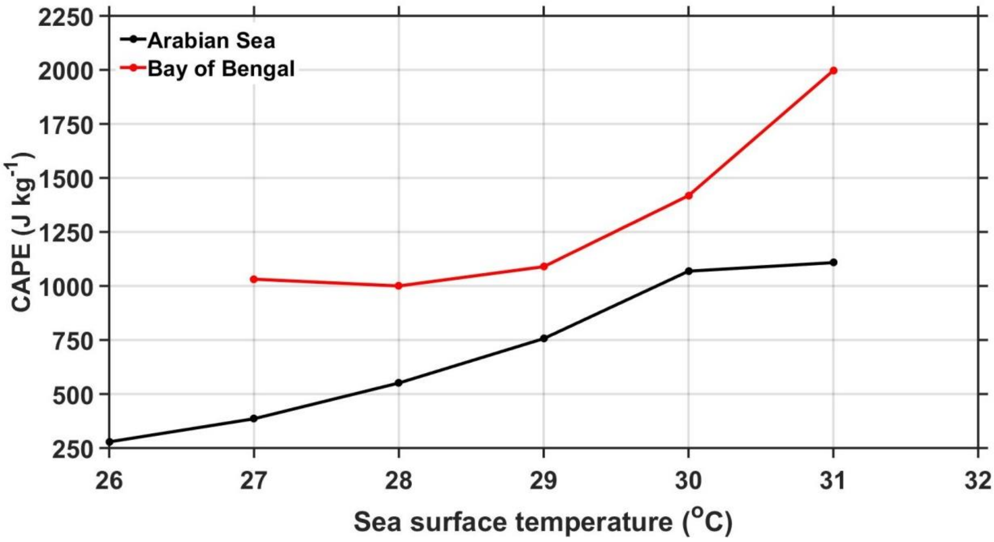

Figure S1: Variation of mean CAPE (in J kg^{-1}) with SST over the AS and the BOB during the ISM season.

Formatted: Font: (Default) Times New Roman, 12 pt

Formatted: Font: (Default) Times New Roman, 12 pt

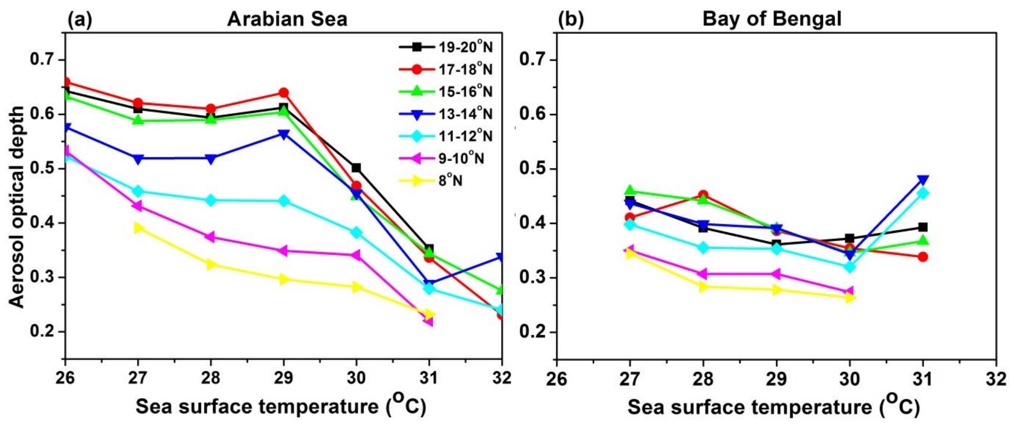

Figure ~~8~~S2: (a) and (b), respectively, represent latitudinal variation (for every 2° latitude interval) of mean AOD over the AS (between 63°E and 72°E) and the BOB (between 83°E and 92°E).

Replies to Reviewer

At the outset, we thank the reviewer for positive and constructive comments that improved the quality of the manuscript.

Comment: It is not clear the SST effect is the primary cause of the variability of vertical structure of precipitation. The authors should examine the SST effect on this variability under similar monsoon westerlies conditions, following the paper by Takahashi and Dado (2018) showing that SST makes a positive contribution toward rainfall in the Philippines during the summer Monsoon, but the monsoon westerly is the primary driver of the variation in rainfall.

Reply: *It is true that SST alone cannot explain all the observed variability. SST, of course, is the main forcing parameter, but the vertical structure is dictated by several atmospheric factors, like temperature inversions, atmospheric instability, availability of moisture (in the mid-troposphere), wind shear, etc. Takahashi and Dado (2018) have shown that zonal wind variations can also explain some variability of rain. To examine the impact of zonal wind on rainfall over the Arabian Sea and Bay of Bengal, the data are segregated into 3 wind regimes* as *weak (monsoon westerlies lies between 0 and 6 m s^{-1}), moderate (monsoon westerlies lies between 6 to 12 m s^{-1}) and strong (monsoon westerlies > 12 m s^{-1}) winds. The median vertical profiles of reflectivity are computed for each SST bin for deep and shallow systems. These median reflectivity profiles for shallow and deep systems at each SST bin and for each wind category are shown in Figures R1, R2, R3 & R4. Two important observations are noted from these figures. 1. Vertical profiles of reflectivity show considerable variation (2-5 dBZ) in all wind categories over the Arabian Sea, but such variations are absent over the Bay of Bengal. It implies that the reported differences in reflectivity profiles over the Arabian Sea and Bay of Bengal exist in all wind regimes. 2. The variation in reflectivity with SST increases with weak to strong wind regime over the Arabian Sea, indicating some influence of wind on reflectivity (rainfall) variation.*

The above information is included in the revised manuscript (but not figures).

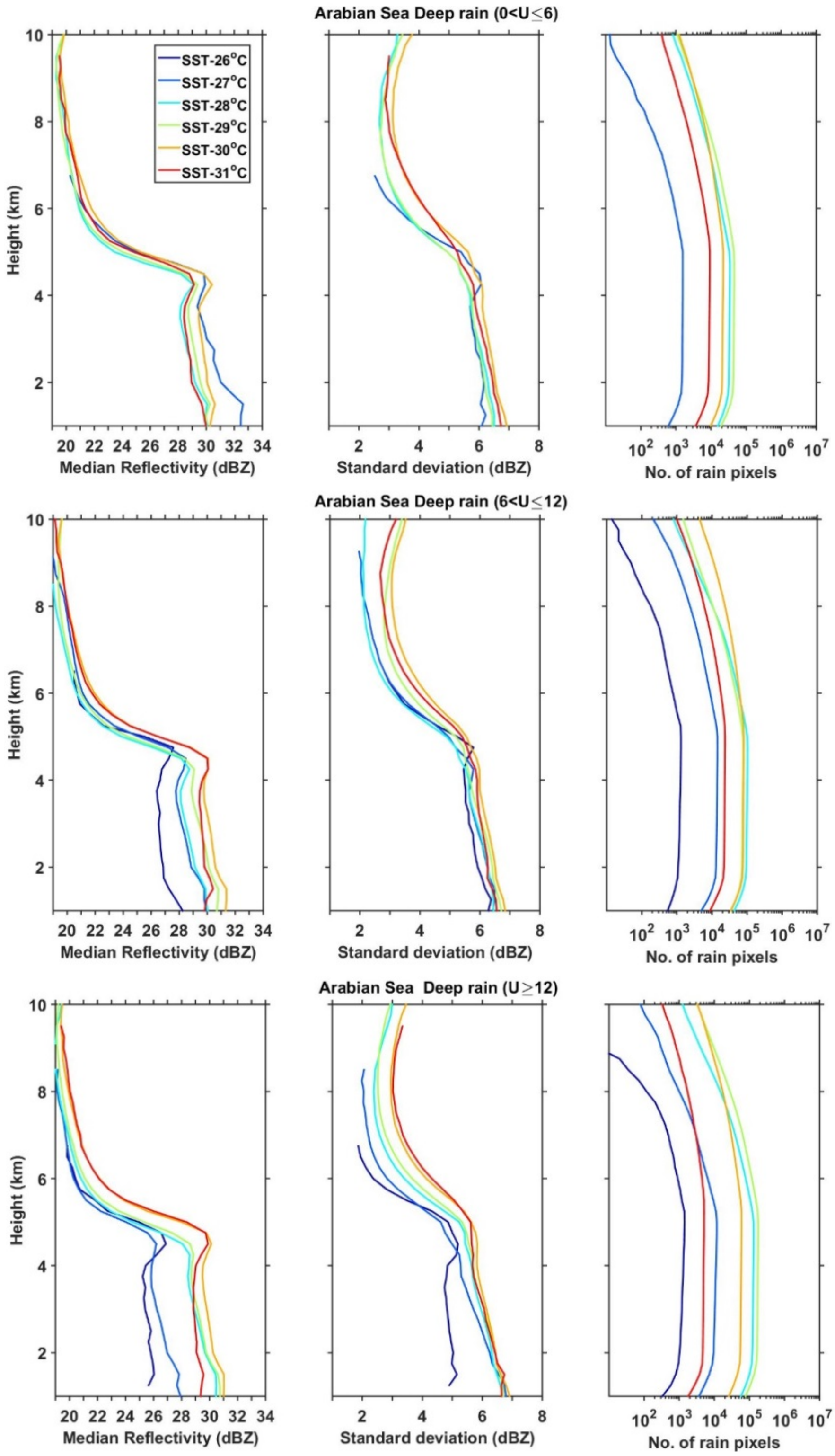

Figure R1: *Vertical profiles of median reflectivity and standard deviation during weak, moderate and strong westerly wind regimes corresponding to deep systems as a function of SST over the AS during the ISM season. Also shown are the number of conditional reflectivity pixels at each altitude used for the estimation of the median and standard deviation.*

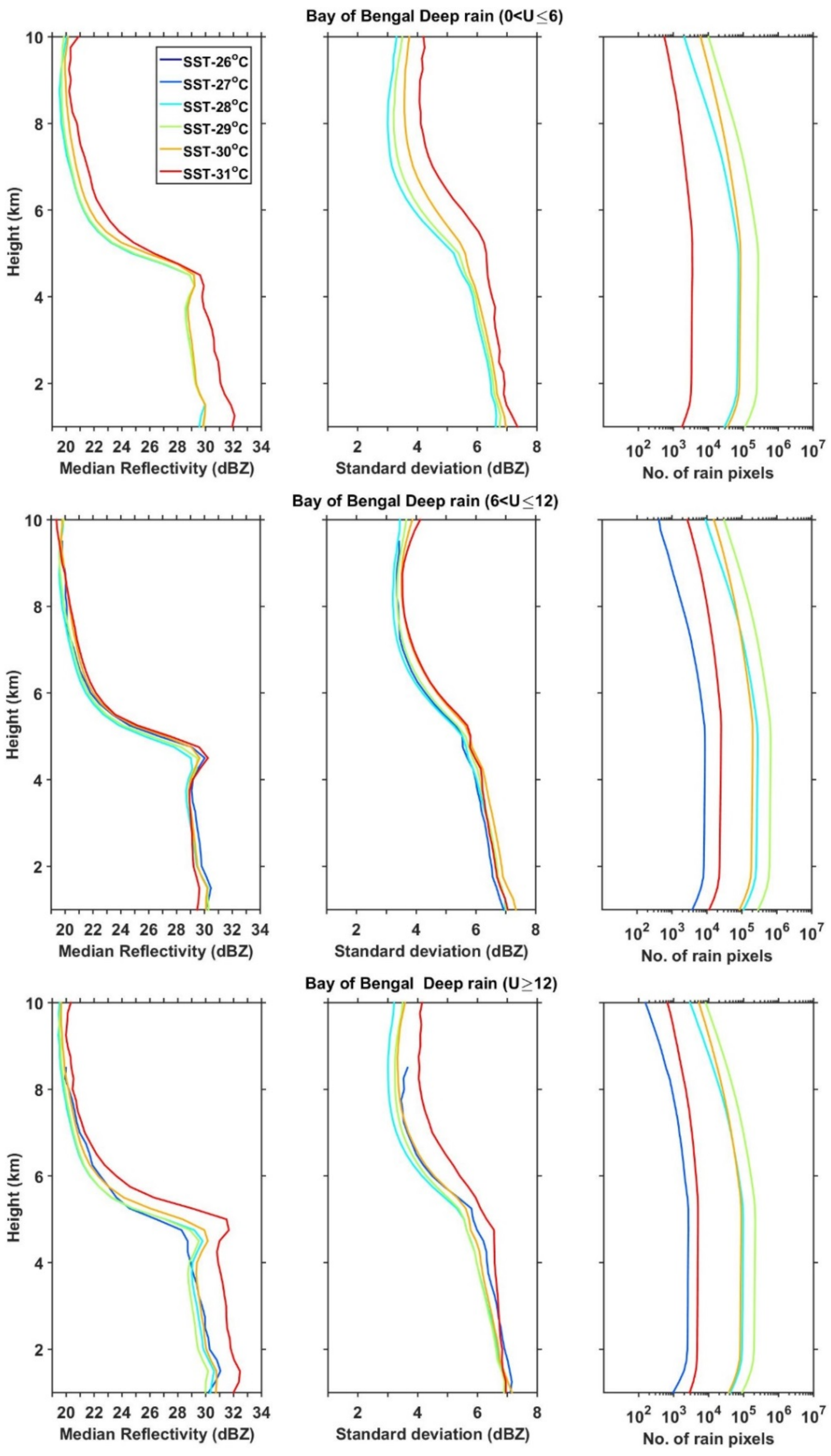

Figure R2: *Vertical profiles of median reflectivity and standard deviation during weak, moderate and strong westerly wind regimes corresponding to deep systems as a function of SST over the BOB during the ISM season. Also shown are the number of conditional reflectivity pixels at each altitude used for the estimation of the median and standard deviation*.

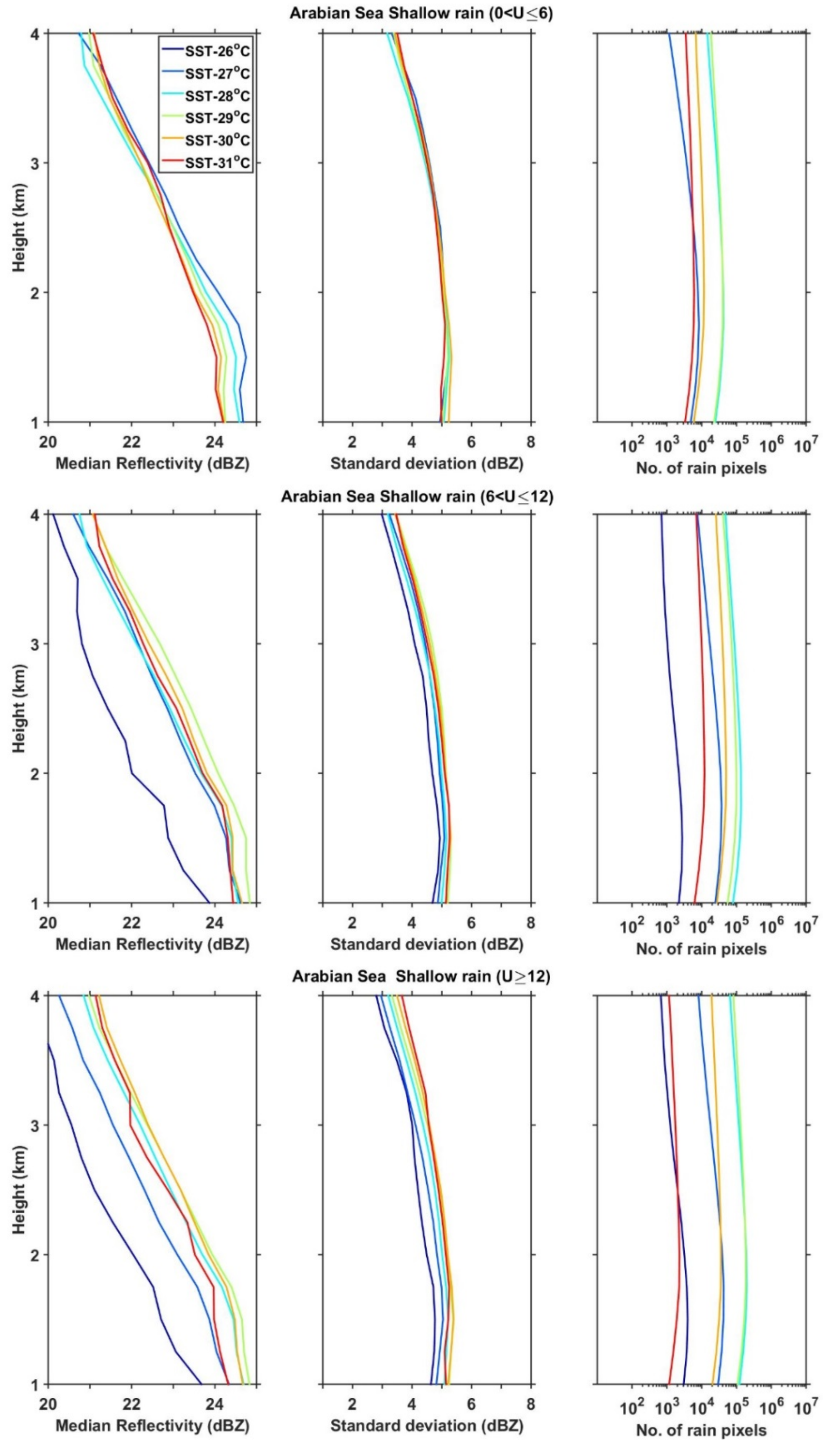

Figure R3: *Vertical profiles of median reflectivity and standard deviation during weak, moderate and strong westerly wind regimes corresponding to shallow systems as a function of SST over the AS during the ISM season. Also shown are the number of conditional reflectivity pixels at each altitude used for the estimation of the median and standard deviation*.

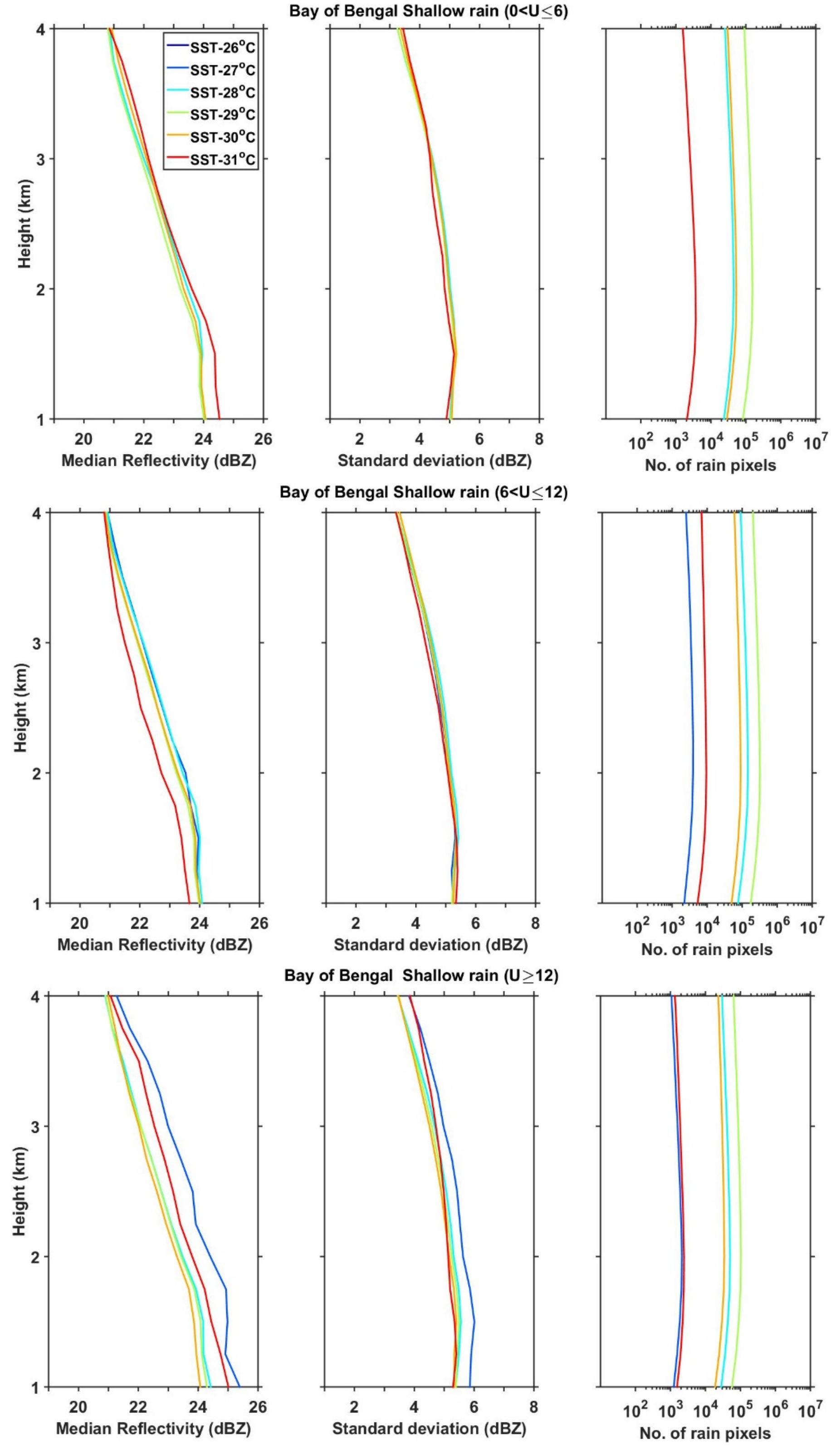

Figure R4: *Vertical profiles of median reflectivity and standard deviation during weak, moderate and strong westerly wind regimes corresponding to shallow systems as a function of SST over the BOB during the ISM season. Also shown are the number of conditional reflectivity pixels at each altitude used for the estimation of the median and standard deviation.*

Comment: I cannot agree with the arguments described in Line 283-285, since cloud effective radius (CER) is not simply linked to precipitation size (i.e. Z-R). The authors should refer to the review by Rosenfeld, D., and C. W. Ulbrich (2003) describing that microphysically “continental” clouds with greater concentrations of small cloud droplets produce greater concentrations of large rain drops and smaller concentrations of small rain drops compared to microphysically “maritime” clouds with small concentrations of large cloud droplets.

Reply: *We do agree with the reviewer that is it not entirely correct to directly link CER to raindrop size (reflectivity), because several microphysical and dynamical processes occur during the cloud drop growth (collision-coalescence, riming, etc.) to rain drop and also its descent (evaporation, etc.) to the ground (Rosenfeld and Ulbrich, 2003; Rao et al., 2009; Radhakrishna et al. 2009). The slope of the vertical profile of reflectivity can provide the dominant microphysical processes occurring during the drop evolution (Saikranthi et al. 2014; Rao et al. 2016). In the present study, the reflectivity gradients are negative (i.e., reflectivity increases in magnitude with decreasing height) at all SST’s, albeit with varying magnitude. It indicates that, on average, there is a low-level hydrometeor growth at all SST’s over both Arabian Sea and Bay of Bengal. Since the microphysical process at all SST’s is same, we linked CER and raindrop size. Since both the study regions (Arabian Sea and Bay of Bengal) are oceanic regions, it is a reasonable approximation. However, such approximations may not necessarily be valid over continental regions (or continental clouds) and dry regions (where evaporation of raindrops plays a dominant role) (Radhakrishna et al. 2009; Saikranthi et al. 2014; Rao et al. 2006).*

Comment: It is not clear the definition of deep systems shown in Fig. 3. If deep systems include both convection and stratiform precipitation, they should be separated. I would suggest the authors refer to the paper by Kobayashi et al. (2018) describing vertical gradient of stratiform radar reflectivity below the bright band.

Reply: *The main objective of the paper is to understand the impact of SST (and other atmospheric processes) on the vertical structure of precipitation. Since SST is the surface forcing parameter and triggers only convection (could be shallow or deep)(here convection means the physical process not the type of rain, which we generally refer to as convective rain)(Houze et al. 2015), we primarily focused on these two types of systems. Stratiform rain is the trailing or decaying portion of the convective cell, so, we may not find a direct link between SST and stratiform rain.*

Comment: I speculate that small variation of vertical structure of precipitation with SST over BoB should be explained by the fact that rainfall over BoB is produced by southeastward-propagating systems from the India coast (Yang and Slingo 2001; Li and Carbone 2015) rather than those developed in situ.

Reply: *We do agree with the reviewer that the systems generating along the east coast of India propagate towards the Bay of Bengal at diurnal scale. The local conditions (including SST) play an important role for the propagation of systems (they are not simple advective systems). In that context, it is important to check all the background parameters. All these parameters, like vertical velocity, horizontal wind gradients, AOD, CER and columnar water* *vapor, show smaller variation with SST over the Bay of Bengal than Arabian Sea, indicating that atmospheric conditions are entirely different over the Arabian Sea and Bay of Bengal and are dictating the vertical structure of precipitation.*

Comment: Line 78-80: I would suggest that the authors refer to Kumar et al. (2014) and Shige et al. (2017) describing summer monsoon rainfall over the Western Ghats and Myanmar coast.

Reply: *The above references are added in the introduction of the revised manuscript.*

Variability of vertical structure of precipitation with sea surface temperature over the Arabian Sea and the Bay of Bengal as inferred by TRMM PR measurements

Kadiri Saikranthi[1], Basivi Radhakrishna[2], Thota Narayana Rao[2] and

Sreedharan Krishnakumari Satheesh[3]

[1] *Department of Earth and Climate Science, Indian Institute of Science Education and Research (IISER), Tirupati, India.*

[2] *National Atmospheric Research Laboratory, Department of Space, Govt. of India, Gadanki - 517112, India.*

[3] *Divecha Centre for Climate Change, Centre for Atmospheric and Oceanic Sciences, Indian Institute of Science, Bangalore - 560012, India.*

Address of the corresponding author

Dr. K. Saikranthi,

Department of Earth and Climate Science,

Indian Institute of Science Education and Research (IISER),

Tirupati,

Andhra Pradesh, India.

Email: ksaikranthi@gmail.com

Abstract

Tropical rainfall measuring mission precipitation radar measurements are used to examine the variation of vertical structure of precipitation with sea surface temperature (SST) over the Arabian Sea (AS) and Bay of Bengal (BOB). The variation of reflectivity and precipitation echo top with SST is remarkable over the AS but small over the BOB. The reflectivity increases with SST (from 26°C to 31°C) by ~1 dBZ and 4 dBZ above and below 6 km, respectively, over the AS while, its variation is < 0.5 dBZ over the BOB. The transition from shallow storms at lower SSTs (≤ 27°C) to deeper storms at higher SSTs is strongly associated with the decrease in stability and mid-tropospheric wind shear over the AS. Contrary, the storms are deeper at all SSTs over the BOB due to weaker stability and mid-tropospheric wind shear. At lower SSTs, the observed high aerosol optical depth (AOD) and low total column water vapor (TCWV) over AS results in small cloud effective radius (CER) and weaker reflectivity. As SST increases, AOD decreases and TCWV increases leading to large CER and high reflectivity. The changes in these parameters with SST are marginal over the BOB and hence the CER and reflectivity. The predominance of collision-coalescence process below the bright band is responsible for the observed negative slopes in the reflectivity over both the seas. The observed variations in reflectivity are originated at the cloud formation stage over both the seas and these variations are magnified during the descent of hydrometeors to ground.

1. Introduction

Indian summer monsoon (ISM - June through September) is one of the most complex weather phenomena, involving coupling between the atmosphere, land and ocean. At the boundary of the ocean and atmosphere air-sea interactions play a key role for the coupled Earth system (Wu and Kirtman 2005; Feng et al. 2018). The sea surface temperature (SST) – precipitation relations are the important measures for the air-sea interactions on different temporal scales (Woolnough et al., 2000; Rajendran et al. 2012). Recent studies (Wang et al. 2005; Rajeevan et al. 2012; Chaudhari et al. 2013; 2016; Weller et al. 2016; Feng et al. 2018) have shown that the simulation of ISM can be improved with the exact representation of SST - precipitation relationship. SST modulates the meteorological factors that influence the formation and evolution of different kinds of precipitating systems over tropical oceans (Gadgil et al. 1984; Schumacher and Houze, 2003; Takayabu et al. 2010; Oueslati and Bellon 2015).

The studies dealing with SST and cloud/precipitation population considered whole Indian Ocean as a single entity (Gadgil et al. 1984; Woolnough et al., 2000; Rajendran et al. 2012; Sabin et al. 2012; Meenu et al. 2012; Nair and Rajeev 2014; Roxy 2014). But in reality the Bay of Bengal (BOB) and the Arabian Sea (AS) of Indian Ocean possess distinctly different features (Kumar et al. 2014; Shige et al. 2017; Rajendran et al. 2018; Saikranthi et al. 2019). The monsoon experiment (MONEX) and Bay of Bengal monsoon experiment (BOBMEX) have shown how these two seas are different with respect to each other, in terms of SST, back ground atmosphere and the occurrence of precipitating systems (Krishnamurti 1985; Houze and Churchill 1987; Gadgil 2000; Bhat et al. 2001). The SST in the AS cools between 10 °N and 20 °N during the monsoon season whereas warming is seen in other global Oceans between the same latitudes (Krishnamurthi 1981). SST variability is large over the AS than the BOB at seasonal and intraseasonal scales (Sengupta et al. 2001; Roxy et al. 2013). The monsoonal winds (in particular the low-level jet) are stronger over the AS than BOB (Findlater 1969).

Also, lower-tropospheric thermal inversions are more frequent and stronger over the AS than BOB (Narayanan and Rao 1981; Sathiyamoorthy et al. 2013). Thus, the atmospheric and sea surface conditions and in turn the occurrence of different kinds of precipitating systems are quite different over the BOB and the AS during the ISM period. For instance, long-term measurements of tropical rainfall measuring mission (TRMM) precipitation radar (PR) have shown that shallow systems are more prevalent over the AS, while deeper systems occur frequently over the BOB (Liu et al. 2007; Romatschke et al. 2010; Saikranthi et al. 2014, 2018; Houze et al. 2015).

The aforementioned studies mainly focused on the morphology of vertical structure of precipitation, but, none of them studied the variation of vertical structure of precipitation (in terms of occurrence and intensity) with SST and the differences in the vertical structure over AS and BOB. On the other hand, information on the vertical structure of precipitation is essential for improving the accuracy of rainfall estimation (Fu and Liu 2001; Sunilkumar et al. 2015), understanding the dynamical and microphysical processes of hydrometeor growth/decay mechanisms (Houze 2004; Greets and Dejene 2005; Saikranthi et al. 2014; Rao et al. 2016) and for improving the latent heating retrievals (Tao et al. 2006). SST being the main driving force to trigger precipitating systems through air-sea interactions (Sabin et al. 2012; Nuijens et al. 2017), can alter the vertical structure of precipitation (Oueslati and Bellon 2015). Therefore, the present study aims to understand the variation of vertical structure of precipitation (in terms of precipitation top height and intensity) with SST over the AS and BOB. Besides the SST, vertical structure can be modified by aerosols (or CCN, mostly at the cloud formation stage) and thermodynamics of the ambient atmosphere. For instance, recent studies have shown the impact of surface PM_{10} aerosols in altering the vertical structure of precipitation (Guo et al., 2018). All these parameters, therefore, are considered in the present study to explain the differences in the vertical structure.

2. Data

The present study utilizes 16 years (1998-2013) of TRMM-PR's 2A25 (version 7) dataset, comprising of vertical profiles of attenuation corrected reflectivity (Iguchi et al. 2009), during the ISM. The range resolution of TRMM-PR reflectivity profiles is 250 m with a horizontal footprint size of ~4.3 and 5 km before and after the boosting of its orbit from 350 km to 403 km, respectively. It scans ±17° from nadir with a beam width of 0.71° covering a swath of 215 km (245 km after the boost). The uniqueness of TRMM-PR data is its ability in pigeonholing the precipitating systems into convective, stratiform and shallow rain. This classification is based on two methods namely the horizontal method (H - method) and the vertical method (V - method) (Awaka et al. 2009). The original TRMM-PR 2A25 vertical profiles of attenuation corrected reflectivity are gridded to a three dimensional Cartesian coordinate system with a spatial resolution of 0.05° × 0.05°. The detailed methodology of interpolating the TRMM-PR reflectivity data into the 3D Cartesian grid is discussed in Houze et al. (2007). This dataset is available at the University of Washington website (http://trmm.atmos.washington.edu/).

To understand the observed variations in the vertical structure of precipitation in the light of microphysics of clouds, Moderate Resolution Imaging Spectroradiometer (MODIS) AQUA satellite level 3 data (MYD08) are considered. In particular, the daily atmospheric products of aerosol optical depth (AOD) (Hubanks et al. 2008) and cloud effective radius (CER) liquid (Platnick et al. 2017) during the period 2003 and 2013 have been used. MODIS AOD dataset is a collection of aerosol optical properties at 550 nm wavelength, as well as particle size information. Level 2 MODIS AOD is derived from radiances using either one of the three different algorithms, i.e., over ocean Remer et al. (2005) algorithm, over land the Dark-Target (Levy et al. 2007) algorithm and for brighter land surfaces the Deep-Blue (Hsu et al. 2004) algorithm. CER is nothing but the weighted mean of the size distribution of cloud drops i.e., the ratio of third moment to second moment of the drop size distribution. In the level 3 MODIS daily dataset, aerosol and cloud products of level 2 data pixels with valid retrievals within a calendar day are first aggregated and gridded to a daily average with a spatial resolution of 1° × 1°. For CER grid box values, CER values are weighted by the respective ice/liquid water cloud pixel counts for the spatiotemporal aggregation and averaging processes.

The background atmospheric structure (winds and total column water vapor) and SST information are taken from the European Centre for Medium Range Weather Forecasting (ECMWF) Interim Reanalysis (ERA) (Dee et al. 2011). ERA-Interim runs 4DVAR assimilation twice daily (00 and 12 UTC) to determine the most likely state of the atmosphere at a given time (analysis). The consistency across variables in space and time (during 12-hour intervals) is thus ensured by the atmospheric model and its error characteristics as specified in the assimilation. ERA-Interim is produced at T255 spectral resolution (about 0.75°, ~ 83 km) with a temporal resolution of 6h for upper air fields and 3h for surface fields. The original 0.75° × 0.75° spatial resolution gridded dataset is rescaled to a resolution of 0.125° × 0.125°. The temporal resolution of the dataset used in the present study is 6h (00, 06, 12 and 18 UTC). The equivalent potential temperature (θ_e) is estimated from the ERA-Interim datasets using the following formula (Wallace and Hobbs 2006):

$$\theta_e = \theta exp\left(\frac{L_V w_s}{C_p T}\right) \quad (1)$$

where θ is the potential temperature, L_v is the latent heat of vaporization, w_s is the saturation mixing ratio, C_p is the specific heat at constant pressure and T is the absolute temperature.

The variation of vertical structure of precipitation with SST are studied by considering the dataset between 63 °E – 72 °E and 8 °N – 20 °N over the AS and 83 °E – 92 °E and 8 °N – 21 °N over the BOB. These regions of interest along with the ISM seasonal mean SST over the two seas are depicted in Fig. 1. These regions are selected in such a way that the costal influence on SST is eluded from the analysis. As the rainfall is scanty over the western AS (west of 63°E latitude) during the ISM (Saikranthi et al. 2018), this region is also not considered in the present analysis. The seasonal mean SST is higher over the BOB than in the AS by more than 1 °C during the ISM season, in agreement with Shenoi et al. (2002). The nearest space and time matched SST data from ERA-Interim are assigned to the TRMM-PR and MODIS observations for further analysis.

3. Variation of vertical structure of precipitation with SST

The occurrence (in terms of %) of conditional precipitation echoes (Z ≥ 17 dBZ) at different altitudes as a function of SST over the AS and the BOB is shown in Fig. 2. The variation of precipitation echo occurrence frequency with SST is quite different over both the seas. The top of the precipitation echoes extends to higher altitudes with increasing SST over the AS, while such variation is not quite evident over the BOB. Precipitation echoes are confined to < 8 km at lower SST (< 28 °C) over the AS, but exhibits a gradual rise in height with increase in SST. Large population density of precipitation echoes at lower altitudes is mainly due to the abundant occurrence of shallow storms over the AS (Saikranthi et al. 2014, 2019; Rao et al. 2016). Interestingly, the occurrence of precipitation echoes is seen at higher altitudes even at lower SSTs over the BOB, indicating the presence of deeper storms. Such systems exist at all SST's over the BOB.

To examine the variation of reflectivity profiles with SST, median profiles of reflectivity in each SST bin are computed over the AS and the BOB separately for deep and shallow systems and are depicted in Figs. 3 & 4, respectively. The space- and time-matched conditional reflectivity profiles are grouped into 1°C SST bins and then the median is estimated at each height, only if the number of conditional reflectivity pixels (Figs. 3c; 3f; 4c & 4f) is greater than 500. The median reflectivity profiles corresponding to the deep systems are distinctly different over the AS and the BOB (Figs. 3a & 3d), even at the same SST. Over the

AS, reflectivity of deep systems at different SSTs shows small variations (≤ 1 dBZ) above the melting region (> 5 km), but varies significantly (~ 4.5 dBZ) below the melting level (< 5 km). These variations in reflectivity profiles with SST are negligible (< 0.5 dBZ) over the BOB both above and below the melting region. The reflectivity increases from ~ 26.5 dBZ to ~ 31 dBZ, with increase in SST from 26 °C to 30 °C over the AS, but it is almost the same (~ 30dBZ) at all SST's over the BOB below the melting layer. The standard deviation of reflectivity, representing the variability in reflectivity within the SST bin, is similar at all SSTs over both the seas except for the 26 °C SST over AS. At this SST, the standard deviation is lesser by ~ 1 dBZ than that of other SSTs.

The median reflectivity profiles of shallow storms depicted in Figs. 4a & 4d also show a gradual increase in reflectivity from 20 dBZ to ~ 22 dBZ as SST changes from 26 °C to 31 °C at the precipitation top altitude over the AS and don't show any variation with SST over the BOB. However at 1 km altitude, except at 26 °C SST over the AS, the reflectivity variation with SST is not substantial over both the seas. The standard deviation of reflectivity profiles show ~ 1 dBZ variation with SST (from 26 °C to 31°C) at all altitudes over the AS and don't show any variation over the BOB. The standard deviation of reflectivity for shallow storms varies from 3 to 4 dBZ at the precipitation top altitude and 4.5 to 5.3 dBZ at 1 km altitude over the AS while it shows ~ 4 dBZ at precipitation top and ~ 5.5 dBZ at 1 km altitude over the BOB.

4. Factors affecting the vertical structure of precipitation and their variability with SST

The formation and evolution of precipitating systems over oceans depend on dynamical, thermodynamical and microphysical factors, like SST, wind shear, vertical wind velocity, stability, CER, etc., and need to be considered for understanding the vertical structure of precipitation (Li and Min 2010; Creamean et al. 2013; Chen et al. 2015; Shige and Kummerow 2016; Guo et al 2018).

Deleted:

Formatted: Indent: First line: 1.27 cm

Deleted: reamean

Deleted: Kummerov

Formatted: Font:Not Bold

4.1. Dynamical and thermodynamical factors:

Takahashi and Dado (2018) have shown that zonal wind variations can also explain some variability of rain. To examine the impact of zonal wind on rainfall over the Arabian Sea and Bay of Bengal, the data are segregated into 3 wind regimes as weak (monsoon westerlies lies between 0 and 6 m s^{-1}), moderate (monsoon westerlies lies between 6 to 12 m s^{-1}) and strong (monsoon westerlies > 12 m s^{-1}) winds. The median vertical profiles of reflectivity are computed for each SST bin corresponding to deep and shallow systems (not shown here). Two important observations are noted from these figures. 1) Vertical profiles of reflectivity show considerable variation (2-5 dBZ) in all wind categories over the Arabian Sea, but such variations are absent over the Bay of Bengal. It implies that the reported differences in reflectivity profiles over the Arabian Sea and Bay of Bengal exist in all wind regimes. 2) The variation in reflectivity with SST increases with weak to strong wind regime over the Arabian Sea, indicating some influence of wind on reflectivity (rainfall) variation.

To understand the role of stability/instability, θ_e values computed from (1) using the ERA-Interim datasets during the ISM period over the AS and the BOB are averaged for a season and are depicted in Figs. 5(a) & 5(b), respectively. The surface θ_e (at 1000 hPa) values are larger over the BOB than those over AS for the same SST, indicating that the instability and convective available potential energy (CAPE) could be higher over the BOB. Indeed, higher CAPE is seen over the BOB (Fig. S1, calculated following Emanuel 1994) than AS at all SSTs by a magnitude > 300 J kg^{-1}. The θ_e increases with SST from 358 °K to 368 °K from 27 °C to 31 °C and from 350 °K to 363 °K from 26 °C to 31 °C over the BOB and the AS, respectively. The CAPE also increases with rise in SST over both the seas. To know the stability of the atmosphere θ_e gradients are considered. Irrespective of SST, positive gradients in θ_e are observed between 900 and 800 hPa levels over the AS indicating the presence of strong stable layers. The strength of these stable layers decreases with increasing SST. These stable layers are formed mainly due to the flow of continental dry warm air from Arabian Desert and Africa above the maritime air causing temperature inversions below 750 hPa level over the AS during the ISM period (Narayanan and Rao 1981). However over the BOB, such temperature inversions are not seen in the lower troposphere.

To understand the effect of wind field on the vertical structure of precipitation, profiles of ISM seasonal mean vertical wind velocity and vertical shear in horizontal wind at various SSTs over the AS and the BOB are shown in Figs. 5(c), 5(d) & 5(e), 5(f) respectively. The updrafts are prevalent at all SSTs throughout the troposphere over the BOB, whereas downdrafts are seen in the mid-troposphere (between 200 and 600 hPa levels) up to 27 °C and updrafts in the entire troposphere at higher SSTs over the AS. Also, the magnitude of the vertical wind velocity varies significantly with SST in the mid-troposphere over the AS. Over the BOB, the magnitude of updrafts increases with altitude in the lower and middle troposphere, but doesn't vary much with SST. In the mid-troposphere, updrafts are stronger by > 0.02 Pa S^{-1} over the BOB than over the AS. The profiles shown in Fig. 5(e) & 5(f) are the mean vertical shear in horizontal wind estimated following Chen et al. (2015) at different levels with reference to 950 hPa level. The wind shear increases with increasing altitude at all the SSTs up to 400 hPa, but the rate of increase is distinctly different between the AS and the BOB at SSTs less than 28 °C and nearly the same at higher SSTs. The wind shear decreases systematically with SST (~ 1.5 m s^{-1} for 1° increase in SST) in the middle troposphere over the AS while the change is minimal over the BOB (~ 2 m s^{-1} for 27 °C and 31 °C).

Chen et al. (2015) highlighted the importance of mid-tropospheric wind shear in generating mesoscale local circulations, like low-level cyclonic and upper-level anticyclonic circulations. This feature is apparent over the AS, where down drafts are prevalent in mid-upper troposphere and updrafts in the lower troposphere at lower SSTs. As SST increases, the wind shear decreases and the updraft increases in the mid-troposphere. However, over the BOB the wind shear is relatively week when compared to the AS and hence the updrafts are seen up to 200 hPa level at all SSTs. The weaker CAPE and stable mid-troposphere coupled with upper- to mid- tropospheric downdrafts at lower SSTs over the AS inhibit the growth of precipitating systems to higher altitudes and in turn precipitate in the form of shallow rain. This result is in accordance with the findings of Shige and Kummerow (2016) that showed the static stability at lower levels inhibits the growth of clouds and promotes the detrainment of clouds over the Asian monsoon region and is considered as an important parameter in determining the precipitation top height. As SST increases large CAPE and updrafts in the middle troposphere collectively support the precipitating systems to grow to higher altitudes, as evidenced in Fig. 2a. On the other hand, large CAPE and updrafts in the middle troposphere prevalent over the BOB at all SSTs are conducive for the precipitating systems to grow to higher altitudes as seen in Fig. 2b.

4.2. Microphysical factors

The observed differences in reflectivity profiles of precipitation with SST could be originated at the cloud formation stage itself or manifested during the evolution stage or due to both. Information on AOD and CER would be ideal to infer microphysical processes at the cloud formation stage. CER values are mainly controlled by the ambient aerosols concentration and the available moisture (Twomey 1977; Albrecht 1989; Tao et al. 2012; and Rosenfeld et al. 2014). For fixed liquid water content, as the concentration of aerosols increases, the number of cloud drops increases and CER decreases (Twomey 1977). To understand the variation of AOD and TCWV and the resultant CER with SST, the mean AOD and TCWV for different SST bins are plotted in Figs. 6a & 6b. The mean and standard error are calculated only when the number of data points is more than 100 in each SST bin. AOD decreases from 0.62 to 0.31 with rise in SST from 26 °C to 31 °C over the AS but only from 0.42 to 0.36 as SST varies from 27 °C to 30 °C and then increases at higher SSTs over the BOB. The variation of TCWV with SST (Fig. 6b) shows a gradual increase with SST over the AS while it decreases initially from 27°C to 28°C, and then increases over the BOB. At a given SST the TCWV is more in the BOB (> 8 mm) than in the AS.

The decrease in AOD and an increase in TCWV with SST result in an increase in CER (14.7 μm to 20.8 μm from 26°C to 31°C) over the AS (Fig. 7). On the other hand, CER doesn't show much variation with SST (18.5 μm to 19.5 μm from 27°C to 31°C) over BOB due to smaller variations in AOD and TCWV. This also shows that the cloud droplets are smaller in size at lower SSTs over the AS than BOB, while they are bigger and nearly equal in size at higher SSTs. Since, reflectivity is more sensitive to the particle size ($Z \propto D^6$), the smaller-sized hydrometeors at lower SSTs over the AS yield weaker reflectivity than over the BOB (both for deep and shallow systems). As the SST increases, CER as well as the reflectivity increases over the AS. At higher SSTs, the CER values are approximately equal over both the seas and in turn the observed reflectivities (Figs. 3a & 4a). This suggests that the variations seen in the reflectivity are originated in the cloud formation stage itself.

The hydrometeors also evolve during their descent to the ground due to several microphysical processes. These processes can be inferred from the vertical structure of precipitation or vertical profiles of reflectivity. The median reflectivity profiles of deep systems show a gradual increase from ~ 10 km to 6 km and an abrupt enhancement is seen just below 6 km over both the seas (Figs. 3a & 3d). The sudden enhancement at the freezing level (radar bright band) is primarily due to the aggregation of hydrometeors and change in dielectric factor from ice to water (Fabry and Zawadzki 1995; Rao et al. 2008; Cao et al. 2013). Below the bright band, raindrops grow by collision-coalescence process and reduce their size by either breakup and/or evaporation processes. The collision-coalescence results in negative slope in the reflectivity profile, whereas breakup and evaporation results in positive slope (Liu and Zipser 2013; Cao et al. 2013; Saikranthi et al. 2014; Rao et al. 2016). The observed negative slope (~ - 0.3 dBZ km^{-1}) in the median reflectivity profiles below the bright band indicates dominance of low-level hydrometeor growth over both the seas. The magnitude of the slope decreases with SST over the AS, while it is nearly equal at all SSTs over the BOB. It indicates the growth rate decreases with SST over the AS and remains the same at all SSTs over the BOB. The median reflectivity profiles of shallow systems also show negative slopes (~ -1 dBZ km^{-1}) at all SSTs representing the predominance of low-level hydrometeor growth by collision-coalescence processes over both the seas.

The present analysis shows that the observed reflectivity changes with SST over both the seas originate at the cloud formation stage and magnify further during the descent of hydrometeors to ground.

5. Conclusions

Sixteen years of TRMM-PR 2A25 reflectivity profiles and 11 years of MODIS AOD and CER data are utilized to understand the differences in variation of vertical structure of precipitation with SST over AS and BOB. Precipitation top height increases with SST over the AS indicating that systems grow to higher altitudes with increase in SST while it is almost same at all SSTs representing that the systems are deeper over the BOB. The decrease in stability and mid-tropospheric wind shear with SST over the AS favour the formation of deeper system at higher systems. However the low stability and small wind shear at all SSTs over the BOB help the formation of deeper systems. The variation of reflectivity with SST is found to be remarkable over the AS and marginal over the BOB. The reflectivity increases with rise in SST over the AS and remains the same at all SSTs over the BOB. This change in reflectivity over the AS is more prominent below the freezing level height (~ 4 dBZ) than the above (~ 1 dBZ). Over the AS, the abundance of aerosols and less moisture at SSTs < 27°C result in high concentration of smaller cloud droplets. As SST increases the aerosol concentration decreases and moisture increases leading to the formation of bigger cloud droplets. Thus, the reflectivity increases with rise in SST over the AS. On the other hand, AOD, TCWV and CER do not show substantial variation with SST over the BOB and hence the change in reflectivity is small. Over the BOB, the mid troposphere is wet and hydrometeor's size at the formation stage is nearly the same at all SSTs. The evolution of hydrometeors during their descent is also similar at all SST's. The collision-coalescence process is predominant below the bright band region over both the seas and is responsible for the observed negative slope in the reflectivity profiles.

Acknowledgements

The authors would like to thank Prof. Robert Houze and his team for the interpolated 3D gridded TRMM-PR dataset (http://trmm.atmos.washington.edu), ECMWF (http://data-portal.ecmwf.int/) team for providing the ERA-Interim dataset and MODIS (https://ladsweb.modaps.eosdis.nasa.gov/) science team for providing the AOD and CER dataset. The authors express their gratitude to Prof. J. Srinivasan for his fruitful discussions and valuable suggestions in improving the quality of the manuscript. The corresponding author would like to thank Department of Science & Technology (DST), India for providing the financial support through the reference number DST/INSPIRE/04/2017/001185. We thank the anonymous referees for their critical comments in improving the quality of the manuscript.

Deleted: two

Formatted: Font:Bold

Formatted: Centered, Space After: 8 pt, Line spacing: multiple 1.08 li, Widow/Orphan control, Adjust space between Latin and Asian text, Adjust space between Asian text and numbers

References

Albrecht, B.A.: Aerosols, cloud microphysics, and fractional cloudiness, *Science*, 245, 1227–1230, 1989.

Awaka, J., Iguchi, T., and Okamoto, K.: TRMM PR standard algorithm 2A23 and its performance on bright band detection, *J. Meteorol. Soc. Jpn*., 87A, 31–52, 2009.

Bhat, G. S., Gadgil, S., Kumar, P. V. H., Kalsi, S. R., Madhusoodanan, P., Murty, V. S., Rao, C. V. P., Babu, V. R., Rao, L.V., Rao, R. R., Ravichandran, M., Reddy, K.G., Rao, P. S., Sengupta, D., Sikka, D. R., Swain, J., and Vinayachandran, P. N.: BOBMEX: The Bay of Bengal Monsoon Experiment, *Bull. Amer. Meteor. Soc.,* 82, 2217–2244, 2001.

Cao, Q., Hong, Y., Gourley, J. J., Qi, Y., Zhang, J., Wen, Y., and Kirstetter, P. E.: Statistical and physical analysis of the vertical structure of precipitation in the mountainous west region of the United States using 11+ years of space borne observations from TRMM precipitation radar, *J. Appl. Meteorol. Climatol.*, 52, 408-424, 2013.

Chaudhari, H. S., Pokhrel, S., Kulkani, A., Hazra, A., and Saha, S. K.: Clouds-SST relationship and interannual variability modes of Indian summer monsoon in the context of clouds and SSTs: observational and modelling aspects, *Int. J. Climatol.*, doi: 10.1002/ joc.4664, 2016.

Chaudhari, H. S., Pokhrel, S., Mohanty, S., and Saha, S. K.: Seasonal prediction of Indian summer monsoon in NCEP coupled and uncoupled model, *Theor. Appl. Climatol.*, 114, 459–477, doi:10.1007/s00704-013-0854-8, 2013.

Chen, Q., Fan, J., Hagos, S., Gustafson Jr., W. I., and Berg, L. K.: Roles of wind shear at different vertical levels: Cloud system organization and properties, J. Geophys. Res. Atmos., 120, 6551–6574, 2015.

Creamean, J. M., Suski, K. J., Rosenfeld, D., Cazorla, A., DeMott, P. J., Sullivan, R. C., White, A. B., Ralph, F. M., Minnis, P., Comstock, J. M., Tomlinson, J. M., Kimberly A., and

Prather, K. A.: Dust and biological aerosols from the Sahara and Asia influence precipitation in the western U.S., *Science*, 339, 1572–1578, doi:10.1126/science.1227279, 2013.

Dee, D. P., et al.: The ERA-Interim reanalysis: Configuration and performance of the data assimilation system, *Q. J. R. Meteorol. Soc.*, 137, 553–597, 2011.

Emanuel, K. A.: Atmospheric convection. Oxford University Press, Oxford, 1994.

Fabry, F., and Zawadzki, I.: Long-term radar observations of the melting layer of precipitation and their interpretation, *J. Atmos. Sci.,* 52, 838–851, 1995.

Feng, X., Haines, K., Liu, C., de Boisséson, E., and Polo, I., Improved SST-precipitation intraseasonal relationships in the ECMWF coupled climate reanalysis, *Geophys. Res. Lett.*, 45, 3664–3672, 2018.

Findlater, J.: A major low-level air current near the Indian Ocean during the northern summer, *Q. J. R. Meteorol. Soc.*, 95, 362–380, 1969.

Fu, Y., and Liu, G.: The variability of tropical precipitation profiles and its impact on microwave brightness temperatures as inferred from TRMM data, *J. Appl. Meteorol.*, 40, 2130–2143, 2001.

Gadgil, S., Joseph, P. V., and Joshi, N. V.: Ocean atmosphere coupling over monsoonal regions, *Nature*, 312, 141-143, 1984.

Gadgil, S.: Monsoon–ocean coupling. *Current Sci.,* 78, 309–323, 2000.

Geerts, B., and Dejene, T.: Regional and diurnal variability of the vertical structure of precipitation systems in Africa based on space borne radar data, *J. Clim.*, 18, 893–916, 2005.

Guo, J., Liu, H., Li, Z., Rosenfeld, D., Jiang, M., Xu, W., Jiang, J. H., He, J., Chen, D., Min, M., and Zhai, P.: Aerosol-induced changes in the vertical structure of precipitation: a perspective of TRMM precipitation radar, *Atmos. Chem. Phys*., 18, 13329-13343, https://doi.org/10.5194/acp-18-13329-2018, 2018.

Houze, R. A., and Churchill, D. D.: Mesoscale organization and cloud microphysics in a Bay of Bengal depression, *J. Atmos. Sci.*, 44, 1845–1867, 1987.

Houze, R. A., Rasmussen, K. L., Zuluaga, M. D., and Brodzik, S. R.: The variable nature of convection in the tropics and subtropics: A legacy of 16 years of the Tropical rainfall measuring mission satellite, *Rev. Geophys.*, 53, 994–1021, 2015.

Houze, R. A., Wilton, D. C., and Smull, B. F.: Monsoon convection in the Himalayan region as seen by the TRMM precipitation radar, *Q. J. R. Meteorol. Soc.,* 133, 1389-1411, 2007.

Houze, R. A.: Mesoscale convective systems, *Rev. Geophys.*, 42, RG4003, doi: 10.1029/2004RG000150, 2004.

Hsu, N., Tsay, S., King, M., and Herman, J.: Aerosol properties over bright-reflecting source regions, *Geosci. Remote Sens. IEEE Trans.*, 42, 557–569, 2004.

Hubanks, P., King, M., Platnick, S., and Pincus, R.: MODIS atmosphere L3 gridded product algorithm theoretical basis document collection 005 Version 1.1, Tech. Rep. ATBD-MOD-30, NASA, 2008.

Iguchi, T., Kozu, T., Kwiatkowski, J., Meneghini, R., Awaka, J., and Okamoto, K.: Uncertainties in the rain profiling algorithm for the TRMM precipitation radar, *J. Meteor. Soc. Japan*, 87A, 1–30, doi:10.2151/jmsj.87A.1, 2009.

Krishnamurti, T. N.: Summer monsoon experiment – A review. *Mon. Wea. Rev.*, 113, 1590-1626, 1985.

Krishnamurti, T.: Cooling of the Arabian Sea and the onset-vortex during 1979. Recent progress in equatorial oceanography: A report of the final meeting of SCOR WORKING GROUP 47 in Venice, Italy, 1-12, 1981. [Available from Nova Univ., Ocean Science Center, Dania, FL 33004].

Kumar, S., Hazra, A., and Goswami, B. N.: Role of interaction between dynamics,

Formatted: Pattern: Clear

thermodynamics and cloud microphysics on summer monsoon precipitating clouds over the Myanmar coast and the Western Ghats, *Clim. Dyn.*, 43, 911–924, doi:10.1007/s00382-013-1909-3, 2014.

Levy, R., Remer, L., Mattoo, S., Vermote, E., and Kaufman, Y.: Second-generation operational algorithm: Retrieval of aerosol properties over land from inversion of moderate resolution imaging spectroradiometer spectral reflectance, *J. Geophys. Res.*, 112, D13, doi:10.1029/2006JD007811, 2007.

Li, R., and Min, Q.-L.: Impacts of mineral dust on the vertical structure of precipitation, J. Geophys. Res., 115, D09203, doi:10.1029/2009JD011925, 2010.

Liu, C., Zipser, E., and Nesbitt, S. W.: Global distribution of tropical deep convection: Different perspectives using infrared and radar as the primary data source, *J. Climate*, 20, 489-503, 2007.

Liu. C., and Zipser, E. J.: Why does radar reflectivity tend to increase downward toward the ocean surface, but decrease downward toward the land surface?, *J. Geophys. Res. Atmos.*, 118, 135-148, doi: 10.1029/2012JD018134, 2013.

Meenu, S., Parameswaran, K., and Rajeev, K.: Role of sea surface temperature and wind convergence in regulating convection over the tropical Indian Ocean, *J. Geophys. Res. Atmos.*, 117, D14102, 2012.

Nair, A. K. M., and Rajeev, K.: Multiyear CloudSat and CALIPSO observations of the dependence of cloud vertical distribution on sea surface temperature and tropospheric dynamics, *J. Clim.*, 27, 672–683, doi:10.1175/JCLI-D-13-00062.1, 2014.

Narayanan, M. S., and Rao, B. M.: Detection of monsoon inversion by TIROS-N satellite, *Nature*, 294, 546-548, 1981.

Nuijens, L., Emanuel, K., Masunaga, H., and L'Ecuyer, T.: Implications of warm rain in shallow cumulus and congestus clouds for large-scale circulations, *Surv. Geophys.*, 38,

Deleted: .

1257-1282, 2017.

Oueslati, B., and Bellon, G.: The double ITCZ bias in CMIP5 models: interaction between SST, large-scale circulation and precipitation. *Clim. Dyn.*, 44, 585-607, 2015.

Platnick, S., et al.: The MODIS cloud optical and microphysical products: Collection 6 updates and examples from Terra and Aqua, *IEEE Trans. Geosci. Remote Sens*., 55, 502–525, doi:10.1109/TGRS.2016.2610522, 2017.

Rajeevan, M., Unnikrishnan, C. K., and Preethi, B.: Evaluation of the ENSEMBLES multi-model seasonal forecasts of Indian summer monsoon variability, *Clim. Dyn.*, 38, 2257–2274, 2012.

Rajendran, K., Nanjundiah, R. S., Gadgil, S., and Srinivasan, J.: How good are the simulations of tropical SST–rainfall relationship by IPCC AR4 atmospheric and coupled models?, *J. Earth Sys. Sci.*, 121(3), 595–610, 2012.

Rajendran, K., Gadgil, S. and Surendran, S.: Monsoon season local control on precipitation over warm tropical oceans, *Meteorol. Atmos. Phys*., doi:10.1007/s00703-018-0649-7, 2018.

Rao, T. N., Kirankumar, N. V. P., Radhakrishna, B., Rao, D. N., and Nakamura, K.: Classification of tropical precipitating systems using wind profiler spectral moments. Part I: Algorithm description and validation, *J. Atmos. Oceanic Technol.,* 25, 884–897, 2008.

Rao, T. N., Saikranthi, K., Radhakrisna, B., and Rao, S. V. B.: Differences in the climataological characteristics of precipitation between active and break spells of the Indian summer monsoon, *J. Clim.*, 29, 7797-7814, 2016.

Remer, L., Kaufman, Y., Tanr´e, D., Mattoo, S., Chu, D., Martins, J., Li, R., Ichoku, C., Levy, R., Kleidman, R., Eck, T., Vermote, E., and Holben, B.: The MODIS aerosol algorithm, products, and validation, *J. Atmos. Sci*., 62, 947–973, 2005.

Romatschke, U., Medina, S., and Houze, R. A.: Regional, seasonal, and diurnal variations of extreme convection in the South Asian region, *J. Clim.*, 23, 419 –439, 2010.

Rosenfeld, D., et al.: Global observations of aerosol-cloud-precipitation-climate interactions, *Rev. Geophys.*, 52, 750-808, doi:10.1002/2013RG000441, 2014.

Roxy, M., Tanimoto, Y., Preethi, B., Terray, P., and Krishnan, R.: Intraseasonal SST-precipitation relationship and its spatial variability over the tropical summer monsoon region, *Clim. Dyn.*, 41, 45-61, 2013.

Roxy, M.: Sensitivity of precipitation to sea surface temperature over the tropical summer monsoon region—and its quantification, *Clim. Dyn.*, 43, 1159-1169, 2014.

Sabin, T., Babu, C., and Joseph, P.: SST–convection relation over tropical oceans, *Int. J. Climatol*. 33, 1424–1435, 2012.

Saikranthi, K., Radhakrishna, B., Satheesh, S. K., and Rao, T. N.: Spatial variation of different rain systems during El Niño and La Niña periods over India and adjoining ocean, *Clim. Dyn.*, 50, 3671-3685, doi: 10.1007/s00382-017-3833-4, 2018.

Saikranthi, K., Rao, T. N., Radhakrishna, B., and Rao, S. V. B.: Morphology of the vertical structure of precipitation over India and adjoining oceans based on long-term measurements of TRMMPR, *J. Geophys. Res. Atmos.*, 119, 8433–8449, doi: 10.1002/2014JD021774, 2014.

Saikranthi, K., Radhakrishna, B., Rao, T. N., and Satheesh, S. K.: Differences in the association of sea surface temperature - precipitating systems over the Bay of Bengal and the Arabian Sea during southwest monsoon season. *Int. J. Climatol*., doi:10.1002/joc.6074, 2019.

Sathiyamoorthy, V., Mahesh, C., Gopalan, K., Prakash, S., Shukla, B. P., Mathur, A.: Characteristics of low clouds over the Arabian Sea, *J. Geophys. Res. Atmos.*, 118, 13489-13503, 2013.

Deleted: . :

Schumacher, C. and Houze, R. A.: Stratiform rain in the tropics as seen by the TRMM precipitation radar, *J. Climate.*, 16, 1739–1756, 2003.

Sengupta, D., Goswami, B. N., and Senan, R.: Coherent intraseasonal oscillations of ocean and atmosphere during the Asian summer monsoon, *Geophys. Res. Lett.*, 28, 4127–4130, 2001.

Shenoi, S. S. C., Shankar, D., and Shetye, S. R.: Differences in heat budgets of the near-surface Arabian Sea and Bay of Bengal: Implications for the summer monsoon, *J. Geophys. Res.*, 107(C6), 3052, doi:10.1029/2000JC000679, 2002.

Shige, S. and Kummerow, C.D.: Precipitation-Top Heights of Heavy Orographic Rainfall in the Asian Monsoon Region, *J. Atmos. Sci.,* 73, 3009–3024, 2016.

Shige, S., Nakano, Y., and Yamamoto, M. K.: Role of orography, diurnal cycle, and intraseasonal oscillation in summer monsoon rainfall over Western Ghats and Myanmar coast, *J. Climate*, 30, 9365–9381, doi:10.1175/JCLI-D-16-0858.1, 2017.

Sunilkumar, K., Rao, T. N., Saikranthi, K., and Rao, M. P.: comprehensive evaluation of multisatellite precipitation estimates over India using gridded rainfall data, *J. Geophys. Res. Atmos.*, 120, doi:10.1002/2015JD023437, 2015.

Takahashi, H. G., and Dado, J. M. B.: Relationship between sea surface temperature and rainfall in the Philippines during the Asian summer monsoon, *J. Meteor. Soc. Japan*,, 96 (3), 283−290, doi:10.2151/jmsj.2018-03, 2018.

Takayabu, Y. N., Shige, S., Tao, W., and Hirota, N.: Shallow and deep latent heating modes over tropical Oceans observed with TRMM PR spectral latent heating Data, *J. Climate,* 23, 2030–2046, 2010.

Tao, W.-K., Chen, J.-P., Li, Z., Wang, C., and Zhang, C.: Impact of aerosols on convective clouds and precipitation, *Rev. Geophys.*, 50, RG2001, doi:10.1029/2011RG000369, 2012.

Formatted: Pattern: Clear

Formatted: No widow/orphan control, Don't adjust space between Latin and Asian text, Don't adjust space between Asian text and numbers

Tao, W.-K., et al.: Retrieval of latent heating from TRMM measurements, *Bull. Am. Meteorol. Soc.*, 87, 1555–1572, 2006.

Twomey, S.: The influence of pollution on the short wave albedo of clouds, *J. Atmos. Sci.*, 34, 1149–1152, 1977.

Wallace, J. M., and Hobbs, P. V.: Atmospheric science: An introductory survey, Second edition, Academic press, pp. 85, 2006.

Wang, B., Ding, Q., Fu, X., Kang, I.-S., Jin, K., Shukla, J., and Doblas-Reyes, F.: Fundamental challenge in simulation and prediction of summer monsoon rainfall, *Geophys. Res. Lett.*, 32, L15711, doi:10.1029/2005GL022734, 2005.

Weller, R. A., Farrar, J. T., Buckley, J., Mathew, S., Venkatesan, R., Lekha, J. S., Chaudhuri, D., Kumar, N. S., and Kumar, B. P.: Air-sea interaction in the Bay of Bengal, *Oceanography*, 29(2), 28–37, 2016.

Woolnough, S.J., Slingo, J.M., and Hoskins, B.J.: The relationship between convection and sea surface temperature on intraseasonal timescales, *J. Climate,* 13, 2086–2104, 2000.

Wu, R., and Kirtman, B. P.: Roles of Indian and Pacific Ocean air–sea coupling in tropical atmospheric variability, *Clim. Dyn.*, *25*(2–3), 155–170, 2005.

Figure captions

Figure 1: Spatial distribution of ISM mean SST (in °C) obtained from ERA-Interim reanalysis data over the AS (63°E-72°E & 8°N-20°N) and the BOB (83°E-92°E & 8°N-21°N). The regions considered in this analysis over these two seas are shown with the boxes.

Figure 2: (a) and (b) represent the altitudinal distribution of occurrence of conditional reflectivity (≥ 17 dBZ) as a function of SST with respect to precipitation occurrence at that particular SST interval over the AS and the BOB, respectively.

Figure 3: (a), (d) and (b), (e) represent vertical profiles of median reflectivity correspond to deep systems and their standard deviation (in dBZ) with SST over the AS and the BOB, respectively during the ISM season. (c) and (f) show the number of conditional reflectivity pixels at each altitude used for the estimation of the median and standard deviation.

Figure 4: Same as Fig. 3 but for shallow precipitating systems.

Figure 5: (a) and (b), respectively, represent the vertical profiles of mean θ_e (in K) with SST over the AS and the BOB during the ISM season. (c) and (d) and (e) and (f) are same as (a) and (b) but for mean vertical velocity (in Pa s^{-1}) and wind gradient with reference to 950 hPa level (in m s^{-1}).

Figure 6: (a) Mean and standard error of AOD and (b) TCWV (in mm) with SST over the AS and the BOB during ISM.

Figure 7: Variation of mean and standard error of CER liquid (in µm) with SST over the AS and the BOB during the ISM season.

Figures

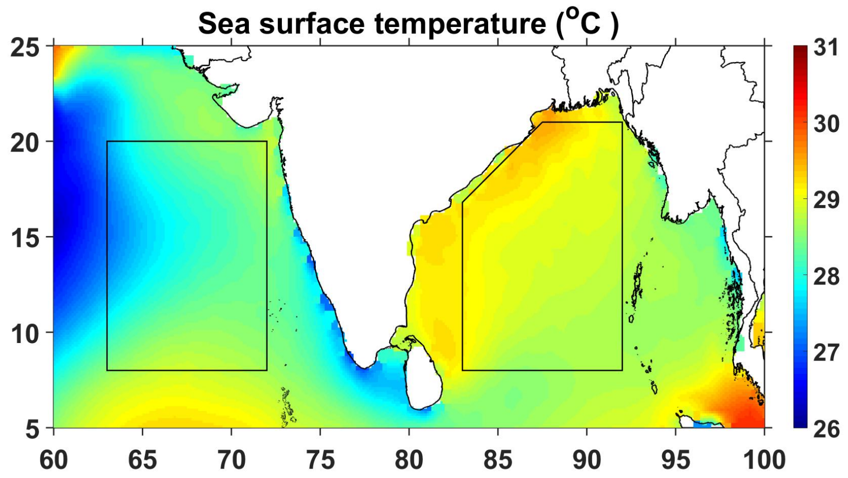

Figure 1: Spatial distribution of ISM mean SST (in °C) obtained from ERA-Interim reanalysis data over the AS (63°E-72°E & 8°N-20°N) and the BOB (83°E-92°E & 8°N-21°N). The regions considered in this analysis over these two seas are shown with the boxes.

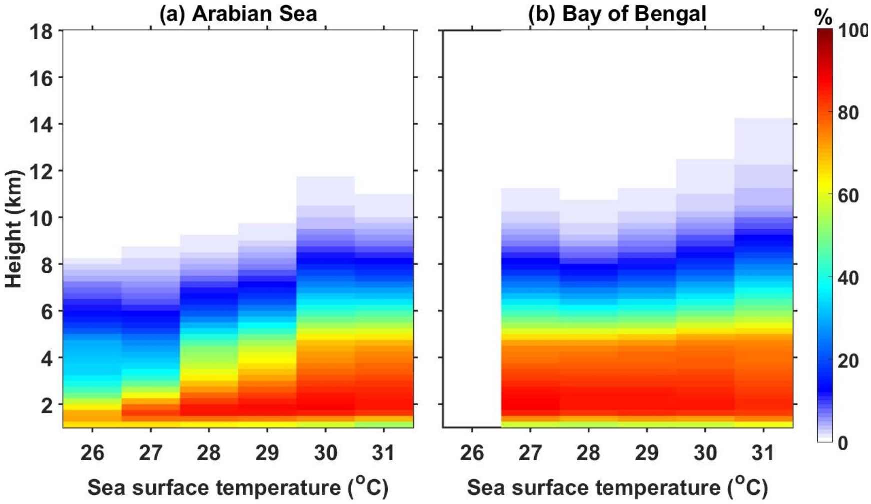

Figure 2: (a) and (b) represent the altitudinal distribution of occurrence of conditional reflectivity (≥ 17 dBZ) as a function of SST with respect to precipitation occurrence at that particular SST interval over the AS and the BOB, respectively.

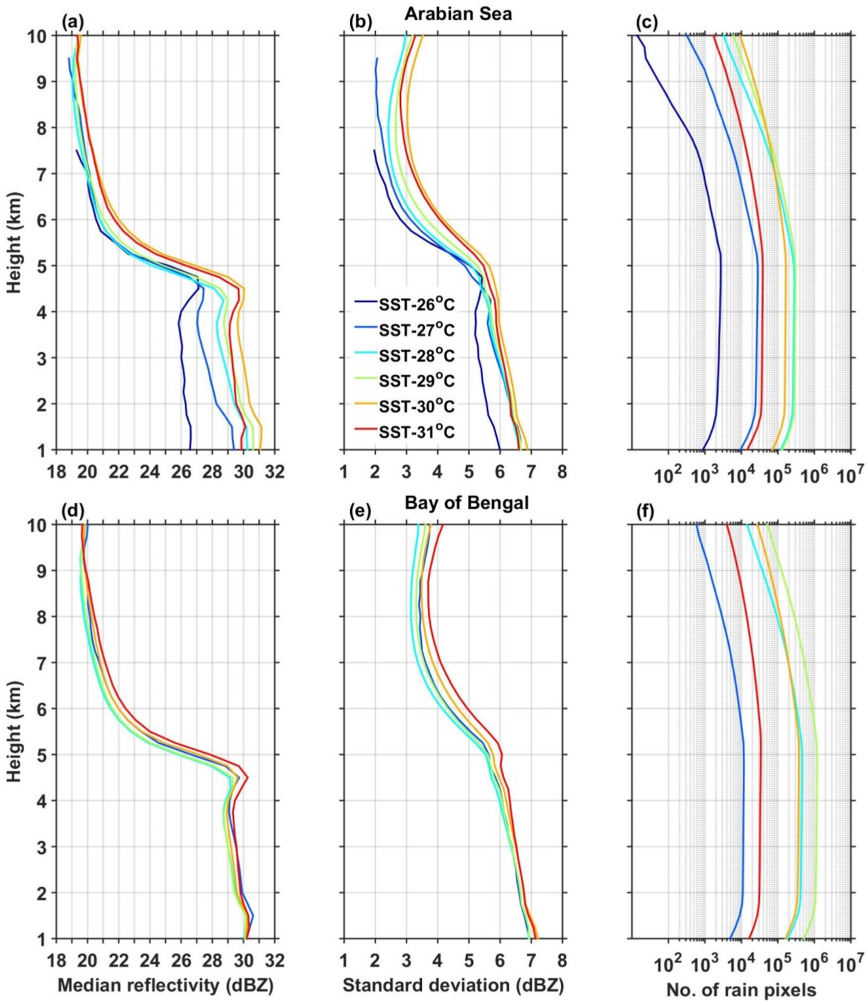

Figure 3: (a), (d) and (b), (e) represent vertical profiles of median reflectivity correspond to deep systems and their standard deviation (in dBZ) with SST over the AS and the BOB, respectively during the ISM season. (c) and (f) show the number of conditional reflectivity pixels at each altitude used for the estimation of the median and standard deviation.

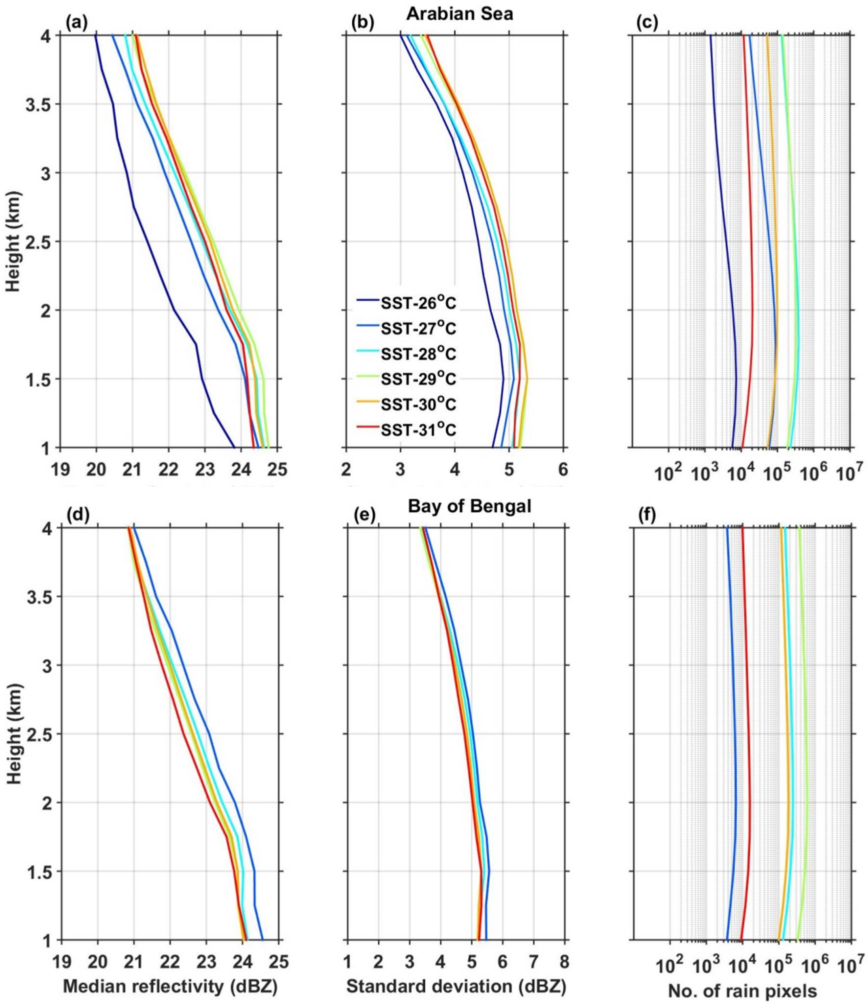

Figure 4: Same as Fig. 3 but for shallow precipitating systems.

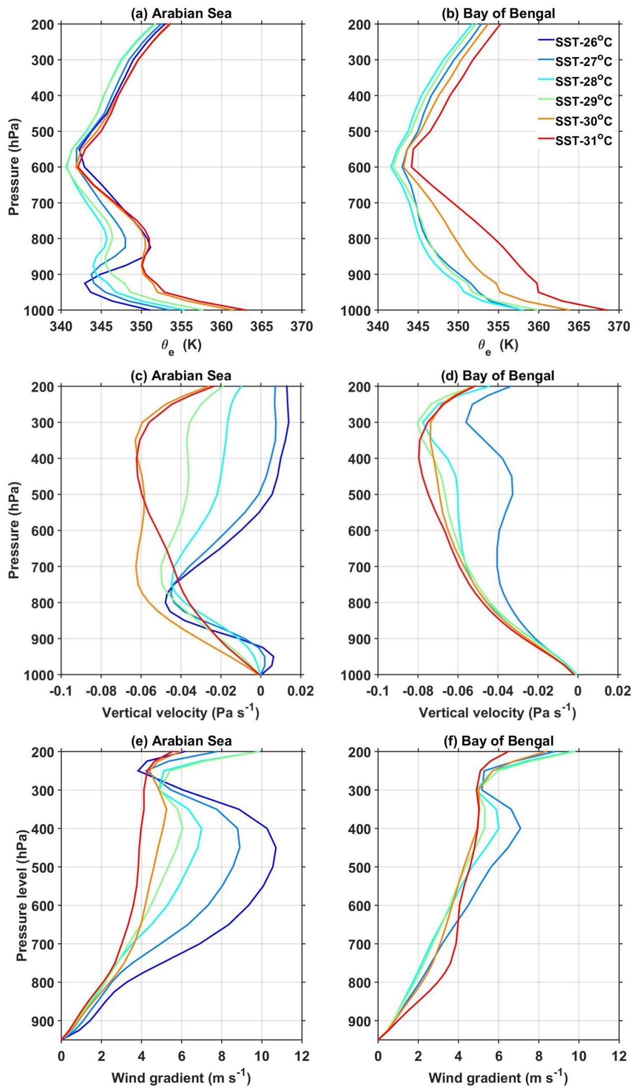

Figure 5: (a) and (b), respectively, represent the vertical profiles of mean θ_e (in K) with SST over the AS and the BOB during the ISM season. (c) and (d) and (e) and (f) are same as (a) and (b) but for mean vertical velocity (in Pa s^{-1}) and wind gradient with reference to 950 hPa level (in m s^{-1}).

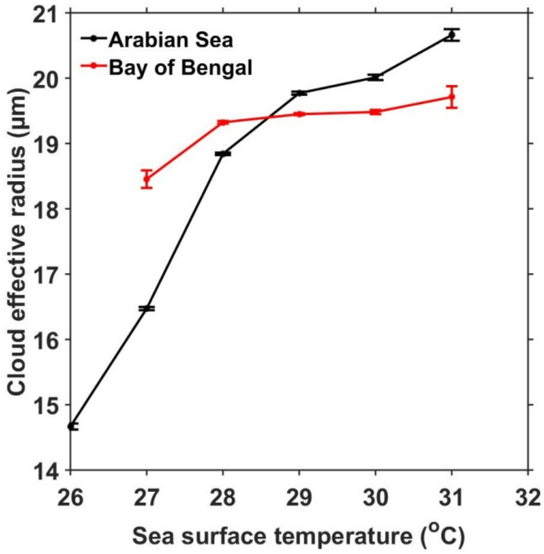

Figure 6: Variation of mean and standard error of CER liquid (in μm) with SST over the AS and the BOB during the ISM season.

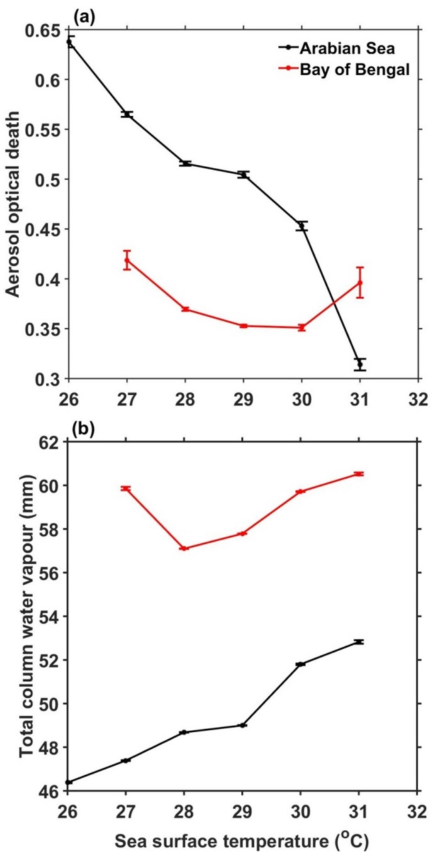

Figure 7: (a) Mean and standard error of AOD and (b) TCWV (in mm) with SST over the AS and the BOB during ISM.

Supplementary material

Satheesh et al. (2006) showed an increase in AOD with increase in latitude over the AS due to the dust advection from Arabia desert regions during ISM season, whereas SST decreases with increase in the latitude. In other words the SST is low and AOD is high in northern AS whereas over the southern AS, SST is high and AOD is low. This contrasting spatial distribution of AOD and SST could cause a negative correlation between AOD and SST as depicted in Fig. 6a. To examine whether the observed decrease in AOD with increase in SST over the AS is due to the latitudinal variation of AOD or exists at all latitudes, we have segregated the data into 2° latitude bins and plotted the mean AOD with SST for all bins and is depicted in Fig. S2. In spite of the magnitude, AOD variation with SST is nearly similar at all latitudes of the AS, i.e., the higher AOD is observed at lower SSTs and vice versa (Fig. S2a). On the other hand the latitudinal variation of AOD with SST over the BOB shown in Fig. S2b also show a decrease in AOD with SST till 30 °C but the magnitude of variation is trivial relative to the AS. Also, as depicted in Fig. 6a AOD increases above 30 °C with SST over the BOB. This indicates that though there is a difference in magnitude of variation, AOD varies with SST over both the seas at all latitudes. This analysis is repeated using the multi-angle imaging spectroradiometer (MISR) dataset (which is not shown here) for small, medium large aerosol particles. Interestingly all three types also show a decrease in AOD with rise in SST over both the seas.

Formatted: Indent: First line: 0 cm

Satheesh, S. K., Moorthy, K. K., Kaufman, Y. J., and Takemura, T.: Aerosol Optical depth, physical properties and radiative forcing over the Arabian Sea, *Meteorol. Atmos. Phys.*, 91, 45–62, doi:10.1007/s00703-004-0097-4, 2006.

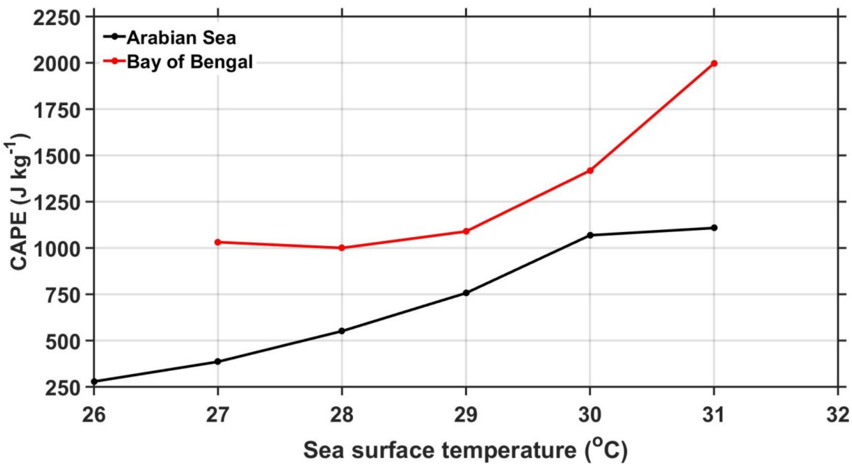

Figure S1: Variation of mean CAPE (in J kg^{-1}) with SST over the AS and the BOB during the ISM season.

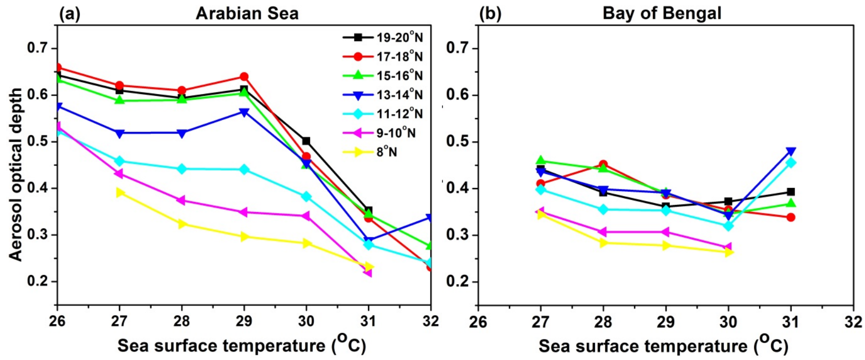

Figure S2: (a) and (b), respectively, represent latitudinal variation (for every 2° latitude interval) of mean AOD over the AS (between 63°E and 72°E) and the BOB (between 83°E and 92°E).

At the outset we thank the reviewer for constructive comments that improved the quality of the manuscript.

Comment: Under weak wind regimes, the reflectivity for deep and shallow systems decreases with increase in SST over AS (Figs. R1 and R3). Why? Is this consistent with the authors' argument that the variations seen in reflectivity are originated in the cloud formations stage itself? This point should be discussed in the manuscript.

Reply: It is true that the reflectivity pattern with SST is somewhat different for weak wind category for reasons not known at present. But, it appears to be interesting and will be pursued later. However, our argument that the variations in reflectivity are originated in the cloud formation is based on TCW, CER and AOD data. To examine the validity of this statement at weak wind regime, we have segregated the above data for weak wind conditions and plotted below for reviewers' reference. The variation of TCW, CER and AOD with SST for weak wind regime is very similar to that of total data, indicating that our argument is still valid even for weak wind regime.

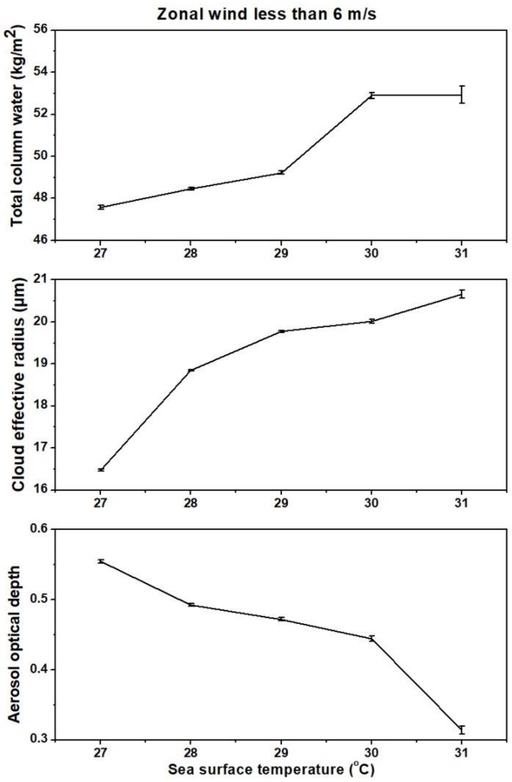

Figure R1: *Variation of mean and standard error of TCW (in kg m^{-2}), CER liquid (in μm) and AOD with SST over the AS during week wind regime.*

Comment: The authors should note their assumption that the microphysical process at all SST's is same in the manuscript.

Reply: Reflectivity profiles show an increase with decreasing height over both seas, albeit with varying magnitude. It indicates that the microphysical growth processes could be the same at all SST's but their efficacy could be different owing to ambient atmospheric conditions.

Comment: Again, the authors should explain the definition of deep and shallow systems (not just refer to Houze et al. 2007) in the manuscript.

Reply: *The deep and shallow systems definitions are included in the revised manuscript. "Profiles are classified as deep (shallow), if their storm top reflectivity ≥ 17 dBZ lies above (1 km below) the 0°C isotherm".*

Comment: L38: Tropical rainfall measuring mission should be Tropical Rainfall Measuring Mission.

Reply: *The typos are corrected in the revised manuscript.*

Comment: L92: tropical rainfall measuring mission should be Tropical Rainfall Measuring Mission.

Reply: *The typos are corrected in the revised manuscript.*

Comment: L103: I would suggest the authors add Tao et al. (2016).

Reply: *The reference is added in the revised manuscript.*

Tao, W.-K., Y. N. Takayabu, S. Lang, S. Shige, W. Olson, A. Hou, G. Skofronick-Jackson, X. Jiang, C. Zhang, W. Lau, T. Krishnamurti, D. Waliser, M. Grecu, P. E. Ciesielski, R. H. Johnson, R. Houze, R. Kakar, N. Nakamura, S. Braun, R. Oki, and A. Bhardwaj, 2016: TRMM Latent Heating Retrieval: Applications and Comparisons with Field Campaigns and Large-Scale Analyses, Meteorological Monographs - Multi-scale Convection-Coupled Systems in the Tropics: A tribute to Dr. Michio Yanai, 56, 2.1-2.34, DOI: 10.1175/AMSMONOGRAPHS-D-15-0013.1.

Comment: L295: the particle size should be the precipitating particle size.

Reply: *'particle size' is replaced with 'precipitating particle size' in the revised manuscript.*

Comment: L305-307: Change in fall speed from ice hydrometers to raindrops should be added.

Reply: *The text "change in fall speed from ice hydrometers to raindrops" is added in the revised manuscript.*

Comment: p. 29: The figure should be Figure 7. p. 30: The figure should be Figure 6.

Reply: *The figures are interchanged in the revised manuscript.*

Variability of vertical structure of precipitation with sea surface temperature over the Arabian Sea and the Bay of Bengal as inferred by TRMM PR measurements

Kadiri Saikranthi[1], Basivi Radhakrishna[2], Thota Narayana Rao[2] and

Sreedharan Krishnakumari Satheesh[3]

[1] *Department of Earth and Climate Science, Indian Institute of Science Education and Research (IISER), Tirupati, India.*

[2] *National Atmospheric Research Laboratory, Department of Space, Govt. of India, Gadanki - 517112, India.*

[3] *Divecha Centre for Climate Change, Centre for Atmospheric and Oceanic Sciences, Indian Institute of Science, Bangalore - 560012, India.*

Address of the corresponding author
Dr. K. Saikranthi,
Department of Earth and Climate Science,
Indian Institute of Science Education and Research (IISER),
Tirupati,

Andhra Pradesh, India.
Email: ksaikranthi@gmail.com

Abstract

Tropical ~~rainfall measuring mission~~Rainfall Measuring Mission precipitation radar measurements are used to examine the variation of vertical structure of precipitation with sea surface temperature (SST) over the Arabian Sea (AS) and Bay of Bengal (BOB). The variation of reflectivity and precipitation echo top with SST is remarkable over the AS but small over the BOB. The reflectivity increases with SST (from 26°C to 31°C) by ~1 dBZ and 4 dBZ above and below 6 km, respectively, over the AS while, its variation is < 0.5 dBZ over the BOB. The transition from shallow storms at lower SSTs (≤ 27°C) to deeper storms at higher SSTs is strongly associated with the decrease in stability and mid-tropospheric wind shear over the AS. Contrary, the storms are deeper at all SSTs over the BOB due to weaker stability and mid-tropospheric wind shear. At lower SSTs, the observed high aerosol optical depth (AOD) and low total column water (TCW) over AS results in small cloud effective radius (CER) and weaker reflectivity. As SST increases, AOD decreases and TCW increases leading to large CER and high reflectivity. The changes in these parameters with SST are marginal over the BOB and hence the CER and reflectivity. The predominance of collision-coalescence process below the bright band is responsible for the observed negative slopes in the reflectivity over both the seas. The observed variations in reflectivity are originated at the cloud formation stage over both the seas and these variations are magnified during the descent of hydrometeors to ground.

1. Introduction

Indian summer monsoon (ISM - June through September) is one of the most complex weather phenomena, involving coupling between the atmosphere, land and ocean. At the boundary of the ocean and atmosphere air-sea interactions play a key role for the coupled Earth system (Wu and Kirtman 2005; Feng et al. 2018). The sea surface temperature (SST) – precipitation relations are the important measures for the air-sea interactions on different temporal scales (Woolnough et al., 2000; Rajendran et al. 2012). Recent studies (Wang et al. 2005; Rajeevan et al. 2012; Chaudhari et al. 2013; 2016; Weller et al. 2016; Feng et al. 2018) have shown that the simulation of ISM can be improved with the exact representation of SST - precipitation relationship. SST modulates the meteorological factors that influence the formation and evolution of different kinds of precipitating systems over tropical oceans (Gadgil et al. 1984; Schumacher and Houze, 2003; Takayabu et al. 2010; Oueslati and Bellon 2015).

The studies dealing with SST and cloud/precipitation population considered whole Indian Ocean as a single entity (Gadgil et al. 1984; Woolnough et al., 2000; Rajendran et al. 2012; Sabin et al. 2012; Meenu et al. 2012; Nair and Rajeev 2014; Roxy 2014). But in reality the Bay of Bengal (BOB) and the Arabian Sea (AS) of Indian Ocean possess distinctly different features (Kumar et al. 2014; Shige et al. 2017; Rajendran et al. 2018; Saikranthi et al. 2019). The monsoon experiment (MONEX) and Bay of Bengal monsoon experiment (BOBMEX) have shown how these two seas are different with respect to each other, in terms of SST, back ground atmosphere and the occurrence of precipitating systems (Krishnamurti 1985; Houze and Churchill 1987; Gadgil 2000; Bhat et al. 2001). The SST in the AS cools between 10 °N and 20 °N during the monsoon season whereas warming is seen in other global Oceans between the same latitudes (Krishnamurthi 1981). SST variability is large over the AS than the BOB at seasonal and intraseasonal scales (Sengupta et al. 2001; Roxy et al. 2013). The monsoonal winds (in particular the low-level jet) are stronger over the AS than BOB (Findlater 1969). Also, lower-tropospheric thermal inversions are more frequent and stronger over the AS than BOB (Narayanan and Rao 1981; Sathiyamoorthy et al. 2013). Thus, the atmospheric and sea surface conditions and in turn the occurrence of different kinds of precipitating systems are quite different over the BOB and the AS during the ISM period. For instance, long-term measurements of ~~tropical rainfall measuring mission~~Tropical Rainfall Measuring Mission (TRMM) precipitation radar (PR) have shown that shallow systems are more prevalent over the AS, while deeper systems occur frequently over the BOB (Liu et al. 2007; Romatschke et al. 2010; Saikranthi et al. 2014, 2018; Houze et al. 2015).

The aforementioned studies mainly focused on the morphology of vertical structure of precipitation, but, none of them studied the variation of vertical structure of precipitation (in terms of occurrence and intensity) with SST and the differences in the vertical structure over AS and BOB. On the other hand, information on the vertical structure of precipitation is essential for improving the accuracy of rainfall estimation (Fu and Liu 2001; Sunilkumar et al. 2015), understanding the dynamical and microphysical processes of hydrometeor growth/decay mechanisms (Houze 2004; Greets and Dejene 2005; Saikranthi et al. 2014; Rao et al. 2016) and for improving the latent heating retrievals (Tao et al. 2006, 2016). SST being the main driving force to trigger precipitating systems through air-sea interactions (Sabin et al. 2012; Nuijens et al. 2017), can alter the vertical structure of precipitation (Oueslati and Bellon 2015). Therefore, the present study aims to understand the variation of vertical structure of precipitation (in terms of precipitation top height and intensity) with SST over the AS and BOB. Besides the SST, vertical structure can be modified by aerosols (or CCN, mostly at the cloud formation stage) and thermodynamics of the ambient atmosphere. For instance, recent studies have shown the impact of surface PM_{10} aerosols in altering the vertical structure of precipitation (Guo et al., 2018). All these parameters, therefore, are considered in the present study to explain the differences in the vertical structure.

2. Data

The present study utilizes 16 years (1998-2013) of TRMM-PR's 2A25 (version 7) dataset, comprising of vertical profiles of attenuation corrected reflectivity (Iguchi et al. 2009), during the ISM. The range resolution of TRMM-PR reflectivity profiles is 250 m with a horizontal footprint size of ~4.3 and 5 km before and after the boosting of its orbit from 350 km to 403 km, respectively. It scans ±17° from nadir with a beam width of 0.71° covering a swath of 215 km (245 km after the boost). The uniqueness of TRMM-PR data is its ability in pigeonholing the precipitating systems into convective, stratiform and shallow rain. This classification is based on two methods namely the horizontal method (H - method) and the vertical method (V - method) (Awaka et al. 2009). The original TRMM-PR 2A25 vertical profiles of attenuation corrected reflectivity are gridded to a three dimensional Cartesian coordinate system with a spatial resolution of 0.05° × 0.05°. The detailed methodology of interpolating the TRMM-PR reflectivity data into the 3D Cartesian grid is discussed in Houze et al. (2007). This dataset is available at the University of Washington website (http://trmm.atmos.washington.edu/). Profiles are classified as deep (shallow), if their storm top reflectivity ≥ 17 dBZ lies above (1 km below) the 0°C isotherm.

To understand the observed variations in the vertical structure of precipitation in the light of microphysics of clouds, Moderate Resolution Imaging Spectroradiometer (MODIS) AQUA satellite level 3 data (MYD08) are considered. In particular, the daily atmospheric products of aerosol optical depth (AOD) (Hubanks et al. 2008) and cloud effective radius (CER) liquid (Platnick et al. 2017) during the period 2003 and 2013 have been used. MODIS AOD dataset is a collection of aerosol optical properties at 550 nm wavelength, as well as particle size information. Level 2 MODIS AOD is derived from radiances using either one of the three different algorithms, i.e., over ocean Remer et al. (2005) algorithm, over land the Dark-Target (Levy et al. 2007) algorithm and for brighter land surfaces the Deep-Blue (Hsu et al. 2004) algorithm. CER is nothing but the weighted mean of the size distribution of cloud drops i.e., the ratio of third moment to second moment of the drop size distribution. In the level 3 MODIS daily dataset, aerosol and cloud products of level 2 data pixels with valid retrievals within a calendar day are first aggregated and gridded to a daily average with a spatial resolution of 1° × 1°. For CER grid box values, CER values are weighted by the respective ice/liquid water cloud pixel counts for the spatiotemporal aggregation and averaging processes.

The background atmospheric structure (winds and total column water) and SST information are taken from the European Centre for Medium Range Weather Forecasting (ECMWF) Interim Reanalysis (ERA) (Dee et al. 2011). ERA-Interim runs 4DVAR assimilation twice daily (00 and 12 UTC) to determine the most likely state of the atmosphere at a given time (analysis). The consistency across variables in space and time (during 12-hour intervals) is thus ensured by the atmospheric model and its error characteristics as specified in the assimilation. ERA-Interim is produced at T255 spectral resolution (about 0.75°, ~ 83 km) with a temporal resolution of 6h for upper air fields and 3h for surface fields. The original 0.75° × 0.75° spatial resolution gridded dataset is rescaled to a resolution of 0.125° × 0.125°. The temporal resolution of the dataset used in the present study is 6h (00, 06, 12 and 18 UTC). The equivalent potential temperature (θ_e) is estimated from the ERA-Interim datasets using the following formula (Wallace and Hobbs 2006):

$$\theta_e = \theta exp\left(\frac{L_V w_s}{C_p T}\right) \tag{1}$$

where θ is the potential temperature, L_v is the latent heat of vaporization, w_s is the saturation mixing ratio, C_p is the specific heat at constant pressure and T is the absolute temperature.

The variation of vertical structure of precipitation with SST are studied by considering the dataset between 63 °E – 72 °E and 8 °N – 20 °N over the AS and 83 °E – 92 °E and 8 °N – 21 °N over the BOB. These regions of interest along with the ISM seasonal mean SST over the two seas are depicted in Fig. 1. These regions are selected in such a way that the costal influence on SST is eluded from the analysis. As the rainfall is scanty over the western AS (west of 63°E latitude) during the ISM (Saikranthi et al. 2018), this region is also not considered in the present analysis. The seasonal mean SST is higher over the BOB than in the AS by more than 1 °C during the ISM season, in agreement with Shenoi et al. (2002). The nearest space and time matched SST data from ERA-Interim are assigned to the TRMM-PR and MODIS observations for further analysis.

3. Variation of vertical structure of precipitation with SST

The occurrence (in terms of %) of conditional precipitation echoes ($Z \geq 17$ dBZ) at different altitudes as a function of SST over the AS and the BOB is shown in Fig. 2. The variation of precipitation echo occurrence frequency with SST is quite different over both the seas. The top of the precipitation echoes extends to higher altitudes with increasing SST over the AS, while such variation is not quite evident over the BOB. Precipitation echoes are confined to < 8 km at lower SST (< 28 °C) over the AS, but exhibits a gradual rise in height with increase in SST. Large population density of precipitation echoes at lower altitudes is mainly due to the abundant occurrence of shallow storms over the AS (Saikranthi et al. 2014, 2019; Rao et al. 2016). Interestingly, the occurrence of precipitation echoes is seen at higher altitudes even at lower SSTs over the BOB, indicating the presence of deeper storms. Such systems exist at all SST's over the BOB.

To examine the variation of reflectivity profiles with SST, median profiles of reflectivity in each SST bin are computed over the AS and the BOB separately for deep and shallow systems and are depicted in Figs. 3 & 4, respectively. The space- and time-matched conditional reflectivity profiles are grouped into 1°C SST bins and then the median is estimated at each height, only if the number of conditional reflectivity pixels (Figs. 3c; 3f; 4c & 4f) is greater than 500. The median reflectivity profiles corresponding to the deep systems are distinctly different over the AS and the BOB (Figs. 3a & 3d), even at the same SST. Over the AS, reflectivity of deep systems at different SSTs shows small variations (≤ 1 dBZ) above the melting region (> 5 km), but varies significantly (~ 4.5 dBZ) below the melting level (< 5 km). These variations in reflectivity profiles with SST are negligible (< 0.5 dBZ) over the BOB both above and below the melting region. The reflectivity increases from ~ 26.5 dBZ to ~ 31 dBZ, with increase in SST from 26 °C to 30 °C over the AS, but it is almost the same (~ 30dBZ) at all SST's over the BOB below the melting layer. The standard deviation of reflectivity, representing the variability in reflectivity within the SST bin, is similar at all SSTs over both the seas except for the 26 °C SST over AS. At this SST, the standard deviation is lesser by ~ 1 dBZ than that of other SSTs.

The median reflectivity profiles of shallow storms depicted in Figs. 4a & 4d also show a gradual increase in reflectivity from 20 dBZ to ~ 22 dBZ as SST changes from 26 °C to 31 °C at the precipitation top altitude over the AS and don't show any variation with SST over the BOB. However at 1 km altitude, except at 26 °C SST over the AS, the reflectivity variation with SST is not substantial over both the seas. The standard deviation of reflectivity profiles show ~ 1 dBZ variation with SST (from 26 °C to 31°C) at all altitudes over the AS and don't show any variation over the BOB. The standard deviation of reflectivity for shallow storms varies from 3 to 4 dBZ at the precipitation top altitude and 4.5 to 5.3 dBZ at 1 km altitude over the AS while it shows ~ 4 dBZ at precipitation top and ~ 5.5 dBZ at 1 km altitude over the BOB.

4. Factors affecting the vertical structure of precipitation and their variability with SST

The formation and evolution of precipitating systems over oceans depend on dynamical, thermodynamical and microphysical factors, like SST, wind shear, vertical wind velocity, stability, CER, etc., and need to be considered for understanding the vertical structure of precipitation (Li and Min 2010; Creamean et al. 2013; Chen et al. 2015; Shige and Kummerow 2016; Guo et al 2018).

4.1. Dynamical and thermodynamical factors:

Takahashi and Dado (2018) have shown that zonal wind variations can also explain some variability of rain. To examine the impact of zonal wind on rainfall over the Arabian Sea and Bay of Bengal, the data are segregated into 3 wind regimes as weak (monsoon westerlies lies between 0 and 6 m s^{-1}), moderate (monsoon westerlies lies between 6 to 12 m s^{-1}) and strong (monsoon westerlies > 12 m s^{-1}) winds. The median vertical profiles of reflectivity are computed for each SST bin corresponding to deep and shallow systems (not shown here). Two important observations are noted from these figures. 1) Vertical profiles of reflectivity show considerable variation (2-5 dBZ) in all wind categories over the Arabian Sea, but such variations are absent over the Bay of Bengal. It implies that the reported differences in reflectivity profiles over the Arabian Sea and Bay of Bengal exist in all wind regimes. 2) The variation in reflectivity with SST increases with weak to strong wind regime over the Arabian Sea, indicating some influence of wind on reflectivity (rainfall) variation.

To understand the role of stability/instability, θ_e values computed from (1) using the ERA-Interim datasets during the ISM period over the AS and the BOB are averaged for a season and are depicted in Figs. 5(a) & 5(b), respectively. The surface θ_e (at 1000 hPa) values are larger over the BOB than those over AS for the same SST, indicating that the instability and convective available potential energy (CAPE) could be higher over the BOB. Indeed, higher CAPE is seen over the BOB (Fig. S1, calculated following Emanuel 1994) than AS at all SSTs by a magnitude > 300 J kg^{-1}. The θ_e increases with SST from 358 °K to 368 °K from 27 °C to 31 °C and from 350 °K to 363 °K from 26 °C to 31 °C over the BOB and the AS, respectively. The CAPE also increases with rise in SST over both the seas. To know the stability of the atmosphere θ_e gradients are considered. Irrespective of SST, positive gradients in θ_e are observed between 900 and 800 hPa levels over the AS indicating the presence of strong stable layers. The strength of these stable layers decreases with increasing SST. These stable layers are formed mainly due to the flow of continental dry warm air from Arabian Desert and Africa above the maritime air causing temperature inversions below 750 hPa level over the AS during the ISM period (Narayanan and Rao 1981). However over the BOB, such temperature inversions are not seen in the lower troposphere.

To understand the effect of wind field on the vertical structure of precipitation, profiles of ISM seasonal mean vertical wind velocity and vertical shear in horizontal wind at various SSTs over the AS and the BOB are shown in Figs. 5(c), 5(d) & 5(e), 5(f) respectively. The updrafts are prevalent at all SSTs throughout the troposphere over the BOB, whereas downdrafts are seen in the mid-troposphere (between 200 and 600 hPa levels) up to 27 °C and updrafts in the entire troposphere at higher SSTs over the AS. Also, the magnitude of the vertical wind velocity varies significantly with SST in the mid-troposphere over the AS. Over the BOB, the magnitude of updrafts increases with altitude in the lower and middle troposphere, but doesn't vary much with SST. In the mid-troposphere, updrafts are stronger by > 0.02 Pa S^{-1} over the BOB than over the AS. The profiles shown in Fig. 5(e) & 5(f) are the mean vertical shear in horizontal wind estimated following Chen et al. (2015) at different levels with reference to 950 hPa level. The wind shear increases with increasing altitude at all the SSTs up to 400 hPa, but the rate of increase is distinctly different between the AS and the

BOB at SSTs less than 28 °C and nearly the same at higher SSTs. The wind shear decreases systematically with SST (~ 1.5 m s^{-1} for 1° increase in SST) in the middle troposphere over the AS while the change is minimal over the BOB (~ 2 m s^{-1} for 27 °C and 31 °C).

Chen et al. (2015) highlighted the importance of mid-tropospheric wind shear in generating mesoscale local circulations, like low-level cyclonic and upper-level anticyclonic circulations. This feature is apparent over the AS, where down drafts are prevalent in mid-upper troposphere and updrafts in the lower troposphere at lower SSTs. As SST increases, the wind shear decreases and the updraft increases in the mid-troposphere. However, over the BOB the wind shear is relatively week when compared to the AS and hence the updrafts are seen up to 200 hPa level at all SSTs. The weaker CAPE and stable mid-troposphere coupled with upper- to mid- tropospheric downdrafts at lower SSTs over the AS inhibit the growth of precipitating systems to higher altitudes and in turn precipitate in the form of shallow rain. This result is in accordance with the findings of Shige and Kummerow (2016) that showed the static stability at lower levels inhibits the growth of clouds and promotes the detrainment of clouds over the Asian monsoon region and is considered as an important parameter in determining the precipitation top height. As SST increases large CAPE and updrafts in the middle troposphere collectively support the precipitating systems to grow to higher altitudes, as evidenced in Fig. 2a. On the other hand, large CAPE and updrafts in the middle troposphere prevalent over the BOB at all SSTs are conducive for the precipitating systems to grow to higher altitudes as seen in Fig. 2b.

4.2. Microphysical factors

The observed differences in reflectivity profiles of precipitation with SST could be originated at the cloud formation stage itself or manifested during the evolution stage or due to both. Information on AOD and CER would be ideal to infer microphysical processes at the cloud formation stage. CER values are mainly controlled by the ambient aerosols concentration and the available moisture (Twomey 1977; Albrecht 1989; Tao et al. 2012; and Rosenfeld et al. 2014). For fixed liquid water content, as the concentration of aerosols increases, the number of cloud drops increases and CER decreases (Twomey 1977). To understand the variation of AOD and total column water (TCW) and the resultant CER with SST, the mean AOD and TCW for different SST bins are plotted in Figs. 6a & 6b. The mean and standard error are calculated only when the number of data points is more than 100 in each SST bin. AOD decreases from 0.62 to 0.31 with rise in SST from 26 °C to 31 °C over the AS but only from 0.42 to 0.36 as SST varies from 27 °C to 30 °C and then increases at higher SSTs over the BOB. The variation of TCW with SST (Fig. 6b) shows a gradual increase with SST over the AS while it decreases initially from 27°C to 28°C, and then increases over the BOB. At a given SST the TCW is more in the BOB (> 8 mm) than in the AS.

The decrease in AOD and an increase in TCW with SST result in an increase in CER (14.7 μm to 20.8 μm from 26°C to 31°C) over the AS (Fig. 7). On the other hand, CER doesn't show much variation with SST (18.5 μm to 19.5 μm from 27°C to 31°C) over BOB due to smaller variations in AOD and TCW. This also shows that the cloud droplets are smaller in size at lower SSTs over the AS than BOB, while they are bigger and nearly equal in size at higher SSTs. Since, reflectivity is more sensitive to the precipitating particle size ($Z \propto D^6$), the smaller-sized hydrometeors at lower SSTs over the AS yield weaker reflectivity than over the BOB (both for deep and shallow systems). As the SST increases, CER as well as the reflectivity increases over the AS. At higher SSTs, the CER values are approximately equal over both the seas and in turn the observed reflectivities (Figs. 3a & 4a). This suggests that the variations seen in the reflectivity are originated in the cloud formation stage itself.

The hydrometeors also evolve during their descent to the ground due to several microphysical processes. These processes can be inferred from the vertical structure of precipitation or vertical profiles of reflectivity. The median reflectivity profiles of deep systems show a gradual increase from ~ 10 km to 6 km and an abrupt enhancement is seen just below 6 km over both the seas (Figs. 3a & 3d). The sudden enhancement at the freezing level (radar bright band) is primarily due to the aggregation of hydrometeors~~ and~~, change in dielectric factor from ice to water and change in fall speed from ice hydrometers to raindrops (Fabry and Zawadzki 1995; Rao et al. 2008; Cao et al. 2013). Below the bright band, raindrops grow by collision-coalescence process and reduce their size by either breakup and/or evaporation processes. The collision-coalescence results in negative slope in the reflectivity profile, whereas breakup and evaporation results in positive slope (Liu and Zipser 2013; Cao et al. 2013; Saikranthi et al. 2014; Rao et al. 2016). The observed negative slope (~ -0.3 dBZ km^{-1}) in the median reflectivity profiles below the bright band indicates dominance of low-level hydrometeor growth over both the seas. The magnitude of the slope decreases with SST over the AS, while it is nearly equal at all SSTs over the BOB. It indicates the growth rate decreases with SST over the AS and remains the same at all SSTs over the BOB. The median reflectivity profiles of shallow systems also show negative slopes (~ -1 dBZ km^{-1}) at all SSTs representing the predominance of low-level hydrometeor growth by collision-coalescence processes over both the seas.

The present analysis shows that the observed reflectivity changes with SST over both the seas originate at the cloud formation stage and magnify further during the descent of hydrometeors to ground.

5. Conclusions

Sixteen years of TRMM-PR 2A25 reflectivity profiles and 11 years of MODIS AOD and CER data are utilized to understand the differences in variation of vertical structure of precipitation with SST over AS and BOB. Precipitation top height increases with SST over the AS indicating that systems grow to higher altitudes with increase in SST while it is almost same at all SSTs representing that the systems are deeper over the BOB. The decrease in stability and mid-tropospheric wind shear with SST over the AS favour the formation of deeper system at higher systems. However the low stability and small wind shear at all SSTs over the BOB help the formation of deeper systems. The variation of reflectivity with SST is found to be remarkable over the AS and marginal over the BOB. The reflectivity increases with rise in SST over the AS and remains the same at all SSTs over the BOB. This change in reflectivity over the AS is more prominent below the freezing level height (~ 4 dBZ) than the above (~ 1 dBZ). Over the AS, the abundance of aerosols and less moisture at SSTs < 27°C result in high concentration of smaller cloud droplets. As SST increases the aerosol concentration decreases and moisture increases leading to the formation of bigger cloud droplets. Thus, the reflectivity increases with rise in SST over the AS. On the other hand, AOD, TCW and CER do not show substantial variation with SST over the BOB and hence the change in reflectivity is small. Over the BOB, the mid troposphere is wet and hydrometeor's size at the formation stage is nearly the same at all SSTs. The evolution of hydrometeors during their descent is also similar at all SST's. The collision-coalescence process is predominant below the bright band region over both the seas and is responsible for the observed negative slope in the reflectivity profiles.

Acknowledgements

The authors would like to thank Prof. Robert Houze and his team for the interpolated 3D gridded TRMM-PR dataset (http://trmm.atmos.washington.edu), ECMWF (http://data-portal.ecmwf.int/) team for providing the ERA-Interim dataset and MODIS (https://ladsweb.modaps.eosdis.nasa.gov/) science team for providing the AOD and CER dataset. The authors express their gratitude to Prof. J. Srinivasan for his fruitful discussions and valuable suggestions in improving the quality of the manuscript. The corresponding author would like to thank Department of Science & Technology (DST), India for providing the financial support through the reference number DST/INSPIRE/04/2017/001185. We thank the anonymous referees for their critical comments in improving the quality of the manuscript.

Formatted: Centered

References

Albrecht, B.A.: Aerosols, cloud microphysics, and fractional cloudiness, *Science*, 245, 1227–1230, 1989.

Awaka, J., Iguchi, T., and Okamoto, K.: TRMM PR standard algorithm 2A23 and its performance on bright band detection, *J. Meteorol. Soc. Jpn*., 87A, 31–52, 2009.

Bhat, G. S., Gadgil, S., Kumar, P. V. H., Kalsi, S. R., Madhusoodanan, P., Murty, V. S., Rao, C. V. P., Babu, V. R., Rao, L.V., Rao, R. R., Ravichandran, M., Reddy, K.G., Rao, P. S., Sengupta, D., Sikka, D. R., Swain, J., and Vinayachandran, P. N.: BOBMEX: The Bay of Bengal Monsoon Experiment, *Bull. Amer. Meteor. Soc.*, 82, 2217–2244, 2001.

Cao, Q., Hong, Y., Gourley, J. J., Qi, Y., Zhang, J., Wen, Y., and Kirstetter, P. E.: Statistical and physical analysis of the vertical structure of precipitation in the mountainous west region of the United States using 11+ years of space borne observations from TRMM precipitation radar, *J. Appl. Meteorol. Climatol.*, 52, 408-424, 2013.

Chaudhari, H. S., Pokhrel, S., Kulkani, A., Hazra, A., and Saha, S. K.: Clouds-SST relationship and interannual variability modes of Indian summer monsoon in the context of clouds and SSTs: observational and modelling aspects, *Int. J. Climatol.*, doi: 10.1002/ joc.4664, 2016.

Chaudhari, H. S., Pokhrel, S., Mohanty, S., and Saha, S. K.: Seasonal prediction of Indian summer monsoon in NCEP coupled and uncoupled model, *Theor. Appl. Climatol.*, 114, 459–477, doi:10.1007/s00704-013-0854-8, 2013.

Chen, Q., Fan, J., Hagos, S., Gustafson Jr., W. I., and Berg, L. K.: Roles of wind shear at different vertical levels: Cloud system organization and properties, J. Geophys. Res. Atmos., 120, 6551–6574, 2015.

Creamean, J. M., Suski, K. J., Rosenfeld, D., Cazorla, A., DeMott, P. J., Sullivan, R. C., White, A. B., Ralph, F. M., Minnis, P., Comstock, J. M., Tomlinson, J. M., Kimberly A., and Prather, K. A.: Dust and biological aerosols from the Sahara and Asia influence precipitation in the western U.S., *Science*, 339, 1572–1578, doi:10.1126/science.1227279, 2013.

Dee, D. P., et al.: The ERA-Interim reanalysis: Configuration and performance of the data assimilation system, *Q. J. R. Meteorol. Soc.*, 137, 553–597, 2011.

Emanuel, K. A.: Atmospheric convection. Oxford University Press, Oxford, 1994.

Fabry, F., and Zawadzki, I.: Long-term radar observations of the melting layer of precipitation and their interpretation, *J. Atmos. Sci.*, 52, 838–851, 1995.

Feng, X., Haines, K., Liu, C., de Boisséson, E., and Polo, I., Improved SST-precipitation intraseasonal relationships in the ECMWF coupled climate reanalysis, *Geophys. Res. Lett.*, 45, 3664–3672, 2018.

Findlater, J.: A major low-level air current near the Indian Ocean during the northern summer, *Q. J. R. Meteorol. Soc.*, 95, 362–380, 1969.

Fu, Y., and Liu, G.: The variability of tropical precipitation profiles and its impact on microwave brightness temperatures as inferred from TRMM data, *J. Appl. Meteorol.*, 40, 2130–2143, 2001.

Gadgil, S., Joseph, P. V., and Joshi, N. V.: Ocean atmosphere coupling over monsoonal regions, *Nature*, 312, 141-143, 1984.

Gadgil, S.: Monsoon–ocean coupling. *Current Sci.,* 78, 309–323, 2000.

Geerts, B., and Dejene, T.: Regional and diurnal variability of the vertical structure of precipitation systems in Africa based on space borne radar data, *J. Clim.*, 18, 893–916, 2005.

Guo, J., Liu, H., Li, Z., Rosenfeld, D., Jiang, M., Xu, W., Jiang, J. H., He, J., Chen, D., Min, M., and Zhai, P.: Aerosol-induced changes in the vertical structure of precipitation: a perspective of TRMM precipitation radar, *Atmos. Chem. Phys*., 18, 13329-13343, https://doi.org/10.5194/acp-18-13329-2018, 2018.

Houze, R. A., and Churchill, D. D.: Mesoscale organization and cloud microphysics in a Bay of Bengal depression, *J. Atmos. Sci.*, 44, 1845–1867, 1987.

Houze, R. A., Rasmussen, K. L., Zuluaga, M. D., and Brodzik, S. R.: The variable nature of convection in the tropics and subtropics: A legacy of 16 years of the Tropical rainfall measuring mission satellite, *Rev. Geophys.*, 53, 994–1021, 2015.

Houze, R. A., Wilton, D. C., and Smull, B. F.: Monsoon convection in the Himalayan region as seen by the TRMM precipitation radar, *Q. J. R. Meteorol. Soc.,* **133**, 1389-1411, 2007.

Houze, R. A.: Mesoscale convective systems, *Rev. Geophys.*, 42, RG4003, doi: 10.1029/2004RG000150, 2004.

Hsu, N., Tsay, S., King, M., and Herman, J.: Aerosol properties over bright-reflecting source regions, *Geosci. Remote Sens. IEEE Trans*., 42, 557–569, 2004.

Hubanks, P., King, M., Platnick, S., and Pincus, R.: MODIS atmosphere L3 gridded product algorithm theoretical basis document collection 005 Version 1.1, Tech. Rep. ATBD-MOD-30, NASA, 2008.

Iguchi, T., Kozu, T., Kwiatkowski, J., Meneghini, R., Awaka, J., and Okamoto, K.: Uncertainties in the rain profiling algorithm for the TRMM precipitation radar, *J. Meteor. Soc. Japan*, 87A, 1–30, doi:10.2151/jmsj.87A.1, 2009.

Krishnamurti, T. N.: Summer monsoon experiment – A review. *Mon. Wea. Rev*., 113, 1590-1626, 1985.

Krishnamurti, T.: Cooling of the Arabian Sea and the onset-vortex during 1979. Recent progress in equatorial oceanography: A report of the final meeting of SCOR WORKING GROUP 47 in Venice, Italy, 1-12, 1981. [Available from Nova Univ., Ocean Science Center, Dania, FL 33004].

Kumar, S., Hazra, A., and Goswami, B. N.: Role of interaction between dynamics, thermodynamics and cloud microphysics on summer monsoon precipitating clouds over the Myanmar coast and the Western Ghats, *Clim. Dyn*., 43, 911–924, doi:10.1007/s00382-013-1909-3, 2014.

Levy, R., Remer, L., Mattoo, S., Vermote, E., and Kaufman, Y.: Second-generation operational algorithm: Retrieval of aerosol properties over land from inversion of moderate resolution imaging spectroradiometer spectral reflectance, *J. Geophys. Res*., 112, D13, doi:10.1029/2006JD007811, 2007.

Li, R., and Min, Q.-L.: Impacts of mineral dust on the vertical structure of precipitation, J. Geophys. Res., 115, D09203, doi:10.1029/2009JD011925, 2010.

Liu, C., Zipser, E., and Nesbitt, S. W.: Global distribution of tropical deep convection: Different perspectives using infrared and radar as the primary data source, *J. Climate*, 20, 489-503, 2007.

Liu. C., and Zipser, E. J.: Why does radar reflectivity tend to increase downward toward the ocean surface, but decrease downward toward the land surface?, *J. Geophys. Res. Atmos.*, 118, 135-148, doi: 10.1029/2012JD018134, 2013.

Meenu, S., Parameswaran, K., and Rajeev, K.: Role of sea surface temperature and wind convergence in regulating convection over the tropical Indian Ocean, *J. Geophys. Res. Atmos.*, 117, D14102, 2012.

Nair, A. K. M., and Rajeev, K.: Multiyear CloudSat and CALIPSO observations of the dependence of cloud vertical distribution on sea surface temperature and tropospheric dynamics, *J. Clim*., 27, 672–683, doi:10.1175/JCLI-D-13-00062.1, 2014.

Narayanan, M. S., and Rao, B. M.: Detection of monsoon inversion by TIROS-N satellite, *Nature*, 294, 546-548, 1981.

Nuijens, L., Emanuel, K., Masunaga, H., and L'Ecuyer, T.: Implications of warm rain in shallow cumulus and congestus clouds for large-scale circulations, *Surv. Geophys*., 38, 1257-1282, 2017.

Oueslati, B., and Bellon, G.: The double ITCZ bias in CMIP5 models: interaction between SST, large-scale circulation and precipitation. *Clim. Dyn.*, 44, 585-607, 2015.

Platnick, S., et al.: The MODIS cloud optical and microphysical products: Collection 6 updates and examples from Terra and Aqua, *IEEE Trans. Geosci. Remote Sens*., 55, 502–525, doi:10.1109/TGRS.2016.2610522, 2017.

Rajeevan, M., Unnikrishnan, C. K., and Preethi, B.: Evaluation of the ENSEMBLES multi-model seasonal forecasts of Indian summer monsoon variability, *Clim. Dyn.*, 38, 2257–2274, 2012.

Rajendran, K., Nanjundiah, R. S., Gadgil, S., and Srinivasan, J.: How good are the simulations of tropical SST–rainfall relationship by IPCC AR4 atmospheric and coupled models?, *J. Earth Sys. Sci.*, 121(3), 595–610, 2012.

Rajendran, K., Gadgil, S. and Surendran, S.: Monsoon season local control on precipitation over warm tropical oceans, *Meteorol. Atmos. Phys*., doi:10.1007/s00703-018-0649-7, 2018.

Rao, T. N., Kirankumar, N. V. P., Radhakrishna, B., Rao, D. N., and Nakamura, K.: Classification of tropical precipitating systems using wind profiler spectral moments. Part I: Algorithm description and validation, *J. Atmos. Oceanic Technol.*, 25, 884–897, 2008.

Rao, T. N., Saikranthi, K., Radhakrisna, B., and Rao, S. V. B.: Differences in the climataological characteristics of precipitation between active and break spells of the Indian summer monsoon, *J. Clim.*, 29, 7797-7814, 2016.

Remer, L., Kaufman, Y., Tanr´e, D., Mattoo, S., Chu, D., Martins, J., Li, R., Ichoku, C., Levy, R., Kleidman, R., Eck, T., Vermote, E., and Holben, B.: The MODIS aerosol algorithm, products, and validation, *J. Atmos. Sci*., 62, 947–973, 2005.

Romatschke, U., Medina, S., and Houze, R. A.: Regional, seasonal, and diurnal variations of extreme convection in the South Asian region, *J. Clim.*, 23, 419 –439, 2010.

Rosenfeld, D., et al.: Global observations of aerosol-cloud-precipitation-climate interactions, *Rev. Geophys.*, 52, 750-808, doi:10.1002/2013RG000441, 2014.

Roxy, M., Tanimoto, Y., Preethi, B., Terray, P., and Krishnan, R.: Intraseasonal SST-precipitation relationship and its spatial variability over the tropical summer monsoon region, *Clim. Dyn.*, 41, 45-61, 2013.

Roxy, M.: Sensitivity of precipitation to sea surface temperature over the tropical summer monsoon region—and its quantification, *Clim. Dyn.*, 43, 1159-1169, 2014.

Sabin, T., Babu, C., and Joseph, P.: SST–convection relation over tropical oceans, *Int. J. Climatol*. 33, 1424–1435, 2012.

Saikranthi, K., Radhakrishna, B., Satheesh, S. K., and Rao, T. N.: Spatial variation of different rain systems during El Niño and La Niña periods over India and adjoining ocean, *Clim. Dyn.*, 50, 3671-3685, doi: 10.1007/s00382-017-3833-4, 2018.

Saikranthi, K., Rao, T. N., Radhakrishna, B., and Rao, S. V. B.: Morphology of the vertical structure of precipitation over India and adjoining oceans based on long-term measurements of TRMMPR, *J. Geophys. Res. Atmos.*, 119, 8433–8449, doi: 10.1002/2014JD021774, 2014.

Saikranthi, K., Radhakrishna, B., Rao, T. N., and Satheesh, S. K.: Differences in the association of sea surface temperature - precipitating systems over the Bay of Bengal and the Arabian Sea during southwest monsoon season. *Int. J. Climatol*., doi:10.1002/joc.6074, 2019.

Sathiyamoorthy, V., Mahesh, C., Gopalan, K., Prakash, S., Shukla, B. P., Mathur, A.: Characteristics of low clouds over the Arabian Sea, *J. Geophys. Res. Atmos.*, 118, 13489-13503, 2013.

Schumacher, C. and Houze, R. A.: Stratiform rain in the tropics as seen by the TRMM precipitation radar, *J. Climate.*, 16, 1739–1756, 2003.

Sengupta, D., Goswami, B. N., and Senan, R.: Coherent intraseasonal oscillations of ocean and atmosphere during the Asian summer monsoon, *Geophys. Res. Lett.*, 28, 4127–4130, 2001.

Shenoi, S. S. C., Shankar, D., and Shetye, S. R.: Differences in heat budgets of the near-surface Arabian Sea and Bay of Bengal: Implications for the summer monsoon, *J. Geophys. Res.*, 107(C6), 3052, doi:10.1029/2000JC000679, 2002.

Shige, S. and Kummerow, C.D.: Precipitation-Top Heights of Heavy Orographic Rainfall in the Asian Monsoon Region, *J. Atmos. Sci.*, 73, 3009–3024, 2016.

Shige, S., Nakano, Y., and Yamamoto, M. K.: Role of orography, diurnal cycle, and intraseasonal oscillation in summer monsoon rainfall over Western Ghats and Myanmar coast, *J. Climate*, 30, 9365–9381, doi:10.1175/JCLI-D-16-0858.1, 2017.

Sunilkumar, K., Rao, T. N., Saikranthi, K., and Rao, M. P.: comprehensive evaluation of multisatellite precipitation estimates over India using gridded rainfall data, *J. Geophys. Res. Atmos.*, 120, doi:10.1002/2015JD023437, 2015.

Takahashi, H. G., and Dado, J. M. B.: Relationship between sea surface temperature and rainfall in the Philippines during the Asian summer monsoon, *J. Meteor. Soc. Japan*,, 96 (3), 283−290, doi:10.2151/jmsj.2018-03, 2018.

Takayabu, Y. N., Shige, S., Tao, W., and Hirota, N.: Shallow and deep latent heating modes over tropical Oceans observed with TRMM PR spectral latent heating Data, *J. Climate*, 23, 2030–2046, 2010.

Tao, W.-K., Chen, J.-P., Li, Z., Wang, C., and Zhang, C.: Impact of aerosols on convective clouds and precipitation, *Rev. Geophys.*, 50, RG2001, doi:10.1029/2011RG000369, 2012.

Tao, W.-K., et al.: Retrieval of latent heating from TRMM measurements, *Bull. Am. Meteorol. Soc.*, 87, 1555–1572, 2006.

Tao, W.-K., et al.: TRMM latent heating retrieval: Applications and comparisons with field campaigns and large-scale analyses, *Meteorological Monographs - Multi-scale Convection-Coupled Systems in the Tropics: A tribute to Dr. Michio Yanai*, 56, 2.1-2.34, doi:10.1175/AMSMONOGRAPHS-D-15-0013.1, 2016.

Twomey, S.: The influence of pollution on the short wave albedo of clouds, *J. Atmos. Sci.*, 34, 1149–1152, 1977.

Wallace, J. M., and Hobbs, P. V.: Atmospheric science: An introductory survey, Second edition, Academic press, pp. 85, 2006.

Wang, B., Ding, Q., Fu, X., Kang, I.-S., Jin, K., Shukla, J., and Doblas-Reyes, F.: Fundamental challenge in simulation and prediction of summer monsoon rainfall, *Geophys. Res. Lett*., 32, L15711, doi:10.1029/2005GL022734, 2005.

Weller, R. A., Farrar, J. T., Buckley, J., Mathew, S., Venkatesan, R., Lekha, J. S., Chaudhuri, D., Kumar, N. S., and Kumar, B. P.: Air-sea interaction in the Bay of Bengal, *Oceanography*, 29(2), 28–37, 2016.

Woolnough, S.J., Slingo, J.M., and Hoskins, B.J.: The relationship between convection and sea surface temperature on intraseasonal timescales, *J. Climate*, 13, 2086–2104, 2000.

Wu, R., and Kirtman, B. P.: Roles of Indian and Pacific Ocean air–sea coupling in tropical atmospheric variability, *Clim. Dyn.*, *25*(2–3), 155–170, 2005.

Figure captions

Figure 1: Spatial distribution of ISM mean SST (in °C) obtained from ERA-Interim reanalysis data over the AS (63°E-72°E & 8°N-20°N) and the BOB (83°E-92°E &

8°N-21°N). The regions considered in this analysis over these two seas are shown with the boxes.

Figure 2: (a) and (b) represent the altitudinal distribution of occurrence of conditional reflectivity (≥ 17 dBZ) as a function of SST with respect to precipitation occurrence at that particular SST interval over the AS and the BOB, respectively.

Figure 3: (a), (d) and (b), (e) represent vertical profiles of median reflectivity correspond to deep systems and their standard deviation (in dBZ) with SST over the AS and the BOB, respectively during the ISM season. (c) and (f) show the number of conditional reflectivity pixels at each altitude used for the estimation of the median and standard deviation.

Figure 4: Same as Fig. 3 but for shallow precipitating systems.

Figure 5: (a) and (b), respectively, represent the vertical profiles of mean θ_e (in K) with SST over the AS and the BOB during the ISM season. (c) and (d) and (e) and (f) are same as (a) and (b) but for mean vertical velocity (in Pa s^{-1}) and wind gradient with reference to 950 hPa level (in m s^{-1}).

Figure 6: (a) Mean and standard error of AOD and (b) TCW (in kg m^{-2}) with SST over the AS and the BOB during ISM.

Figure 7: Variation of mean and standard error of CER liquid (in μm) with SST over the AS and the BOB during the ISM season.

Figures

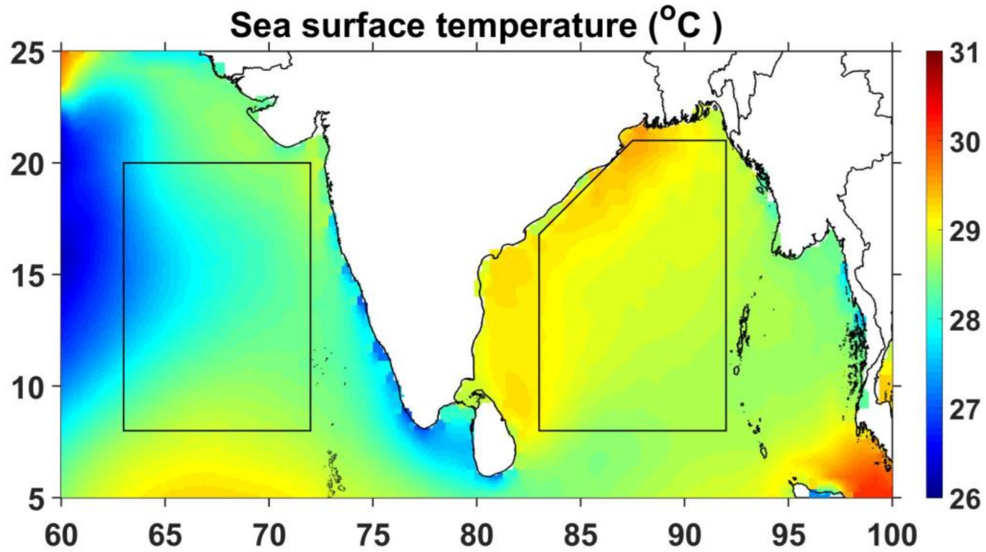

Figure 1: Spatial distribution of ISM mean SST (in °C) obtained from ERA-Interim reanalysis data over the AS (63°E-72°E & 8°N-20°N) and the BOB (83°E-92°E & 8°N-21°N). The regions considered in this analysis over these two seas are shown with the boxes.

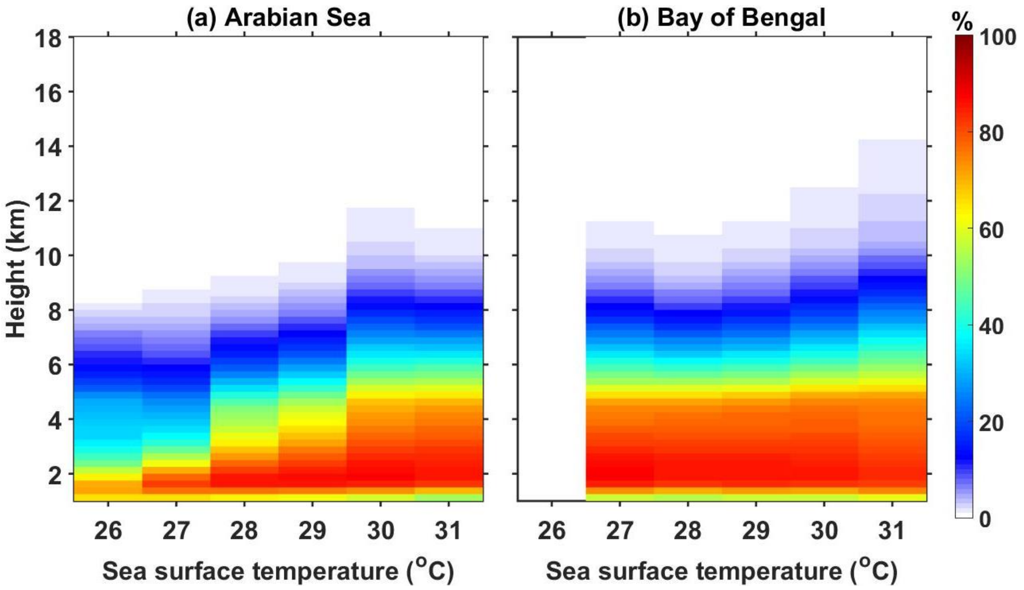

Figure 2: (a) and (b) represent the altitudinal distribution of occurrence of conditional reflectivity (≥ 17 dBZ) as a function of SST with respect to precipitation occurrence at that particular SST interval over the AS and the BOB, respectively.

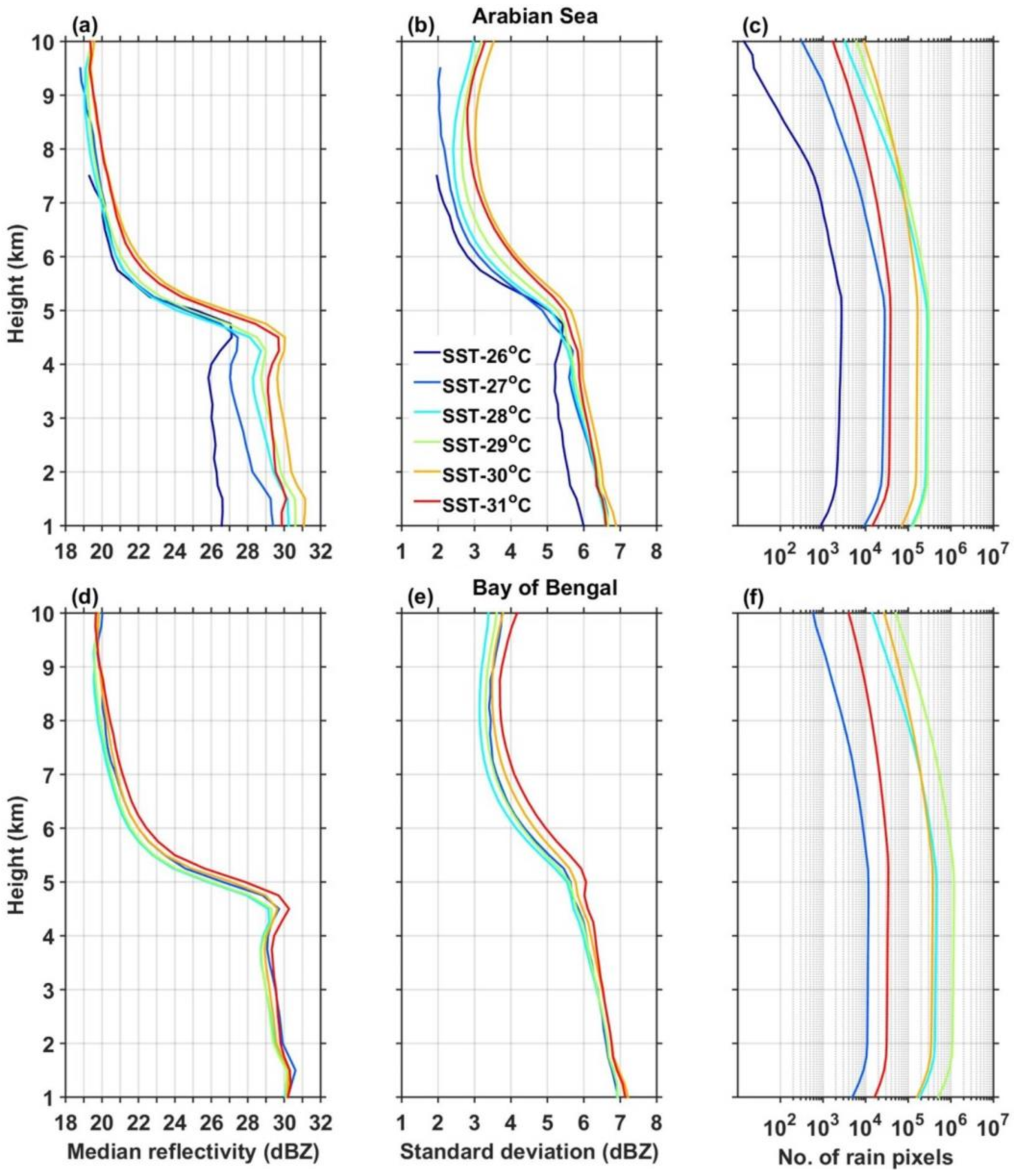

Figure 3: (a), (d) and (b), (e) represent vertical profiles of median reflectivity correspond to deep systems and their standard deviation (in dBZ) with SST over the AS and the

BOB, respectively during the ISM season. (c) and (f) show the number of conditional reflectivity pixels at each altitude used for the estimation of the median and standard deviation.

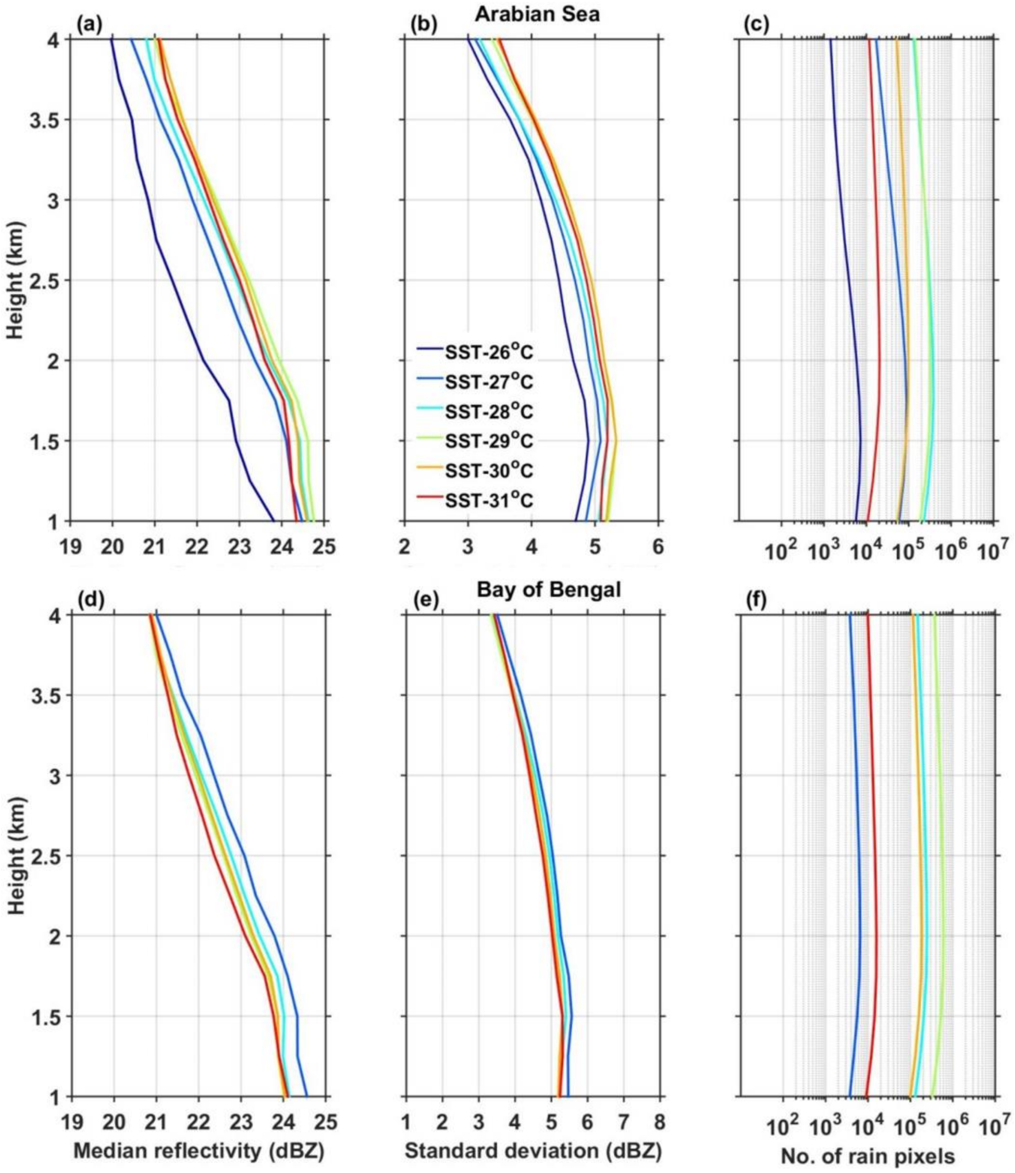

Figure 4: Same as Fig. 3 but for shallow precipitating systems.

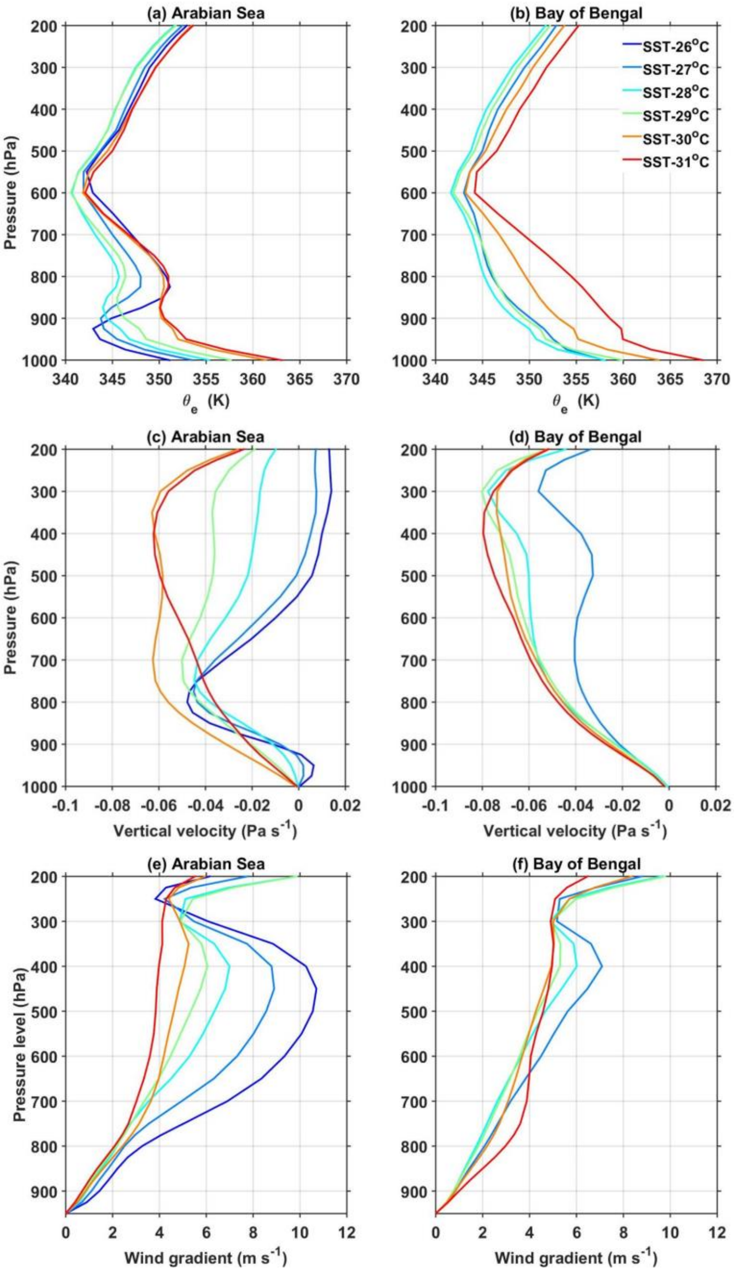

Figure 5: (a) and (b), respectively, represent the vertical profiles of mean θ_e (in K) with SST over the AS and the BOB during the ISM season. (c) and (d) and (e) and (f) are same as (a) and (b) but for mean vertical velocity (in Pa s^{-1}) and wind gradient with reference to 950 hPa level (in m s^{-1}).

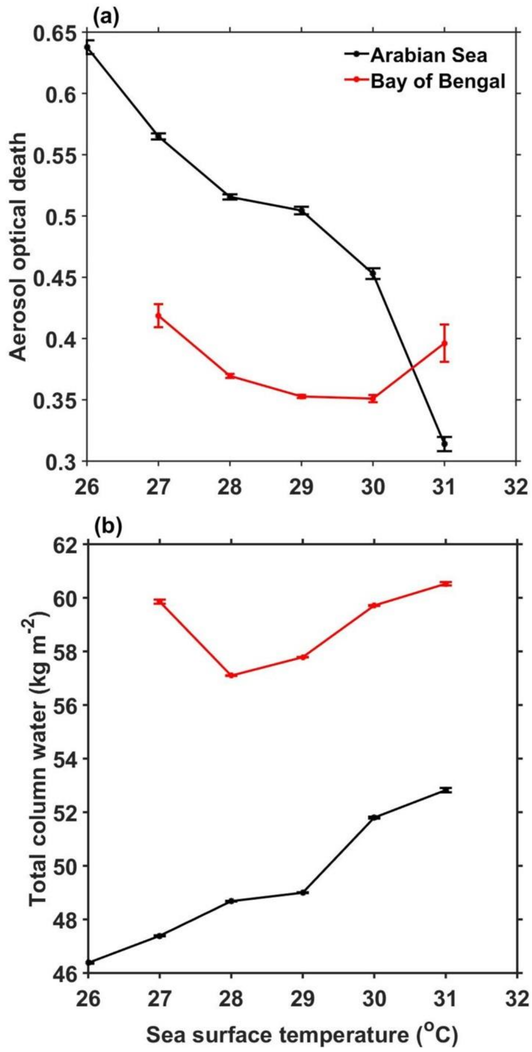

Figure 6: (a) Mean and standard error of AOD and (b) TCW (in kg m^{-2}) with SST over the AS and the BOB during ISM.

Formatted: Font: (Default) Times New Roman, 12 pt

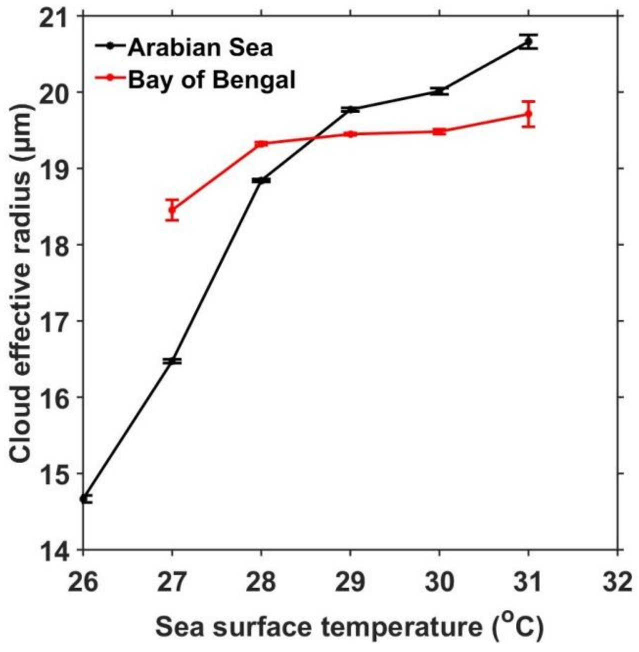

Figure 7~~Figure 6~~: Variation of mean and standard error of CER liquid (in μm) with SST over the AS and the BOB during the ISM season.

Supplementary material

Satheesh et al. (2006) showed an increase in AOD with increase in latitude over the AS due to the dust advection from Arabia desert regions during ISM season, whereas SST decreases with increase in the latitude. In other words the SST is low and AOD is high in northern AS whereas over the southern AS, SST is high and AOD is low. This contrasting spatial distribution of AOD and SST could cause a negative correlation between AOD and SST as depicted in Fig. 6a. To examine whether the observed decrease in AOD with increase in SST over the AS is due to the latitudinal variation of AOD or exists at all latitudes, we have segregated the data into 2° latitude bins and plotted the mean AOD with SST for all bins and is depicted in Fig. S2. In spite of the magnitude, AOD variation with SST is nearly similar at all latitudes of the AS, i.e., the higher AOD is observed at lower SSTs and vice versa (Fig. S2a). On the other hand the latitudinal variation of AOD with SST over the BOB shown in Fig. S2b also show a decrease in AOD with SST till 30 °C but the magnitude of variation is trivial relative to the AS. Also, as depicted in Fig. 6a AOD increases above 30 °C with SST over the BOB. This indicates that though there is a difference in magnitude of variation, AOD varies with SST over both the seas at all latitudes. This analysis is repeated using the multi-angle imaging spectroradiometer (MISR) dataset (which is not shown here) for small, medium large aerosol particles. Interestingly all three types also show a decrease in AOD with rise in SST over both the seas.

Satheesh, S. K., Moorthy, K. K., Kaufman, Y. J., and Takemura, T.: Aerosol Optical depth, physical properties and radiative forcing over the Arabian Sea, *Meteorol. Atmos. Phys.*, 91, 45–62, doi:10.1007/s00703-004-0097-4, 2006.

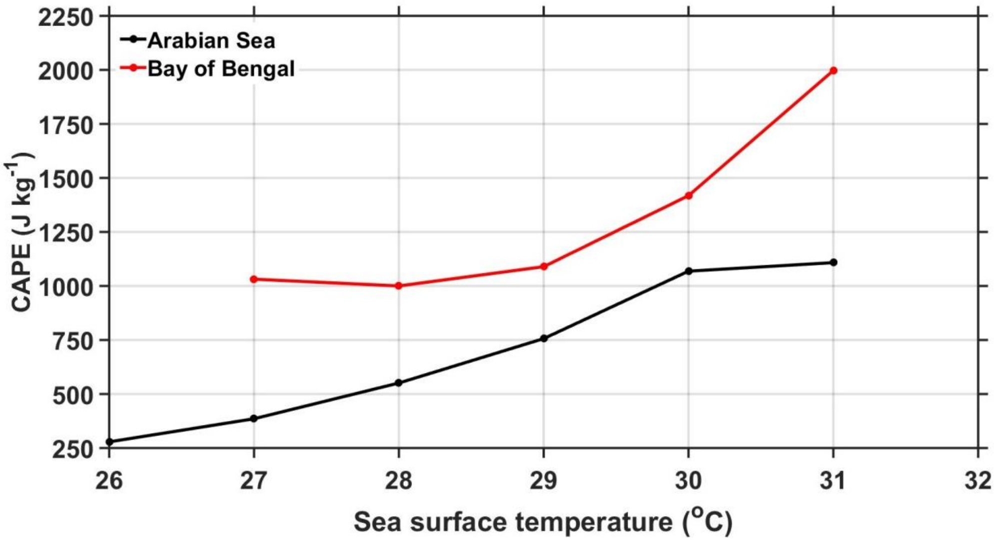

Figure S1: Variation of mean CAPE (in J kg^{-1}) with SST over the AS and the BOB during the ISM season.

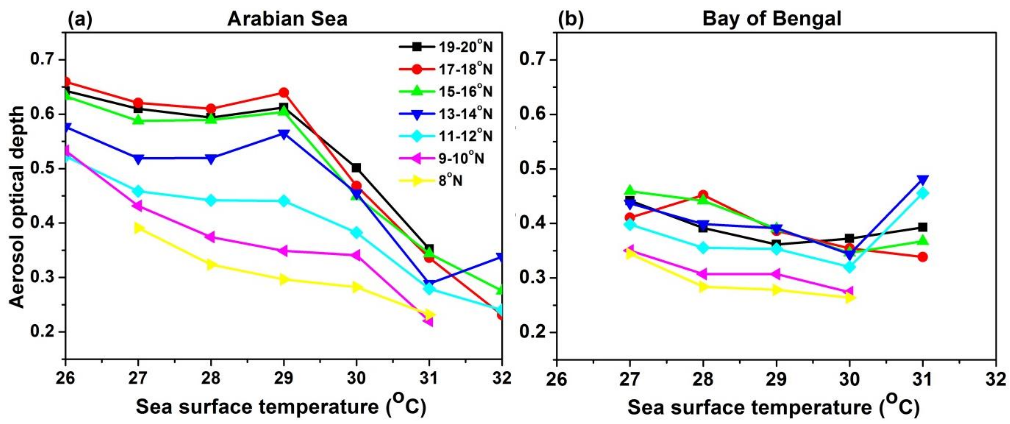

Figure S2: (a) and (b), respectively, represent latitudinal variation (for every 2° latitude interval) of mean AOD over the AS (between 63°E and 72°E) and the BOB (between 83°E and 92°E).